FreedomCAR FUEL Partnership

Energy Storage Research & Development

2003 Annual Progress Report

Less dependence on foreign oil, and eventual transition to an emissions-free, petroleum-free vehicle

FreedomCAR & Vehicle Technologies Program

U.S. Department of Energy
Energy Efficiency and Renewable Energy
Bringing you a prosperous future where energy is clean, abundant, reliable, and affordable

U.S. Department of Energy
Office of FreedomCAR and Vehicle Technologies
1000 Independence Avenue S.W.
Washington, D.C. 20585-0121

FY 2003

Progress Report for Energy Storage Research and Development

Energy Efficiency and Renewable Energy
FreedomCAR and Vehicle Technologies

Tien Q. Duong
Manager, Energy Storage R&D

May 2004

TABLE OF CONTENTS

TABLE OF CONTENTS (CONT.)

I. INTRODUCTION

The promise of alternative vehicles which achieve better fuel economy, emit fewer harmful emissions, yet perform as well or better than typical internal combustion engine (ICE) vehicles, appears to be closer than ever. Manufacturers continue to pursue and introduce new technologies that achieve those goals because of increased concern about and attention to air pollution, petroleum consumption, and reliance on foreign sources of that petroleum.

Several hybrid-electric vehicles (HEVs) have been introduced into the U.S. market over the past three years, including the Toyota Prius and the Honda Insight and HEV Civic. The challenge is for the United States to work towards energy independence and market leadership while maintaining consumer choice and mobility. The Energy Storage Research and Development Effort is working to help address these challenges.

I.A. FreedomCAR and Vehicle Technologies Program Overview

Transportation consumes two-thirds of all petroleum consumed in the United States, and is therefore a natural place to focus efforts on increased efficiencies. With this in mind, on January 9, 2003 the Department of Energy (DOE) and the leadership of General Motors Corporation, Ford Motor Company, and DaimlerChrysler Corporation announced the creation of the FreedomCAR Partnership.[1] This partnership is focused on funding high-reward/high-risk research that promises improvements in critical components needed for more fuel efficient, cleaner vehicles and provides ongoing guidance and expertise to DOE's energy storage activity. Such collaboration with automakers and battery manufacturers enhances the potential for success and the relevancy of these programs.

The DOE FreedomCAR & Vehicle Technologies (FCVT) Program office[2] works with industry to develop advanced transportation technologies that reduce the nation's use of imported oil and improve its air quality. Some of the technologies being supported by this office include hybrid systems R&D, electric vehicle R&D, materials technologies R&D, advanced fuels R&D, and advanced combustion R&D. The program also maintains a diverse set of R&D activities in light and heavy vehicle technologies.

[1] For more information, please see http://www.uscar.org/Media/2002issue1/p1_freedomcar.htm, or www.ott.doe.gov/pdfs/freedomcar_plan.pdf.

[2] See http://www.eere.energy.gov/vehiclesandfuels/.

I.B. Energy Storage Research & Development Overview

Energy storage technologies, including batteries as well as ultracapacitors, have been identified as critical enabling technologies for advanced, fuel-efficient, light and heavy duty vehicles. The Energy Storage Research and Development Effort within the FCVT Program is responsible for advancing innovative batteries for a wide range of vehicle applications, including HEVs, battery electric vehicles (EVs), the potential 42 volt vehicle system (42V), as well as fuel cell vehicles (FCVs). The office is working in close partnership with the automotive industry, represented by the United States Advanced Battery Consortium (USABC).[3]

The current effort is comprised of three major activities, battery technology development, applied battery research, and long-term exploratory research. The work done in each of these is described below:

Battery Technology Development is subdivided into three closely related sets of activities: full system development, technology assessment, and benchmark testing.

- *Full System Development* - In cooperation with the USABC, efforts are focused on developing and evaluating a cost-optimized liquid cooled NiMH monoblock module for HEVs, on addressing the issues that reduce the useful life of lithium ion batteries in EVs, on reducing the cost of lithium ion HEV modules, and on developing an advanced lithium sulfur (Li/S) battery system that has the potential of meeting all EV targets, including cost.

- *Technology Assessment* - Technology assessments are conducted on newly emerging technologies prior to full system development. These 12-month projects assess a developer's overall capabilities and validate technical claims through independent testing. Current assessment projects include cells based on Lithium-ion gel technology, a spinel based chemistry, and a new $LiFePO_4$ cathode active material.

- *Benchmark Testing* - Benchmark testing of emerging technologies is important for remaining abreast of the latest industry developments. Working with the national laboratories, FCVT purchases and independently tests hardware against the manufacturer's specifications and the most applicable technical targets. Recently completed benchmark testing included Lithium-ion/ manganese spinel chemistries against HEV and EV targets.

Applied Battery Research is focused on addressing the cross-cutting barriers that face Lithium-ion systems which are closest to meeting all of the technical energy and power requirements for vehicle applications. Five national laboratories participate in this activity, each bringing its own expertise to three critical barrier areas: life, abuse tolerance, and cost. In addition, this activity concentrates on Technology Transfer to ensure that the research results and lessons learned are effectively provided to the U.S. automotive and battery manufacturers.

[3] The USABC partnership was formed in 1991 between DaimlerChrysler, Ford, and General Motors to initiate a domestic advanced battery industry based on new technology.

Long-term Battery Research addresses fundamental problems of chemical instabilities that impede the development of advanced batteries. This research provides a better understanding of why systems fail, develops models that predict system failure and permit system optimization, and investigates new and promising materials. The work presently concentrates on six research areas: advanced cell chemistry, non-carbonaceous anodes, new electrolytes, novel cathode materials, advanced diagnostics and analytical methods, and phenomenological modeling.

This report highlights the activities and progress achieved in the Energy Storage Research and Development Effort during FY 2003. We are pleased with the progress made during the year and look forward to continued work with our industrial, government, and scientific partners to overcome the challenges that remain to delivering advanced energy storage systems for vehicle applications.

Tien Q. Duong
Manager, Energy Storage Research and Development
FreedomCAR and Vehicle Technologies Program

II. BATTERY TECHNOLOGY DEVELOPMENT

Introduction

Battery technology development is one of the primary activities of the energy storage effort. It is subdivided into four mission areas: *system development*, aimed at developing advanced batteries for a wide range of vehicle applications; *technology assessment*, to assess developers' current capabilities and validate technical claims*; benchmark testing* of emerging technologies in order to remain abreast of the latest industry developments; and *Small Business Innovative Research (SBIR),* that provides valuable support to EV and HEV battery development efforts.

II.A. System Development

System development, in turn, is divided into two programmatic areas: Vehicle High Power Energy Storage that focuses on development of batteries for HEVs, 42V systems, and FCVs; and Electric Vehicle Battery Research and Development that supports the development of battery technologies to enable commercially competitive EVs. All battery system development for light duty vehicles is conducted in collaboration with industry through the United States Advanced Battery Consortium (USABC). All of the USABC subcontracts to develop advanced light vehicle batteries for hybrid and electric vehicles are awarded under a competitive process and are cost-shared.

II.A.1 Vehicle High-Power Energy Storage

Introduction

Under the leadership of the OFCVT, the Vehicle High-Power Energy Storage activity is part of a multifaceted effort to develop and perfect the technologies needed to encourage the commercial adoption of cleaner, more fuel-efficient hybrid-electric vehicles. The Vehicle High-Power Energy Storage activity supports the FreedomCAR Partnership.

Lightweight, durable, and affordable high-power batteries are one of the critical technologies essential for the continuing development of hybrid vehicles, 42V vehicular systems, and fuel cell vehicles. The Vehicle High-Power Energy Storage activity is focused on overcoming the main technical barriers associated with commercialization of these advanced vehicles by concentrating on four major areas, namely:

Cost

The current cost of nickel-metal hydride and lithium-based batteries (the most promising high-power battery chemistries) is prohibitively high, both on a kW and a kWh basis. The main cost drivers being addressed are the high cost of raw materials and materials processing, and cell and module packaging cost.

Battery Life

A 15-year calendar life is required to reduce overall system costs and to make the technology more attractive to consumers. Nickel-metal hydride (NiMH) batteries have a calendar life of

over 6 years in real world applications. The life of lithium-based batteries is estimated to be 15 years, according to reports from Saft America Inc., as shown in Table II-1.

Table II-1. Performance of High-Power Lithium-ion Batteries (2003)

Performance	*Current Lithium-ion*	*System Target*
Specific Power (W/kg, 18s discharge)	900[4]	625
Power Density (W/L)	1,450	780
Specific Energy (Wh/kg)	75	7.5
Cycle Life (25 Wh cycles)	300,000	300,000
Calendar (yrs)	10	15
Selling Price ($/system @ 100 k/yr)	(Approx. 2-4 times target value)	500

Battery Performance

The barriers related to battery performance are the reduced discharge pulse power available at low temperatures and the loss of available power over time due to use and aging.

Abuse Tolerance

High power batteries are not intrinsically tolerant of abuse such as short circuits, overcharge, over-discharge, mechanical shock, vibration, crush, or fire exposure. Multiple strings of cells pose a problem for lithium-based technologies because they require overcharge and over-discharge protection at the cell level. In addition, challenging thermal management requirements need to be addressed.

The Vehicle High-Power Battery activity was created to develop solutions to these technical challenges by developing low-cost, high-power batteries that meet or exceed the energy storage requirements for HEVs, 42V vehicular systems, and FCVs, as shown Tables II-2–II-4 respectively. Note that these requirements have been developed in close coordination with industry through the USABC technical teams.

Specific objectives of the Vehicle High-Power Energy Storage activity include:

- By 2010, develop an electric drive train energy storage device with a 15-year life at 300 Wh with a discharge power of 25 kW for 18 seconds and $20/kW cost (a FreedomCAR Partnership goal).
- Reduce the production cost of a high-power 25-kW battery (light vehicle) from $3,000 to $750 in 2006 and to $500 in 2010 (priority FCVT goal).
- Establish and continuously reaffirm performance and cost targets for batteries covering the full range of applications, including 42V systems, HEVs, and FCVs.
- Develop hardware for specific applications that can be tested against respective performance targets and used for subsystem benchmarking.

[4] Battery performance calculated from cell performance by applying a Burden Factor based on battery design.

Table II-2. Energy Storage Requirements for High Voltage, Power Assist Hybrid Electric Vehicles (HEVs)

Characteristic	Units	Minimum	Maximum
Pulse discharge power	kW	25 for 10 sec	45 for 10 sec
Max regenerating pulse (10 sec pulse)	kW	20 (50Wh pulse)	35 (97Wh pulse)
Total available energy	kWh	0.3	0.5
Round trip efficiency	%	>90, 25Wh/cycle	>90, 50Wh /cycle
Cycle life	Cycles	300k @ 25Wh (7.5MWh)	300k @ 50Wh (15 MWh)
Cold cranking power at –30°C (three 2-sec pulses, 10-sec rests between)	kW	5	7
Calendar life	Yrs	15	15
Maximum system weight	kg	40	60
Maximum system volume	Liters	32	45
Production cost @ 100k units/year	$	500	800
Maximum operating voltage	Vdc	<400	<400
Minimum operating voltage	Vdc	>0.55 Vmax	>0.55 Vmax
Maximum self discharge	Wh/d	50	50
Operating temperature	°C	-30 to +52	-30 to +52
Survival temperature	°C	-46 to +66	-46 to +66

Table II 3. Energy Storage Requirements for 42V Vehicular Systems

Characteristic	Units	M-HEV	P-HEV
		Commercialization Goals	
Discharge pulse power	kW	13 for 2 sec	18 for 10 sec
Regenerative pulse power	kW	8 for 2 sec	18 for 2 sec
Engine-off accessory load	kW	3 for 5 min	3 for 5 min
Total available energy	kWh	0.3	0.5
Recharge rate	kW	2.6	4.5
Energy efficiency on load profile	%	>90	>90
Cycle life, profiles (engine starts)		150k (450k)	150k (450k)
Cold cranking power at –30°C	kW	8 (21V minimum)	8 (21V minimum)
Calendar life	Yrs	15	15
Maximum system weight	kg	25	35
Maximum system volume	Liters	20	28
Selling price 100k units/year	$	260	360
Maximum operating voltage	Vdc	48	48
Maximum OCV	Vdc	48 (after 1 sec)	48 (after 1 sec)
Minimum operating voltage	Vdc	27	27
Maximum self discharge	Wh/d	<20	<20
Operating temperature range	°C	-30 to +52	-30 to +52

Table II-4. Proposed Battery targets for Fuel Cell Vehicles (FCVs)

Characteristic	Units	Maximum	Minimum
Discharge pulse power	kW	25 for 18 sec	75 for 18 sec
Regenerative pulse power	kW	22 for 10 sec	65 for 10 sec
Total available energy	kWh	1.5	5
Rouind trip efficiency	%	>90	>90
Cycle life	Cycles	TBD (15 year life equivalent)	
Cold cranking power at –30°C (Details TBD)	kW	5	5)
Calendar life	Yrs	15	15
Maximum system weight	kg	40	100
Maximum system volume	Liters	30	75
Production price @ 100k units/year	%	500	1500
Maximum operating voltage	Vdc	</= 440	</= 440
Minimum operating voltage	Vdc	>/= 0.5 Vmax	>/= 0.5 Vmax
Operating temperature range	°C	-30 to +52	-30 to +52
Survival temperature range	°C	-46 to + 66	-46 to + 66

Two candidate battery chemistries have been identified as the most likely to meet these performance and cost targets: NiMH and lithium-based technology. NiMH batteries offer relatively good power capability as a result of the good ionic conductivity of the potassium hydroxide electrolyte. Lithium-based batteries offer an excellent energy density which can be traded for higher power.

The USABC has supported development of these two technologies since the program's inception in 1997 by awarding subcontracts to a number of developers including Saft America (Li ion and NiMH), VARTA (NiMH), Delphi (Li polymer), AVESTOR (Li polymer), Texaco-Ovonic (NiMH) and Electro Energy (bipolar NiMH). Contracts active in 2003 were with Texaco-Ovonic (NIMH) and Saft (Li ion).

NiMH Battery Development

The contract with Texaco-Ovonic was directed at the development of high-power, low-cost, liquid-cooled multi-cell modules that are designed to be assembled into full batteries, see Figure II-1. Properties of the current modules are presented in Table II-5.

Under DOE sponsorship, Texas Ovonic Battery Systems (TOBS) achieved a two-fold increase in specific power and reduced the projected $/kW battery cost by half. The plastic monoblock module evolved from a labor-intensive battery proof-of-concept to one more amendable to mass production. The most recent monoblock provides a lower cost approach, even better adapted to mass production, with the added benefit of significant improvements in packaging efficiency.

The Phase 3 effort, which concluded in 2003, completed technology development needed for a total battery system useable in commercial products. Additional cost reductions were aimed at achieving a selling price of about $750 for a full battery pack system at a mature volume of 100,000 packs per year. Qualification of the battery cycle life and calendar life was also an objective of this effort.

Figure II-1: TOBS Series 1000 NiMH Monoblock

Table II-5. Properties of TOBS NiMH Battery Monoblock

Characteristic	Value
Nominal voltage	12V
Nominal capacity	9 Ah
Nominal power	2.7 kW
Nominal energy (@ 1C rate)	125 Wh
Module weight	2.4 kg
Module volume	1.28 L
Energy density	52 Wh/L
Specific power	1125 W/kg
Power density	2100 W/L

Lithium-ion Battery Development

A contract with Saft to develop high power cells and modules for the HEV application was also completed in FY 2003. To achieve the targeted cost reduction, Saft focused on material cost reduction and process and assembly optimization. The performance and life of the improved low-cost cells were validated in nominal 50-volt modules. At the conclusion of the contract, Saft delivered two full packs to DOE. The packs met all of the FreedomCAR HEV performance targets, except cost, as shown in Table II-1. One of battery packs has completed 300,000 HEV test cycles suffering less than 2% power fade.

Low-cost Separator Development

Studies at the national laboratories have shown that the cost of non-active material components in high-power batteries (packaging, current collectors, and separator) can equal or even exceed the cost of the active materials. The cost of the separator dominates the cost of the non-active materials. Therefore, DOE, in conjunction with the USABC, is supporting research and development efforts in industry to create novel, low cost materials and to improve processing techniques so that currently available materials may be produced in a less costly manner. Support is being provided to the development of a low-cost polypropylene (PP)-based separator using a wet process, an established dry production process applied to PP-based separators, and a nylon-based high-strength low-cost separator. The goal of these tasks is to produce acceptable separators at a cost of $\$1/m^2$. Contractors engaged in this activity include Celgard, Inc., ENTEK Membranes, LLC, Advanced Membrane Systems (AMS), and Ultimate Membrane Technologies (UMT). All four contracts have an industry cost-share of at least 50%.

The goal is to develop a direct replacement for current materials having the following properties:

- Thickness: < 25 microns
- Wettability: Complete Wet Out in Electrolytes
- Puncture Strength: > 300 g/25.4 microns
- Permeability: MacMullin Number of < 11

- Pore Size: < 1 micron
- Moisture Content: < 50 ppm
- Chemical Stability: Stable in Battery for 10 Years

In addition, the separator should have the capability of shutting down at a temperature of 100–110ºC and also have structural stability to 200ºC.

Battery Thermal Management

This work focuses on improving the thermal performance of batteries through thermal characterization, modeling, analysis, and management. The objectives of this work include improving the performance and extending the life of batteries by measuring their thermal properties and improving the thermal design, developing a test procedure for the thermal evaluation of batteries, thermally analyzing cells and modules and making recommendations for better thermal performance, and evaluating the parameters that affect the alternating current (AC) heating of batteries to improve their performance at cold temperatures. Battery and energy storage models and simulation tools have been developed to define the requirements of energy storage systems and to assess their benefits in advanced vehicles. Results of this research are described in the following paragraphs.

Thermal Improvement of Lithium Polymer Cells. The National Renewable Energy Laboratory (NREL) used thermal characterization tools to provide technical support to Compact Power Incorporated (CPI) of Colorado Springs, Colorado, to improve the thermal performance of three generations of Lithium-ion polymer gel batteries. Compact Power's improvements in third-generation cells have resulted in more uniform temperature distribution, lower maximum temperature, and less heat generation, all of which are needed for greater energy efficiency and longer battery operation.

Energy Storage Requirements for Fuel Cell Vehicles. Members of the NREL energy storage and vehicle systems analysis teams collaborated to evaluate the benefits and requirements of energy storage devices (batteries or ultracapacitors) for hybrid FCVs using ADVISOR, Figure II-2. Analyses indicated that batteries or ultracapacitors could capture significant regenerative braking energy, enhancing the fuel economy of FCVs.

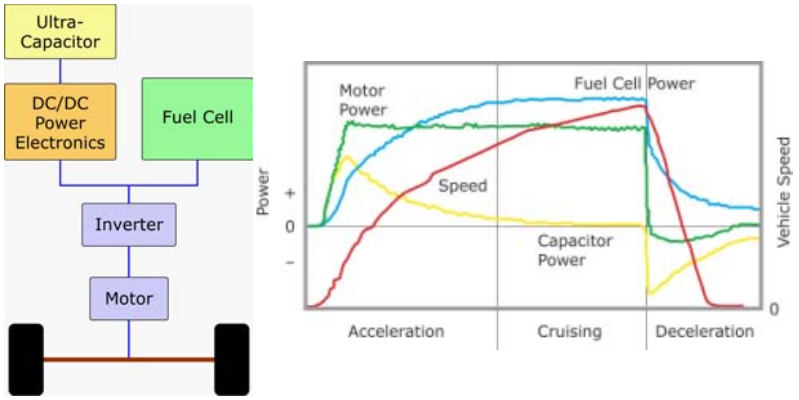

Figure II-2. Energy storage requirements for fuel cells

Battery Preheating. The objective of this work was to investigate the optimal parameters that affect AC preheating of batteries in cold climates. An AC power amplifier was used to provide AC heating to a three-cell Panasonic NiMH module kept at -30ºC, Figure II-3. The impact of current amplitude, frequency, waveform, and duration to improve the pulse power capability of the battery, after applying AC heating pulse, was investigated. An improvement in pulse power capability and an increase in current amplitude and duration were accomplished.

Figure II-3. AC Power amplifier (left) and tested NiMH modules

Thermal Evaluation of Batteries. The objective of this work was to test the thermal management of an advanced battery module for HEV applications, an advanced 12-cell air-cooled Lithium-ion module from Saft. Under repeated 25-Wh PNGV life cycle test profiles and one that was 30% more aggressive, the thermal performance of the battery and its thermal management system kept the battery temperature below 40ºC and the temperature difference less than 2ºC when ambient temperature was 30ºC.

Dual-Source Energy Storage. NREL has developed simulation tools to evaluate the benefits of combining batteries with ultracapacitors for HEVs and FCVs, including a novel control strategy that optimizes the energy and power flow between the ultracapacitor stack and the battery pack. The use of dual-source energy storage could possibly enhance advanced vehicle performance and extend battery life.

Thermal Characterization of Batteries. NREL measured the thermal characteristics (heat capacity and heat generation) of Saft Lithium-ion cells at 0°C, 30°C, and 50°C using the HPPC test. The heat generated by the cell during the PNGV cold cranking test was measured and demonstrated that the cell could meet the test procedure requirements and was 58% efficient at -30°C. Infrared thermal images of a cell as it underwent a 100-amp discharge from 100%-0% state of charge was obtained. No areas of thermal concern or hot spots on the cell were found.

Thermal Analysis of Cells and Batteries. Finite element thermal analysis was used to guide Saft America in the thermal design of their 12-cell module, Figure II-4. NREL evaluated four liquid-cooled designs and found that the design with liquid-cooled plastic jackets around each cell provided the best combination of lowest maximum temperature and lowest temperature difference. Based on NREL's recommendations and the lower mass of this design, Saft has built modules and delivered them to FreedomCAR and NREL for evaluation.

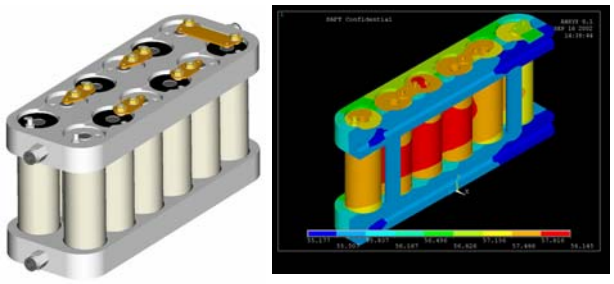

Figure II-4. Thermal analysis of cells in a 42-V module

Future Directions

Looking ahead, the Vehicle High-Power Battery effort will continue to research lower cost separators, will define energy storage requirements for heavy hybrids, will ensure that new materials are made available to manufacturers, and promote information exchange among the various participants in the program. A new contract will be initiated with Saft to focus on 42V systems. In the thermal analysis area, work will continue to improve the thermal performance of batteries and develop models that enable the evaluation for advanced energy storage concepts for EVs and HEVs.

II.A.2 Electric Vehicle Battery Research and Development

Introduction

The Electric Vehicle Battery Research and Development effort supports the development of battery technologies that would enable commercially competitive electric vehicles (EV). The advantage of EVs over other vehicles, (including HEVs) is the fact that they produce no vehicle emissions. Electric Vehicle Battery Research and Development has had several major successes, including the development and introduction of the NiMH battery for EV use. Over 1000 NiMH battery EVs have been put into service in the past several years. The effort conducts extensive benchmarking studies of advanced batteries from the U.S. and abroad. The technical requirements are defined in Table II-6.

Table II-6. U.S. Advanced Battery Consortium Goals for Electric Vehicle Batteries

Primary Criterion	Long-term goals[5] (2005-2008)
Power Density, W/L	460
Specific Power, W/kg (80% DOD/30 sec)	300
Energy Density (Wh/L) (C/3 discharge rate)	230
Specific Energy, Wh/kg (C/3 discharge rate)	150
Life (years)	10
Cycle life (cycles)	1000 (80% DOD) 1,600 (50% DOD) 2670 (30% DOD)
Power and capacity degradation[6] (% of rated spec)	20%
Ultimate price[7] ($/kWh) (10,000 units @ 40 kWh)	<$150 (desired to 75)
Operating environment	-30C to 65 C
Recharge time	< 6 hours
Continuous discharge in 1 hour (no failure)	75% (of rated energy capacity)

[5] For interim commercialization (reflects USABC revisions of September 1996).
[6] Specifics on criteria can be found in *USABC Electric Vehicle Battery Test Procedures Manual, Rev. 2,* DOE/ID 10479, January 1996.
[7] Cost to the original equipment manufacturer.

Secondary Criteria	Long-term goals (2005-2008)
Efficiency (C/3 discharge and C/6 charge[8])	80%
Self-discharge	<20% in 12 days
Maintenance	No maintenance. Service by qualified personnel only.
Thermal loss	Covered by self-discharge
Abuse resistance	Tolerant. Minimized by on-board controls.
Specified by contractor: Packaging constraints, Environmental impact, Safety, Recyclability, Reliability, Overcharge/over-discharge tolerance	

Li ion Battery Development

Saft continued development of the lithium-ion electric vehicle battery with emphasis on meeting interim commercialization goals. Saft engineered and built lithium-ion cells (Figure II-5) to evaluate alternative battery system materials and provided more detailed testing and analysis against USABC and Society of Automotive Engineers criteria for evaluation of abuse to these batteries. This will facilitate acceptance of these batteries by the auto industry. The effort focused on materials research and selection. Recent work has also focused on addressing the gas buildup in cells that reduces their useful life, especially at higher temperatures and states of charge. Saft also conducted comprehensive safety analyses, including testing and failure modes and effects analysis.

Figure II-5. Saft lithium-ion cell and module

As seen in Table II-7, cell performance fell short of the target goals and the cost continues to be a major issue.

Table II-7. Performance of High-Energy Lithium-ion Batteries (2003)

Characteristic	System target[9]	Current Lithium-ion
Specific power, W/kg, 80 % DOD, 3 sec pulse	400	280[10]
Power density, W/L	600	440
Specific energy, Wh/kg @ C/3	200	100
Energy density, Wh/L @ C/3	300	155
Cycle life, cycles @ 80% DOD	1,000	1,000
Selling price, $/kWh for 40 kWh system @ 100,000/yer	100	Approximately 2–4 times the target value

[8] Roundtrip charge/discharge efficiency.

[9] USABC, "Development of Advanced High-performance Batteries of Electric Vehicle Applications," request for proposal information, October 2000

[10] Battery performance calculated from cell performance by applying a burden factor based on battery design.

Development of Lithium-ion batteries for EV applications was concluded in 2003. Future development of this technology will be focused on 42V applications.

Lithium/Sulphur Battery Development

Lithium/sulfur rechargeable batteries offer several possible advantages over the current Lithium-ion rechargeable cells. Because sulfur is less expensive relative to the lithiated metal oxides used for the cathodes in lithium/ion systems, the lithium/sulfur system has the promise of significantly lowering cost per kilowatt-hour of stored energy. In addition, the use of a metallic lithium anode in these cells may allow for improved specific energy and energy density relative to the lithium/ion system which must use a non-reactive matrix material, such as carbon, for the anode. The complex chemistry of the lithium/sulfur cell may also provide a "shuttle mechanism" that would allow the cell to be overcharged without significant safety problems or other adverse effects. Unfortunately, the lithium/sulfur system is not yet mature enough for these potential advantages to be demonstrated in commercial cells.

The DOE, in conjunction with the USABC, is supporting research and development on this technology through long-term contracts with two industrial firms, SCION of Tuscon, AZ, and PolyPlus of Berkeley, CA. Early phases of these activities will focus on issues at the electrode and cell level and concentrate on finding means to improve the anode-electrolyte interface against parasitic reactions and to improve the cells' cycling efficiency. All contracts have industry cost-share of at least 50%.

Future activities

Over the next year, the Electric Vehicle Battery Research and Development effort will focus on testing and demonstrating the performance of the lithium/sulfur cells against the USABC requirements.

II.B. Technology Assessment

Technology assessments are often conducted in order to validate a developer's technical claims by means of independent testing and to gauge the developer's ability to deliver a full-scale, fully packaged battery. The tests are performed both at the developer's facilities and at the DOE national laboratories in order to familiarize the developer with vehicular requirements and USABC testing procedures. The companies also share in the cost of the testing.

Current assessment tasks include cells based on Lithium-ion gel technology, a Lithium-ion system using a spinel-based chemistry, and a new $LiFePO_4$ cathode active material.

II.C. Benchmarking

Benchmark testing of emerging technologies is important for remaining abreast of the latest industry developments. Working with the national laboratories, OFCVT purchases and independently tests hardware against the manufacturer's specifications and the most applicable technical targets.

For example, although ultracapacitors have demonstrated only about 50% of the energy density needed for HEV applications, OFCVT continues to track advances in this technology. Ultracapacitors obtained from commercial sources are being benchmark tested at the Idaho National Engineering and Environmental Laboratory (INEEL) against the FreedomCAR requirements for a High-Power Energy Storage System. Capacitors currently undergoing test at INEEL are listed in Table II-8.

Table II-8. Capacitors Undergoing Benchmark Testing at INEEL

Manufacturer	Ratings Capacitance (F)/Vmax	Electrodes;electrolyte
CCR Corporation[11] (Japan)	2000 F/2.3 V	Carbon/carbon; Et_4NBF_4 in PC
CCR Corporation (Japan)	3000 F/2.3 V	Carbon/carbon; Et_4NBF_4 in PC
Maxwell Technologies, Inc. (USA)	2700 F/2.7 V	Carbon/carbon; Et_4NBF_4 in CH_3CN
Maxwell/Montena (USA/Switzerland)	2600 F/2.5 V	Carbon/carbon; Et_4NBF_4 in CH_3CN
NESS Corporation (Korea)	2500 F/2.7V	Carbon/carbon; Et_4NBF_4 in CH_3CN
NESS Corporation (Korea)	3500 F/2.7V	Carbon/carbon; Et_4NBF_4 in CH_3CN
NESS Corporation (Korea)	5000 F/2.8V	Carbon/carbon; Et_4NBF_4 in CH_3CN
Panasonic (Japan)	1200 F/2.3V	Carbon/carbon; Et_4NBF_4 in CH_3CN
Panasonic (Japan)	2000 F/2.3V	Carbon/carbon; Et_4NBF_4 in CH_3CN
Panasonic (Japan)	2500 F/2.3V	Carbon/carbon; Et_4NBF_4 in CH_3CN
Saft (France)	3500 F/2.7V	Carbon/carbon; Et_4NBF_4 in CH_3CN
Telcordia Technologies (USA)	450 F/2.8V	Carbon/$Li_4Ti_5O_{12}$;$LiBF_4$ in CH_3CN

II.D. Small Business Innovative Research (SBIR)

The Small Business Innovation Research (SBIR) program was created by the Small Business Innovation Development Act of 1982 (P.L. 97-219) and has been reauthorized again until September 30, 2008. The SBIR program was designed to stimulate technological innovation, strengthen the technological competitiveness of small businesses, and use small businesses to meet Federal research and development needs. DOE's SBIR program budget for FY 2003 was about $94 million, based on a set-aside of 2.5%. These funds were used to support an annual competition for Phase I awards of up to $100,000 each for about 9 months to explore the feasibility of innovative concepts. Phase II research effort represents up to $750,000 over a two-year period.

Over the past several years, SBIR/STTR contracts have provided valuable support to EV and HEV battery development efforts. There are currently in place over $4 million in Phase I and Phase II contracts, focused on development of new battery materials and components.

[11] CCR Corporation has been dissolved and is now Nippon Chemi-Con Corporation

Phase II contract topics (~$750,000 each) active in FY 2003 are listed below:

- ***A123 Systems, Inc.*** – An Advanced Cathode Material for Lithium-ion Batteries
- ***Eltron Research, Inc.*** **–** Novel Lithium Ion Conducting Polymer Electrolytes for Lithium Ion Batteries
- ***Farasis, Inc.*** **–** Stabilized Lithium Manganese Oxide Spinel Cathode for High Power Lithium-ion Batteries
- ***MER Corp.*** **–** Low Cost Carbon Anodes for Lithium-Ion Batteries
- ***Optodot Corp.*** **–** Low-Cost Nanoporous Sol Gel Separators for Lithium-Based Batteries
- ***T/J Technologies, Inc.*** **–** A Novel Cathode Material for High Power Lithium Rechargeable Batteries
- ***TPL, Inc*** **–** Synthesis of New Solid Polymer Electrolytes
- ***Yardney Technical Products, Inc. (Lithion)*** **–** Development of Low-Cost Salts for Lithium-Ion Rechargeable Batteries

The following Phase I Proposals were funded in FY 2003:

- ***Boundless Corp.*** – Nanowire Cathode Material for Lithium-Ion Batteries
- ***MER Corp.*** – High Performance Solid Polymer Electrolyte for Li Batteries
- ***SION Power Corp.*** – Multi-Layer Anode Stabilization Layer for Preventing Dendrites in Lithium Sulfur Batteries
- ***TechDrive, Inc.*** – Highly Conductive Solvent-Free Polymer Electrolytes for Lithium Rechargeable Batteries
- ***TIAX, LLC.*** – $LiFePO_4$ Cathode Material Designed for Use in Lithium-Ion Batteries
- ***TPL, Inc.*** – Preparation of High Performance Nanocomposite Cathode Material
- ***US Nanocorp, Inc.*** – High Energy Density Rechargeable Lithium Sulfur Battery with Novel Solid Electrolyte

Sample Publications/Presentations include the following

- Zolot, M., "Hybrid Energy Storage Studies Using Batteries and Ultracapacitors for Advanced Vehicles," 12th International Seminar on Double Layer Capacitors, Deerfield Beach, FL.
- Vlahinos, A., Kelly, K., Pesaran, A., and Penney, T., "Empowering Engineers to Generate Six-Sigma Quality Designs," First Annual Quality Symposium, American Society for Quality, Automotive Division, Livonia, MI, February 25, 2003.
- Vlahinos, A., Pesaran, A., and Stuart, T., "Cooling and Preheating of Batteries in Hybrid Electric Vehicles," Proceedings of the 6th ASME-JSME Thermal Engineering Joint Conference, Kona, HI, March 16-20, 2003.
- Keyser. M.A., Pesaran, A., Mihalic, M., Yu, J.-S., Kim, S-R., Alamgir, M., and Rivers, D., "Thermal Characterization of Advanced Lithium-Ion Polymer Cells," Proceedings of the Third Advanced Automotive Battery Conference, Nice, France, June 10-12, 2003.
- Markel, T., Zolot, M., Wipke, K.B., and Pesaran, A.A. "Energy Storage System Requirements for Hybrid Fuel Cell Vehicles," Advanced Automotive Battery Conference, Nice, France, June 10-13, 2003.

III. APPLIED BATTERY RESEARCH

III.A. Introduction

Applied Battery Research focuses on high-power battery development in support of the FreedomCAR Partnership's goal of affordable cars and light trucks that will reduce U.S. dependence on foreign petroleum and reduce emissions, yet will not impact its historic mobility and freedom of vehicle choice.

Started in late 1998 as the Advanced Technology Development (ATD) Program, Applied Battery Research focuses on finding solutions to barriers that are impeding U.S. battery manufacturers in their efforts to produce and market high-power batteries for use in hybrid electric vehicles (HEVs). The major challenges are: life, abuse tolerance, and cost. Of these, abuse tolerance is the single most important issue for U.S. automotive manufacturers and all other activities are being pursued with a continual consideration of their impact on the safety of the battery.

Focus

A *Calendar Life* of 15 years is required to meet the California emissions standards. The calendar life of the current generation of lithium-based batteries is approximately 6–10 years, although there are encouraging estimates which place the life very close to 15 years. To address issues associated with the calendar life of high-power batteries, the Applied Battery Research Activity is:

- Developing and validating accelerated life test methods,
- Developing a life-test validation protocol that may be used by battery manufactures and automobile companies to confirm the life of HEV batteries,
- Identifying life-limiting mechanisms
- Evaluating advanced cell components and chemistries that address these life-limiting mechanisms and extend cell life, and
- Modeling and designing battery thermal management systems, since many mechanisms that lead to poor calendar life are enhanced as the temperature increases.

Abuse Tolerance is a primary requirement for a battery in an automotive application. Current high-power batteries are not intrinsically tolerant of abuse such as short circuits, overcharge, overdischarge, mechanical shock, vibration, crush, or fire exposure. In addition, thermal management requirements faced during stressful periods in a driving cycle need to be addressed. Current related research activities include:

- Specifying relevant abuse conditions and desired responses to those conditions, along with developing abuse testing standards,
- Testing and evaluating novel chemistries and cell designs that exhibit enhanced abuse tolerance,
- Developing detection and management controls for battery state-of-charge, battery temperature, and electrical faults, and
- Developing *in situ* overcharge protection.

The current *cost* of high-power lithium-based cells is prohibitively high, but is continuing to decrease. The main cost drivers being addressed are the high cost of raw materials, materials

processing cost, cell and module packaging cost, and failsafe electric and mechanical safety devices. Specific research activities include:

- Evaluating lower cost cell components: electrolytes, anodes, and cathodes,
- Developing low-cost processing methods for producing high-power batteries,
- Working with potential U.S. suppliers to implement low-cost material production, and
- Developing low-cost cell packaging alternatives.

Recently, a new effort to evaluate and improve low temperature performance has begun. An overview of how these focus areas are being addressed in this activity is shown in Figure III-1. Some preliminary results are presented below.

Participants

The Applied Battery Research Activity requires the close coordination of five national laboratories: Argonne National Laboratory (ANL), Brookhaven National Laboratory (BNL), Idaho National Engineering and Environmental Laboratory (INEEL), Lawrence Berkeley National Laboratory (LBNL), and Sandia National Laboratories (SNL). Close communication is maintained with battery developers, automobile manufacturers, and related corporations to ensure that the issues being investigated will be of direct benefit to the U.S. battery manufacturing and automotive communities. To make a significant impact on the cost barriers, contacts with over a dozen battery component vendors have been established. In addition, close ties are maintained with other government organizations involved in battery research through the Interagency Power Working Group. This ensures that relevant technical issues and solutions are disseminated amongst all interested government agencies

This activity has focused its efforts over the past year on testing and diagnosing a second generation chemistry (called Gen 2 throughout this report), detailed in Table III-1. This chemistry was chosen based on issues identified with the Gen 1 chemistry, and based on the HEV battery performance and safety requirements.

The following sections highlight the activities and progress achieved in the Applied Battery Research Effort during FY 2003. The results presented are representative only. Full, detailed, experimental, theoretical, and analytical results are available upon request. The materials for these summaries were provided by the national laboratories, universities, and industrial firms that participated in this exciting work. These organizations are listed in Appendix A of this report.

Table III-1. ATD Gen 2 Cell Chemistry

Characteristic	Values
Size	18650 553 Baseline cells & 651 Variant C cells
Positive Electrode	8 wt% PVdF binder 4 wt% SFG-6 graphite 4 wt% carbon black 84 wt% $LiNi_{0.8}Co_{0.15}Al_{0.05}O_2$ - Baseline 84 wt% $LiNi_{0.8}Co_{0.1}Al_{0.10}O_2$ - Variant C
Negative Electrode	8 wt% PVdF binder 92 wt% MAG-10 graphite
Electrolyte	1.2 M $LiPF_6$ in EC:EMC (3:7 by wt)
Separator	25 mm thick PE (Celgard)

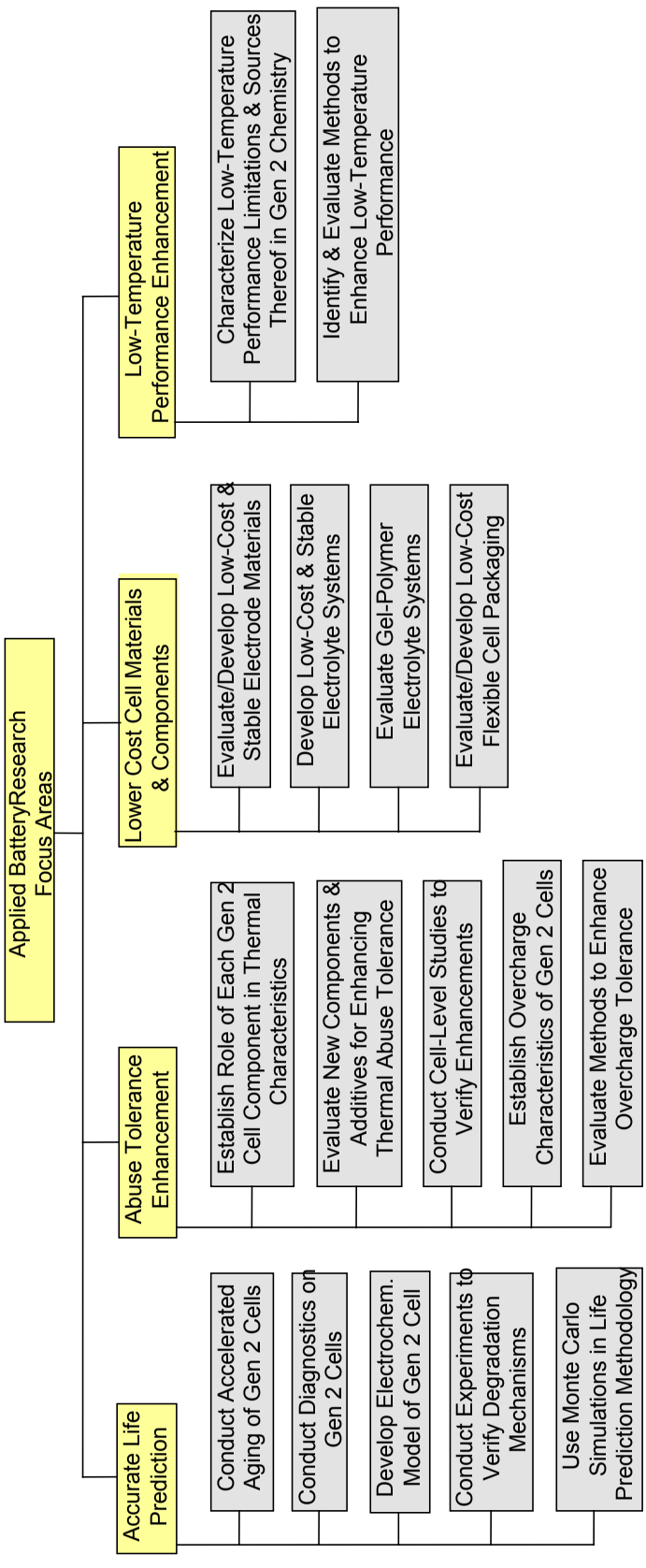

Figure III-1. Applied Battery Research Focus Areas

III.B Calendar and Cycle Life

Objectives

- Age Lithium-ion cells under controlled conditions for diagnostics evaluation, analyze performance.
- Help identify and quantify the factors responsible for power fade through analysis of aged cells.
- Provide analyzed performance data to enable correlations against diagnostic results and facilitate selection of most useful tools.
- Develop aging protocols and explore new tests, analyses, and modeling methodologies related to calendar and cycle life and provide results to battery developers and other laboratories.
- Develop life models and correlations to gain understanding of fade mechanisms.
- Develop accelerated life test (ALT) methodology and ALT manual.

Approach

- Perform independent, but coordinated, performance testing at INEEL, ANL, and SNL using cell-specific test plans.
- Utilize end-of-test criteria to provide diagnostics laboratories aged cells at specified intervals based upon power fade.
- Analyze performance data based upon the *PNGV Battery Test Manual*, Revision 3, to help identify factors that limit cell life.
- Measure the Gen 2 baseline performance and evaluate electrochemistry improvements of the variant chemistry cells.
- Correlate capacity fade, resistance and impedance growth, power fade, and changes in differential capacity against calendar and cycle life.

Accomplishments/Findings

- Completed performance analysis of all available Gen 2 characterization and life-testing data.
- Determined that impedance growth at the cathode boundary appears to be the greatest contributor to power fade.
- Assembled test results from all three test laboratories and identified state-of-charge (SOC), temperature and time dependent trends.
    - Fade increases with temperature.
    - Fade increases with SOC.
    - Fade is generally lowest for the calendar-life cells, in the middle for the cycle-life cells, and highest for the accelerated-life cells at a given test temperature and SOC.
    - Fade begins as a parabolic function of time and changes to a linear time dependence.
- Developed models to explain the impedance growth with time.
- Refined ATD test procedures and coordinated methodologies between participating laboratories.

Future Studies

Power and capacity fade

- Complete life testing and data analyses for the Gen 2 baseline and Variant C cells.
- Develop phenomenological hypotheses to explain performance degradation and power fade.

- Continue to develop predictive models for calendar life and cycle life.

Models & Correlations

- Continue developing and assessing correlations and models to aid diagnostics work and for ALT manual.
- Utilize T-cell experiments to segregate anode and cathode contributions to capacity and power fade.

ALT Manual

- Include cycle-, calendar-, and combined-life tests in the manual.
- Use screening tests to assess stress factor relationships, with stress factors including temperature, SOC, pulse current, and DSOC.

Sample Publications

- **201st ECS meeting, May 12-17, 2002 (Philadelphia, PA):** "Pathway to Understanding Fading Mechanisms in Lithium-Ion Batteries," B. Y. Liaw, R. G. Jungst, E. P. Roth, H. L. Case, D. H. Doughty
- **Surface Changes on $LiNi_{0.8}Co_{0.2}O_2$ Particles During Testing of High-Power Lithium-Ion Cells**, D. P. Abraham, R.D. Twesten, M. Balasubramanian, I. Petrov, J. McBreen, K. Amine, *Electrochem. Commun.* **4**, 620 (2002).
- **Microscopy and Spectroscopy of Lithium Nickel Oxide Based Particles Used in High-Power Lithium-Ion Cells**, D. P. Abraham, R.D. Twesten, M. Balasubramanian, J. Kropf, D. Fischer, J. McBreen, I. Petrov, K. Amine, *J. Electrochem. Soc.,* accepted for publication.
- **Experimental Design and Analysis for Accelerated Degradation Tests with Lithium-ion Cells**, E. V. Thomas, E. P. Roth, D. H. Doughty, and R. G. Jungst, August 2003, Sandia National Laboratories Technical Report, SAND2003-2897.

III.B.1 Introduction

The purpose of the calendar and cycle life testing activities is to enhance the operating life of advanced HEV batteries. Towards that end, researchers are working to identify capacity and power fade mechanisms, refine accelerated life tests, and develop life validation models applicable to a wide range of advanced chemistries. The national laboratories contributing to life testing and analysis, and their primary responsibilities, are:

- ANL: Calendar-life testing and life modeling
- LBNL: Calendar and cycle life diagnostics
- INEEL: Cycle-life testing and life modeling
- SNL: Accelerated-life testing and life modeling

The specific researchers who contributed materials for this section and for the other sections of this report are listed in Appendix A.

The Applied Battery Research activity has made tremendous progress over the past year in understanding the sources and causes of power and capacity fade in Gen 2 baseline cells. This is, perhaps, the first time such a comprehensive analysis of a battery chemistry has been undertaken with such an aim.

III.B.2 Status

A summary of the cells that have been and are being tested at various states of charge (SOC) and temperature is shown in Table III-2. Note that the baseline and Variant C chemistries are specified in Table III-1, page 18.

Table III-2. Test cell matrix

	Temp. (°C)	Chemistry		
		Baseline		Variant C
Calendar Life (60% SOC only)	45 55	2 15		10
Cycle Life (60% SOC only)	25 45	15 15		14
		State of Charge		
		60%	80%	100%
Accelerated Life (Baseline only)	25 35 45 55	3 3 3 3	3 3 3 5	3 3 5 5

Aging of Gen 2 cells is largely completed. During 2003, an interim evaluation report and draft ALT protocol report have been issued and are available upon request. In 2004, the cycle and calendar life teams will complete work on an ALT verification manual which will be provided to battery and automobile manufacturers as a tool to determine if a battery has been adequately tested to ensure that it will meet life requirements.

III.B.3 Sample Experimental Results

A large number of experiments have been used to characterize and diagnose the cycle and calendar life of Gen 2 cells. In particular, researchers are using techniques such as AFM, EDX, EIS, GC, IR, NMR, Raman, SIMS, TEM, XRD, XPS, and soft x-ray XAS and XRD. Appendix B contains a complete list of acronyms.

Researchers used these and other techniques to measure cell characteristics such as Area Specific Impedance (ASI), Discharge ASI Growth, Useable Energy, Available Power, Discharge Power at various SOC, Available-Power Fade, and Power Fade vs. Discharge ASI Growth
This section presents a representative sample of experimental and theoretical results, and illustrates how those results were used to reach the conclusions presented in this section.

III.B.3.1 Power and Capacity Fade

A plot of power and C/1 capacity fade as a function of the logarithm of test time is shown in Figure III-2 and Figure III-3, respectively, for both baseline and Var C cells. The most intriguing features in these figures are the two distinct slopes in the curves for the baseline cells. This feature suggests that the degradation process follows two different stages with different time dependences. (This two-function behavior is not yet seen in the Variant C cells.)

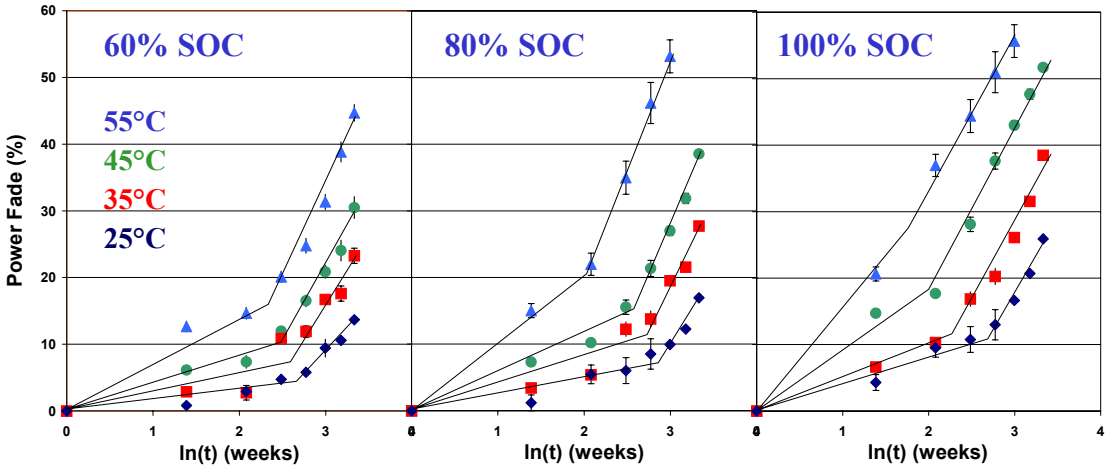

Figure III-2. Power Fade of Gen 2 Baseline Cells

The amount of actual fade averaged over cells tested under the same condition was then plotted against the reciprocal temperature (at which they were aged). A sample plot of the logarithm of power capability loss (PCL) is shown in Figure III-4 for 80% SOC. Note that the slope of each curve in Figure III-4 represents the activation energy of the power fade at each stage.

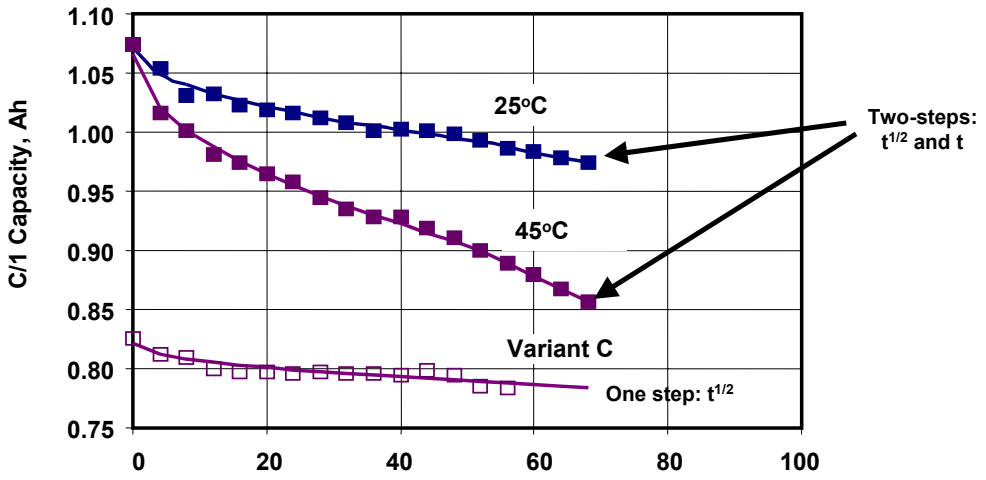

Figure III-3. Capacity Fade of Gen 2 Baseline and Variant C Cells

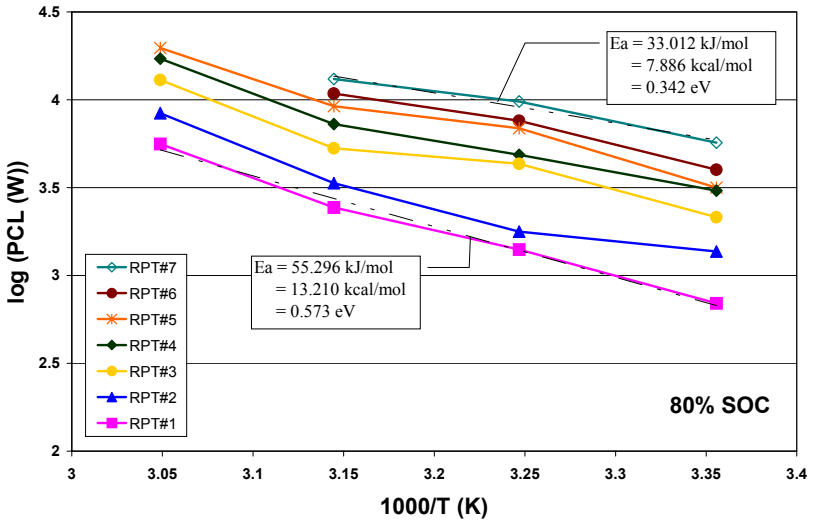

Figure III-4 Arrhenius plot of power fade versus reciprocal temperature for cells aged at 80% SOC

There are several features in Figure III-4, and in related plots for 60% and 100% SOC, that are noteworthy.

1) In the beginning of aging, the cells aged at 100% SOC at higher temperatures (35 to 55°C) seemed to conform to the same degradation mechanism, while the 25°C data deviated. The cells aged at 80% and 60% SOC did not reflect that trend, and four data points at different temperatures seem to conform to a single mechanism.
2) The activation energies representing the first stage are in the order of 51.5 kJ/mol at 100% SOC, 55.3 kJ/mol at 80% SOC, to 58.9 kJ/mol at 60% SOC (not shown).
3) As aging progresses, the slopes of the Arrhenius curves begin to shift. The trend at 100% SOC seems to conform to one mechanism at the second stage, where the slope of the Arrhenius curve becomes shallower and the activation energy is lower than that of the first stage, in the order of 25.1 kJ/mol.

The same trend seems to be followed in 80% and 60% SOC as well. The activation energy at the second stage is 33.0 and 28.9 kJ/mol for 80% and 60% SOC, respectively.

Following these intriguing results, the changes in power capability, rate capacity, and impedance were analyzed and correlations among these properties were investigated. It has been found that all these behaviors follow a similar Arrhenius behavior with activation energies of approximately 50 kJ/mol in the initial aging stage. *The correlation suggests that the power and capacity fades are related to the cells' impedance changes.*

The associated Arrhenius plots for both C/1 and C/25 were investigated and plotted. Observations can be summarized as follows:

1) The Arrhenius behaviors for C/1 and C/25 seem to be different in nature. Up to 12 weeks, the activation energy of the first stage C/1 capacity fade varies from 56.8 kJ/mol to about

37.5 kJ/mol at 12 weeks. In the second stage, the activation energy varies in the range of 37-50 kJ/mol with a mean value of approximately 45 kJ/mol.

2) A different trend is seen in the C/25 capacity fade. Although a trace of the two-stage degradation is observed, the activation energy varies only slightly between 27 and 36 kJ/mol. This value is similar to the one in the second stage of power fade.

The impedance changes for a cell aged for 12 weeks at 100% SOC were also analyzed. The interfacial and total cell impedance activation energies are 53.6 kJ/mol and 52.0 kJ/mol, respectively.

Since only two randomly selected cells were picked as examples for illustrating the Arrhenius behavior of the impedance changes, their behavior might not be representative. Additional analysis will be performed to verify their correlation with the general trends observed in the power and capacity fades.

Finally, microcalorimetry results have been obtained from two unaged cells at 80% SOC. The static heat generation rates from the cells were measured in the microcalorimeter at five different temperatures from 25°C to 65°C. The resulting heat output shows an Arrhenius behavior with an activation energy ranging from 48.0 kJ/mol to 61.8 kJ/mol. These values give a mean activation energy of 54.9 kJ/mol, which is surprisingly similar to the activation energy observed in the first stage of degradation for power and C/1 capacity fade.

Additional conclusions associated with cell power and capacity fade are:

- The capacity fades (C/1 and C/25) generally show the same trends as the ASI growth, EIS growth, and power fade.
- Power degradation correlates with interfacial impedance changes in the cell, primarily from the cathode, independent of aging temperature and time.
- The correlation among activation energies derived from power fade, capacity fades, and impedance changes in aged cells, and microcalorimetry data from unaged cells, suggests:
    - In the 1st stage, the activation energy from power fade, C/1 capacity fade, impedance growth, and microcalorimetry are very similar, suggesting that they might come from the same origin.
- The activation energies derived from power fade and C/1 capacity fade follow a similar trend, suggesting that the source of degradation in the second stage for power and C/1 capacity fade might be related.
- Statistical analysis of the power fade indicates three distinct phases:
    - Phase 1 (to 4 weeks): temperature accelerates *mechanism 1*, 100% SOC is inconsistent with 60% and 80% SOC, time dependence is unknown
    - Phase 2 (to 40% power fade): temperature and SOC accelerate *mechanism 2* at *predictable rates* for a large portion of temperature/SOC space, $t^{3/2}$ dependence
    - Late phase (beyond 40% power fade): not clear, relevance not clear.

This statistical analysis also resulted in a recommendation to schedule RPTs uniformly in log(time) to provides more frequent RPTs relatively early in time.

A summary of the findings associated with each of the major battery components follows:

- **Al current collector -** Not affected by aging
- **PVdF binder -** No obvious degradation
- **Carbons (anode) -** Bulk carbon content unaffected, carbon-black agglomeration possible, graphite not damaged during aging
- **Oxide (cathode) -** Bulk property variations observed**,** surface films change on aging.

A preponderance of experimental data shows that the power fade in Gen 2 cells originates at the cathode. In addition, an increase in interfacial resistance appears to mirror the increase in power fade very closely. A sample of those results is presented below.

EIS Measurements. 3-electrode impedance measurements have been performed on the cathode and anode electrodes in round cells (~1" diameter). This data indicates that the impedance of the aged cathode is significantly higher than that of the aged anode. This observation is consistent with those reported by Delphi (Abstract # 358 and 359) and NTT (Abstract # 363) at the 11th IMLB meeting (June 23-28, 2002, Monterey, CA).

X-ray Diffraction Studies on Cathodes Harvested from Various Cells. X-ray diffraction studies were conducted on cathode laminates extracted from cells that were previously discharged to ~3.1V. Figure III-5 shows the c-lattice parameter that was calculated for the oxide and graphite particles. The c-parameter of the oxide particles from the 0% PF cell is greater than that of the fresh Gen 2 cathode. This data indicates that the 0% PF sample contains less lithium, which is expected because the cell formation cycle consumes lithium to form the SEI layer. The data further shows that the c-parameter is greater for the aged cells, which indicates that lithium is consumed during aging, and is consistent with the lower capacities of the aged cells.

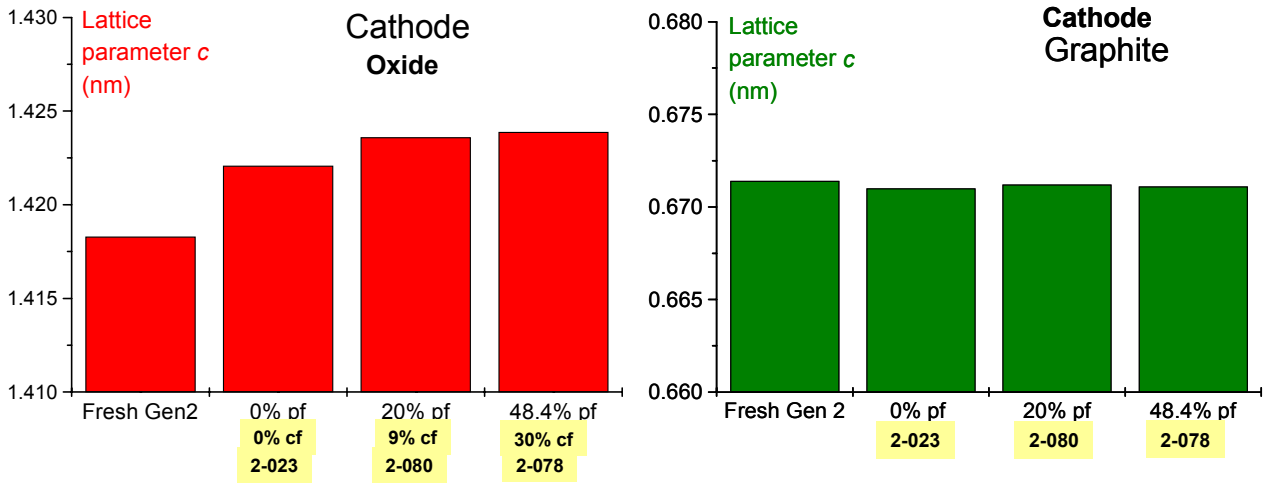

Figure III-5. X-ray diffraction data from the oxide and graphite of Gen 2 dells. The fresh laminate was not exposed to any electrolyte

A number of additional tests also show that the positive electrode is the major contributor to impedance rise. Lab-scale cell reference electrode impedance data is shown in Figure III-6. Similarly, HPPC tests, as shown in Figure III-7, provide complementary information showing that impedance rise is mainly associated with the positive electrode.

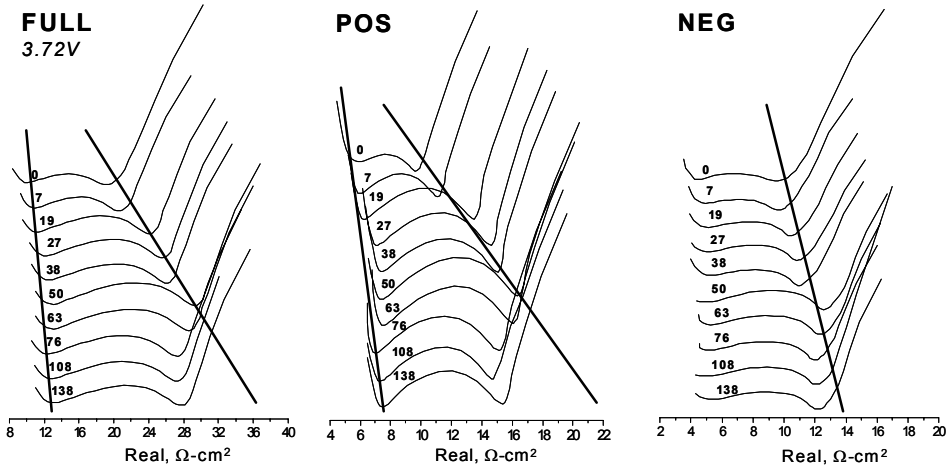

Figure III-6. Impedance of the full Gen 2 cell, and the positive and negative electrodes

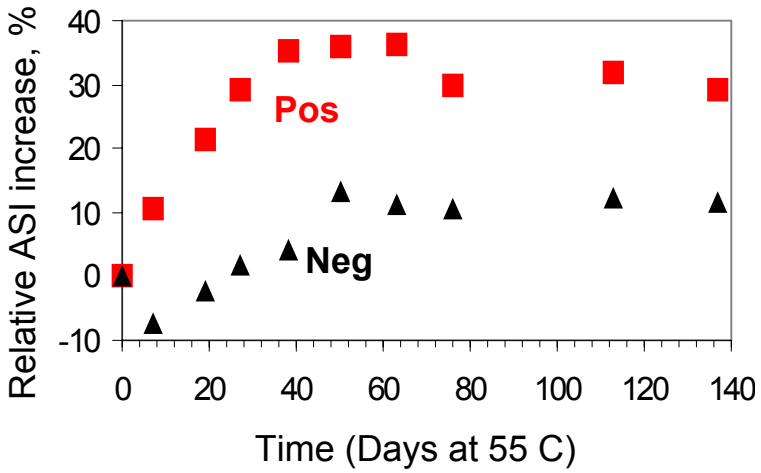

Figure III-7. ASI data suggests that the positive electrode impedance increase arises from the oxide.

.

III.B.3.2 Capacity and Power Loss Interpretation

However, the interpretation of this data, that is, identification of the cause of the impedance rise, is still under investigation. The following discussion provides a sampling of the experimental results related to this search.

Capacity data from all cathodes from the 55°C and 45°C cells are shown in Figure III-8. The data clearly indicate that the capacities of the aged cathodes are lower than that of the cathode from the control (0% CF) cell. This capacity loss could result from several effects, including:

- Oxide particle isolation, which may result from (a) breakup of secondary particles into fragments that are not in contact with the conductive carbon, (b) partially insulating films on the oxide surface, and (c) retreat of carbon away from the main particles.
- Oxide particle damage, which may include (a) changes in the layering structure of the particle bulk, and (b) changes in the ionic conductivity of the $Li_xNi_{1-x}O$-type layer on the oxide surface that may result from variations in Li content.

Normalizing for the capacity variations of the different cells indicates that the average thermodynamic voltage is lower for cells prepared with the aged cathode, which may result from variations in or on the oxide particles.

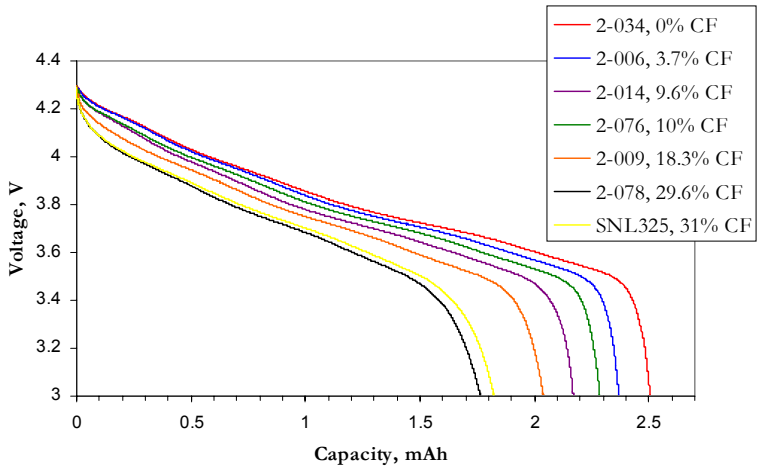

Figure III-8. Capacity data from coin cells with cathodes (vs Li) harvested from 18650-cells.

The capacity data from half cells with anodes harvested from the 55°C and 45°C cells are shown in Figure III-9. Although the cells with the aged anodes appeared to show capacity degradation, the behavior is not consistent. For example, the 10% capacity fade anode half-cell shows a capacity of ~3.04 mAh, which was larger than that measured for the 10% capacity fade cell.

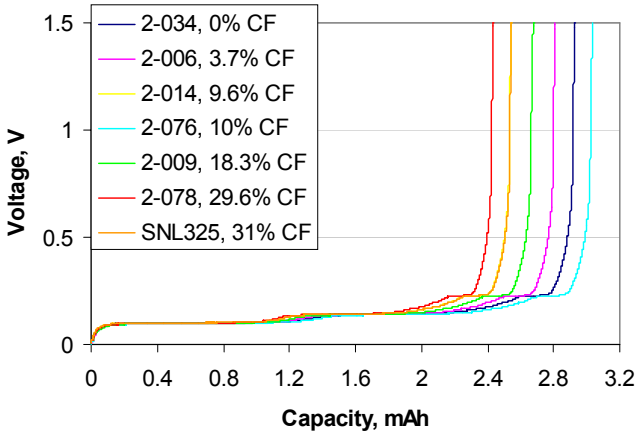

Figure III-9. Capacity data from coin cells with anodes (vs Li) harvested from 18650-cells.

Raman microscopy of cathodes. In prior reports and meetings, color-coded Raman microscopy of Gen 2 cathode and anode surfaces indicated a loss of carbon at the cathode surface following aging, specifically cell storage and cycling at elevated temperatures. Recently, a Raman micro-analysis of the cross-sections of cathode samples (Figure III-10) has been performed from a cycled cell and compared with the results with a fresh Gen 2 cathode. The results were consistent with earlier observations and indicate that changes in the bulk (*i.e.*, sub-surface) cathode/elemental-carbon concentration ratio accompanied cell aging. No clear carbon distribution pattern was observed across the electrode thickness. However, the extent of carbon retreat observed at the cathode surface was greater than in the bulk electrode.

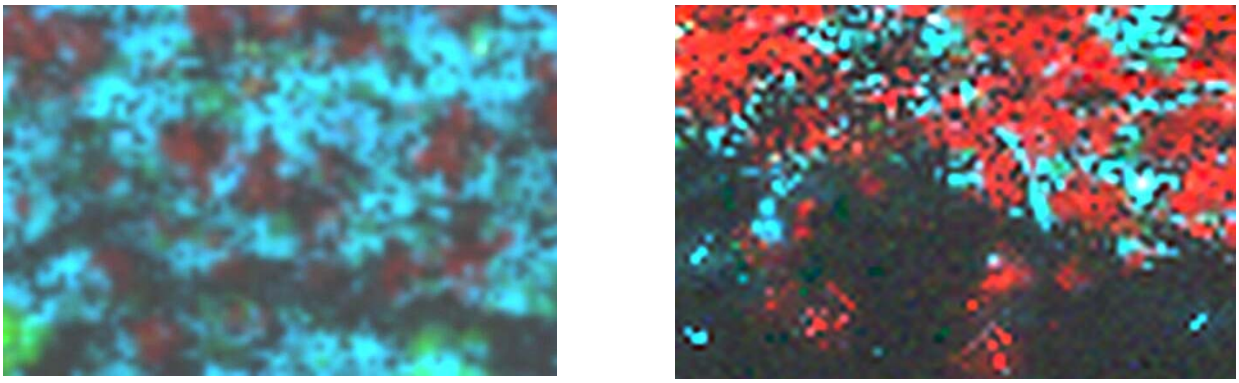

Figure III-10. Raman microscopy images of the cross-section of a fresh Gen-2 cathode (left-hand panel), and the cathode with 52% power fade (right-hand panel). The current collector is at the lower edges of the images and the separator is at the upper edge of the images.

From earlier diagnostic tests, it was determined that non-uniform intrinsic electronic properties of the cathode particles combined with carbon recession or rearrangement can provide a consistent scenario of power and capacity degradation. The reductions may be due to reduced electronic access to the oxide active material. It should also be noted, however, that there is currently no evidence that carbon is being "lost," from the cathode, see Figure III-11.

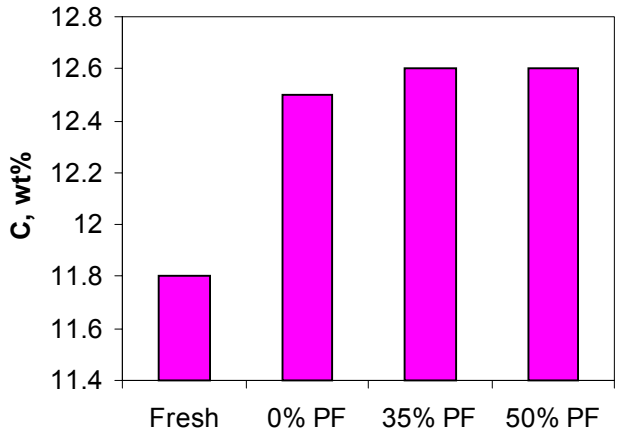

Figure III-11. Total carbon percent as a function of power fade

TEM/EDX Surface layer formed on cathodes following air exposure. Cathode materials with high Ni content are susceptible to oxidative delithiation by atmospheric oxygen and CO_2 to form Li_2CO_3.[12] Recent work in the Long-Term Research activity has shown that Gen 2 electrodes with Li_2CO_3 accumulations exhibit a high impedance. Evidence for particle isolation in these electrodes comes from XRD patterns showing the presence of both charged and discharged cathode particles at the end of charge. Because a similar mechanism (accumulation of solid phases with low electronic and/or ionic conductivity) may be a significant contributor to cell power fade, it is useful to study the morphology and distribution of these Li_2CO_3 deposits.

A small sample of the cathode from a cell exposed to air for one year was examined by TEM/EDX, and the results were compared with those from an unexposed sample obtained shortly after receipt of the cell. In the TEM image (Figure III-12a) of the fresh material, no surface layer is visible, whereas on the exposed grains (Figure III-12b) a layer varying in thickness from a few nm to more than 100 nm is evident. EDX analysis shows that this layer contains large quantities of carbon, oxygen, fluorine, and phosphorus. The spectrum from the center of the grain shows only the cathode active material. It is clear that the deposit (shown by XRD to be primarily Li_2CO_3) covers the oxide surface in a conformal manner, rather than appearing as segregated particles. Although no solid layer is evident in fresh, DMC-washed, samples of Gen 2 cathodes with high power fade, such a layer may be too thin to be observed and/or removed by washing.

[12] K. Matsumoto, R. Kuzuo, T. Kaname, A. Yamanaka, *J. Power Sources*, **81**, 558 (1999).

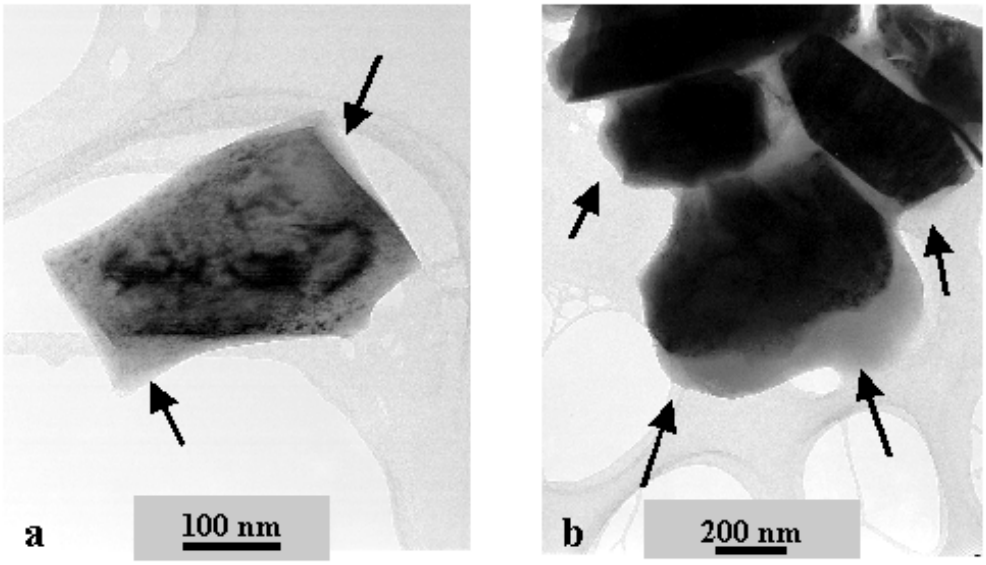

Figure III-12. TEM images of a) unexposed and b) air-exposed $LiNi_{0.8}Co_{0.15}Al_{0.05}O_2$ cathode grains.

XRD studies of thermal decomposition of cathodes from charged cells. High resolution XRD was used to observe effects associated with thermal decomposition of charged $Li_{1-x}Ni_{0.8}Co_{0.15}Al_{0.05}O_2$ at low temperatures. Figure III-13 and Figure III-14. show high resolution XRD patterns for $Li_{0.33}Ni_{0.8}Co_{0.15}Al_{0.05}O_2$ (100% SOC nominal) in the absence and presence of electrolyte, respectively. In the absence of electrolyte, no changes are seen until about 200ºC. In the presence of the electrolyte, decomposition reactions are observed at a temperature as low as 135ºC.

Time resolved XRD measurements were also taken on uncharged electrodes and on electrodes charged to 5.2 V. Complete XRD spectra for the thermal decomposition of a cathode that was charged to 5.2 V in the presence of excess electrolyte show decomposition reactions for the cathode material at temperatures as low as 150ºC. At ambient temperature the graphite peak cannot be seen, perhaps due to the intercalation of PF_6^- into the graphite in the cathode. At 140ºC, the intercalation compound appears to decompose and the graphite peak appears. In the case of uncharged cathodes with excess electrolyte, decomposition reactions do not begin until approximately 300˚C.

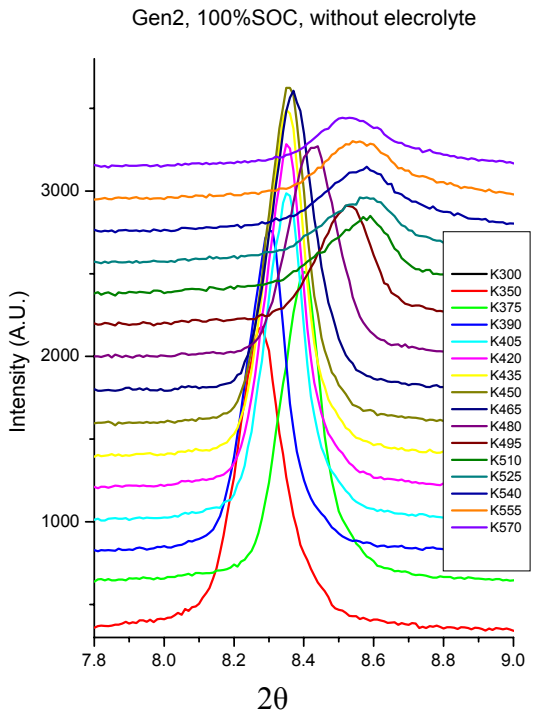

Figure III-13. High resolution XRD patterns in the vicinity of the (003) peak during the decomposition of $Li_{033}Ni_{0.8}Co_{0.15}Al_{0.05}O_2$ that had been washed and dried.

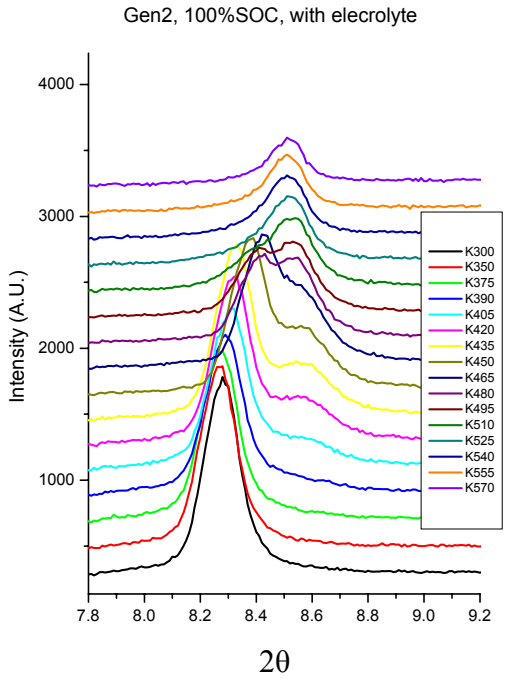

Figure III-14. High resolution XRD patterns in the vicinity of the (003) peak during the decomposition of $Li_{033}Ni_{0.8}Co_{0.15}Al_{0.05}O_2$ in the presence of excess electrolyte.

XPS Study of Gen 2 Cathodes. XPS data from Gen 2 cathodes with various levels of power fade indicate that the cathode surface films change on cell aging; furthermore, a clear correlation with cell power fade is observed. Recently, researchers presented spectra from cathode samples that were rinsed in DMC in an N_2 glove-box. The spectra were collected using XPS under ultra-high vacuum conditions. The data from these measurements are shown in Figure III-15. Data from a fresh sample that indicate locations of the graphite, PVdF binder and oxide peaks are shown for comparison.

The intensities of the graphite peaks are lower for the high power fade samples. However, because analysis shows that the total content of carbon was unchanged, the lower graphite peak intensity indicated that the graphite may be covered by a surface film/layer. The intensity of the PVdF binder peak also decreases with aging, which indicates coverage by a surface film.

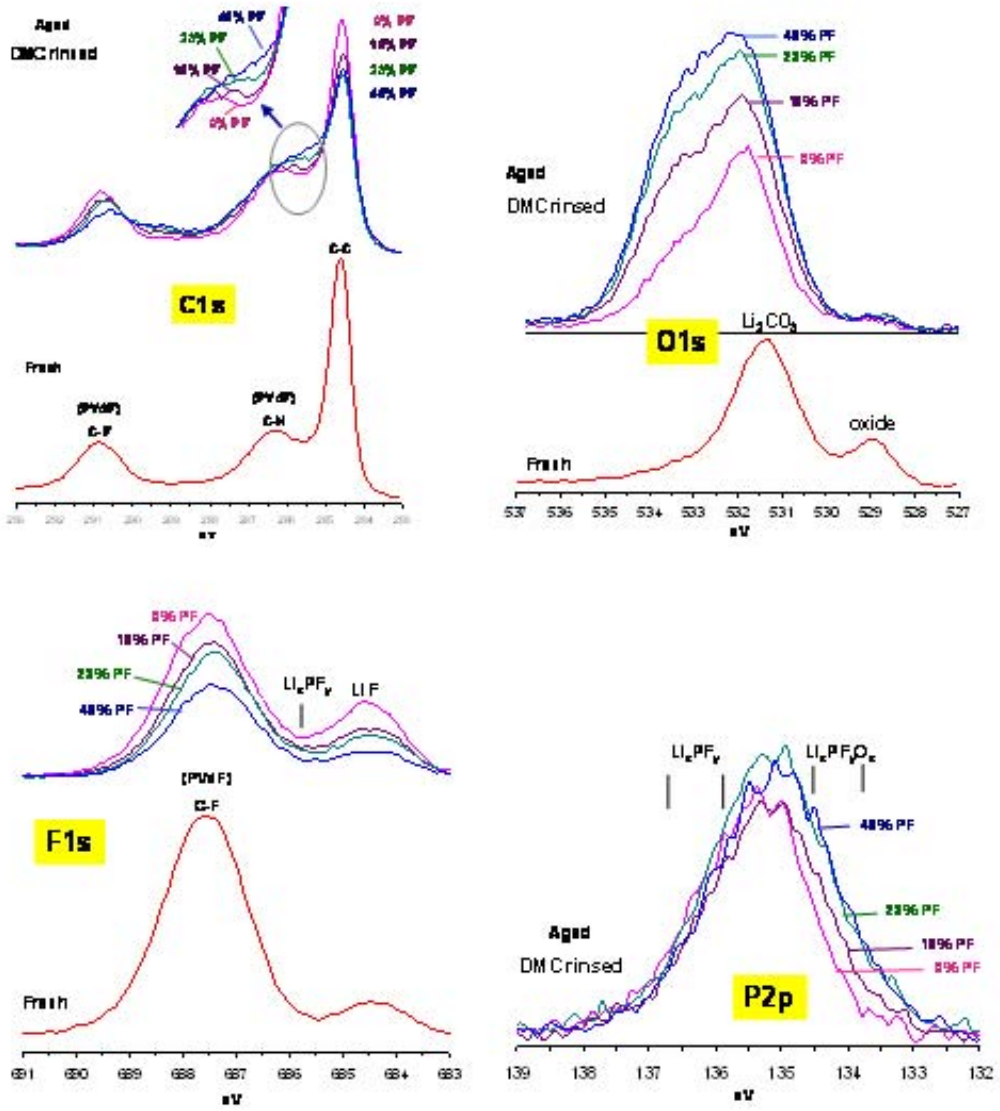

Figure III-15. C1s, O1s, F1s and P2p XPS data from DMC-rinsed cathode samples from cells that showed from 0% to 48% power fade

The O1s spectra show a clear and consistent intensity increase on aging. Because the original oxide peak is not visible, it is clear that the oxide is covered by a surface film. Li_2CO_3, which is known to be a contaminant of the original oxide surface, is not present. Experiments have shown that Li_2CO_3 reacts with the Gen 2 electrolyte, evolving CO_2.

Li_xPF_y is present in the film even after DMC rinsing. Because $LiPF_6$ would be soluble in DMC, its presence indicates that Li_xPF_y is an integral component of the cathode surface film. The intensity increases with sample age, indicating that the surface film is enriched on aging. The species may play an important role in cathode impedance increase because an increasing quantity of it in the surface film would enhance its resistance to lithium ion migration.

III.B.4 Cell Transport and Electrolyte Model Development

There are two modeling efforts ongoing. The first is aimed at examining the impedance rise in Gen 2 cells (see Section III.B.4.1). The second aims to determine the optimum solvent/salt combination to optimize electrolyte conductivity over a given temperature range (see Section III.B.4.2).

III.B.4.1 Modeling of Cell Impedance and Capacity Fade

The goal of this modeling effort is to associate changes that are seen in the post-test diagnostic studies with the loss of electrochemical performance as measured by the HPPC tests. While both electrodes are being modeled, special emphasis has been placed on the positive electrode because experimental evidence indicates that it is responsible for the majority of the impedance rise in the Gen 2 cells.

An electrochemical model capable of simulating the Gen 2 positive electrode under HPPC tests has been developed. The methodology for this electrochemical model follows the work of Prof. John Newman at Berkeley. Concentrated solution theory is used to describe salt transport through the electrolyte, and volume averaged transport equations account for the composite electrode geometry.

The model contains all the phenomena included in the previously developed AC impedance electrochemical model for the positive electrode, with 35 parameters: 18 were set by cell construction, obtained from literature, or estimated; seven were measured independently of reference electrode cell measurements, including electrolyte transport and thermodynamic information; and 10 were obtained by fitting impedance results from reference electrode cell measurements

Reasonable agreement was obtained between the simulations and experiment using the initial parameter values which were determined from HPPC tests. That is, all parameters were originally determined based on other measurements or on physical reasonableness. The agreement was improved by adjusting one of the bulk diffusion parameters and one of the parameters associated with the interfacial phenomena. This adjustment was somewhat arbitrary in that multiple parameters could have been adjusted to improve the fit, and indeed it is likely that several of the parameters are off slightly rather than just one or two. Figure III-16 shows a simulation of the positive electrode HPPC test after adjusting two parameters.

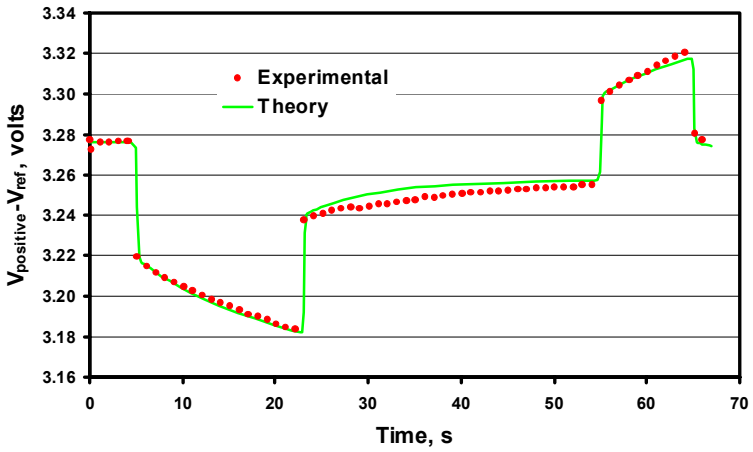

Figure III-16. Simulation of the Positive Electrode HPPC Test after Adjusting Two Parameters

The HPPC electrochemical model was used to examine ways of reducing the positive electrode impedance or at least slow the growth in impedance. Increasing the electrode thickness is one such method that is both simple and effective. Simulations indicate that the positive electrode impedance decreases dramatically with electrode thickness, as shown in Figure III-17. This improvement in performance essentially results from an increase in the electrochemically active area. Another advantage of increasing the electrode thickness is that the electrode has more area available for the current to spread into, thus reducing the impact of increasing interfacial impedance on the overall electrode impedance. However, the current density and the path length also increase with electrode thickness, which would lead to transport problems for very thick electrodes.

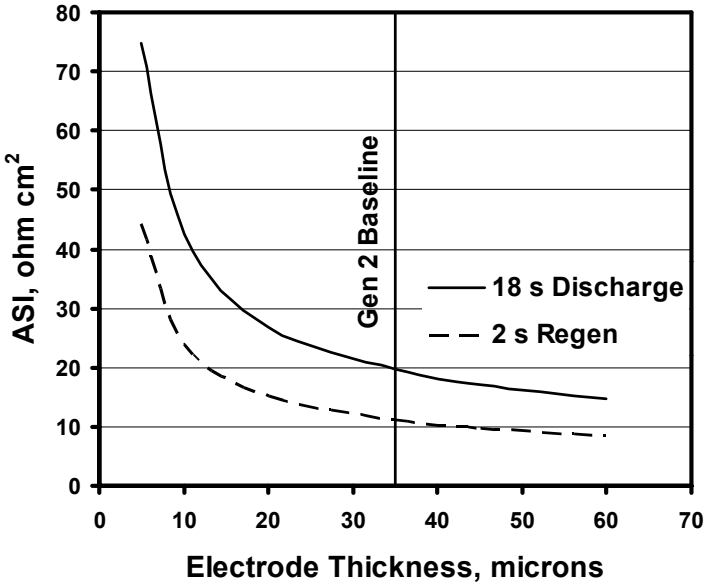

Figure III-17. Positive electrode HPPC impedance as a function of electrode thickness

The HPPC electrochemical model is now being used to study aging effects in the positive electrode. The impedance rise associated with the known capacity fade of the positive electrode has been determined, assuming that the capacity fade is caused by isolation of active particles. The results from these simulations are in agreement with the AC impedance calculations conducted earlier and it is found that the capacity fade can only account for a fraction of the impedance rise.
Some combination of three sources are responsible the observed impedance increase in 18650 cells:

- Changes in the electrolyte/oxide interfacial structure and/or properties,
- Loss of positive electrode capacity, particularly isolation of the oxide particles, and/or
- Loss of electronic conductivity between the carbon and oxide.

III.B.4.2 Electrolyte Modeling

As mentioned above, the second modeling effort aims to determine the optimum solvent/salt combination to optimize the electrolyte conductivity over a given temperature range. Over the past year, this model has been expanded to handle more complicated electrolytes with multiple solvents and salts. Currently the model can accommodate up to 10 solvents per electrolyte mixture, has been successfully tested on ternary and quaternary solvent systems, and has proved useful for temperatures ranging from -60 to 80°C.

The solvents and salts that have had their properties entered into the model, and are therefore available for modeling, are shown in Table III-3.

Table III-3. Components in library

Solvent	Salt
Propylene carbonate (PC)	$LiClO_4$
Ethylene carbonate (EC)	$LiPF_6$
Gamma-butyrolactone (γBL)	$LiBF_4$
1,2 dimethoxyethane (DME)	LiBoB
ethylmethyl carbonate (EMC)	LiCl
diethyl carbonate (DEC)	LiBr
dimethyl carbonate (DMC)	
ethyl acetate (EA)	
ethylene glycol (EG)	
water	

The model has been validated for the multi-solvent systems EC-DEC-DMC-$LiPF_6$, and EC-DEC-DMC-EA- $LiPF_6$. The model results indicate that the PC-EA (3:7)-LiBOB system is superior to EC-EMC (3:7)-$LiPF_6$ due to a number of considerations:

- lower viscosity
- smaller solvated diameters for Li+
- higher transference numbers for Li+
- higher Li+ diffusivity

Therefore, the PC-EA-LiBOB system could be better suited for high power applications where cells do not undergo prolonged storage.

With these results, a solvent composition of EC-DMC-γBL-EA-LiBOB of 2:1:1:6, 1:1:3:5, or 0.5:1.5:4:4 (mass basis) could produce acceptable electrolyte performance over the entire ranges of temperature of interest.

III.B.5 Influence of Experimental Uncertainty

One of the general concerns associated with experimental work is the uncertainty associated with the results. Error bars, although available, are often not included on individual plots as they may mask the result being presented. Recently, the Applied Battery Research Teams evaluated the experimental uncertainty associated with both capacity and power fades. Their results are presented in Table III-4. Important points associated with these results are:

- Uncertainty values are for one standard deviation.
- Capacity fade is a measured parameter. The uncertainty is tied to calibration drift of test equipment which is based on the manufacturer's specifications (0.02% of full scale).
- Power fade is a derived parameter. The uncertainty assumes that the parameters upon which this depends are independent.

Table III-4. Uncertainty in Capacity and Power Fade

	Temp (^{o}C)	Time (Weeks)	Capacity Fade (%)	**Capacity Fade Uncertainty (%)**	Available Power Fade (%)	**Power Fade Uncertainty (%)**
Baseline	25	76	13.8	±**0.22**	29.8	±**1.65**
	45	68	30.1	±**0.17**	50.1	±**1.50**
Variant C	45	56	5.4	±**0.30**	33.5	±**1.65**

It is seen that the uncertainty is relatively small, and is not a strong function of capacity or power fade.

III.C Abuse Tolerance

Goals and objectives

- Determine response of cells to thermal abuse and overcharge.
- Investigate advanced chemistries to overcome abuse tolerance issues.
- Show relationship between abuse tolerance and chemistry, develop physical understanding through advanced diagnostics.
- Support hypotheses through chemical modeling.

Major Accomplishments

- Three temperature regimes during thermal runaway have been identified**:**
  - Room Temperature to 125°C – Onset of thermal runaway occurs at the anode
  - 125°C - 180°C – Venting and accelerated heating (cathode and anode participate)
  - 180°C and above – Explosive decomposition (cathode followed by anode reaction)
- Identified the major source and mechanism of gas and heat generation, EMC produces gas, EC produces heat. "Ring Opened" EC results in EMC decomposition and increased gas generation.
- Achieved increased thermal abuse tolerance through improvements in electrolyte salt, electrolyte additives and anode carbon. LiBETI salt shows improved heat and gas generation performance.
- Quantitatively characterized cell response to overcharge by identifying regions of heat and gas generation that trigger thermal runaway:
  - Cell heat generation increases at 125% SOC at all charging rates, indicating departure from normal cell electrochemical operation
  - Overcharge limited by separator melt at low power supply potentials
  - High thermal impulse at separator melt can result in thermal runaway
  - Cell heating during overcharge studies is non-ohmic, i.e. heat output does not increase with square of current, electrochemistry is contributing to the heat output
  - Low-rate charging can result in a more unstable cell
- Demonstrated new diagnostic approach at BNL, characterized high-temperature cathode degradation reactions.
- Developed new 18650 test cell build capability to study thermal abuse.
- Cycling and abuse testing causes the precipitation of LiF and P species from $LiPF_6$ decomposition on both cathode and anode.

Future Studies

- Quantitatively determine effect of additives and new materials on thermal abuse response of cell components and full cells.
- Investigate new solvent/salt combinations that may lead to increased thermal stability and reduced gas generation.
- Apply advanced diagnostic techniques to determine thermal decomposition products and mechanisms.
- Model cell thermal response with measured cell component thermophysical parameters.

Sample Publications

- **40th Power Sources Meeting**, June 10-13, 2002 (Cherry Hill, NJ):
  - "Thermal Runaway and Gas Generation in Li-ion Cells", E. Roth, C. Crafts.
  - "Correlation of Impedance Increase with Electrical Performance Degradation of Li-Ion Cells", G. Nagasubramanian,
  - "Lithium-Ion Cell Accelerated Aging and Life Prediction", R. G. Jungst, D. H. Doughty, B.Y. Liaw, G. Nagasubramanian, H. L. Case and E. V. Thomas.
- **IMLB 11**, June 23-28, 2002 (Monterey, CA):
  - "Thermal and Gas Generating Reactions in Li-ion Cells Under Thermal Abuse Conditions", E. P. Roth, C.C. Crafts, D. H. Doughty.
  - "Accelerated Calendar and Pulse Life Analysis of Li-Ion Cells", R. Jungst, G. Nagasubramanian, H. Case, B. Y. Liaw, A. Urbina, T. Paez, and D. Doughty.
  - "Correlation of Arrhenius Behaviors in Power and Capacity Fades with Cell Impedance and Heat Generation in Cylindrical Lithium-Ion Cells", E. P. Roth, B. Y. Liaw, R. Jungst, G. Nagasubramanian, H. Case, and D.H. Doughty.
  - "Study of Phase Diagram in Li1-XCoO2 and Li1-XNiO2 Cathode Materials", B.Y. Liaw, X.Q. Yang, J. McBreen and D. H. Doughty.

III.C.1 Introduction

The purpose of the abuse tolerance research is to investigate the abuse tolerance of existing cells, understand the causes of poor abuse tolerance, and investigate and test abuse tolerance mitigation approaches including additives, new or modified materials, or other approaches. The use of high-power Lithium-ion cells in hybrid electric vehicles is predicated on both the electrical performance of the cells and their inherent safety under normal and abusive conditions. The thermal response of the cells is determined by the intrinsic thermal reactivity of its components and the thermal interactions in the full cell. Calorimetric techniques such as Accelerating Rate Calorimetry (ARC) and Differential Scanning Rate Calorimetry (DSC) were used to measure these and other thermophysical properties.

III.C.2 Abuse Tolerance Experimental Results

III.C.2.1 Thermal Response of Heated Cells with and without Additives

ARC measurements are being used to determine thermal runaway profiles, and the volume and composition of evolved gases. Cells are heated to a temperature just below the vent temperature and are then punctured and the gas analyzed directly by the GC system. Figure III-18 shows sample ARC data for the Gen 2 baseline cell.

Work to determine the relative effects of improved anode carbon and additives on heat and gas generation is continuing. The 100 mAh prismatic cells that are being used in these tests were defined by this activity and built at Quallion. The cells have either the standard Gen 2 MAG10 carbon or the GDR carbon which has been shown to have more stable thermal properties. The electrolyte includes the Gen 2 EC:EMC based material as well as an electrolyte with VEC and TPP additives, which have been shown by this activity to reduce the thermal output of the cells under

abusive conditions. Cells with an EC:PC:EMC + 2% VEC electrolyte were also measured. Table III-5 lists the cell compositions, those shown in green have undergone test.

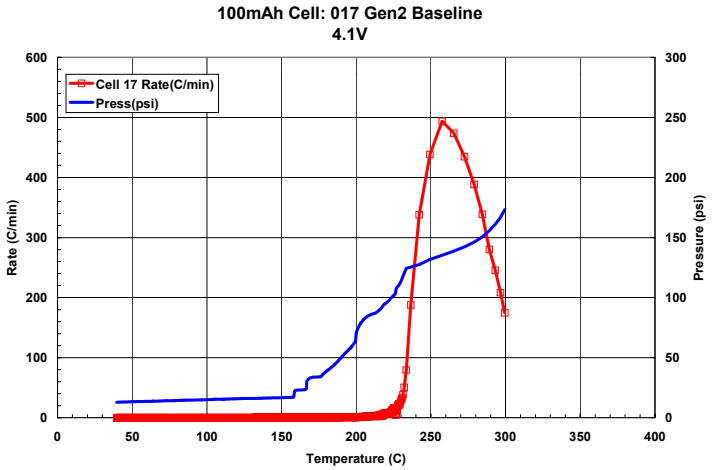

Figure III-18. ARC data (heat rate/pressure) for Gen 2 baseline thermal mitigation cell.

Table III-5. Matrix of Cell Compositions for 100mAh Cells

Cell ID	Positive	Negative	Electrolyte	Peak Rate (C/min)	Gas Vol. (ml)	Max Temp (C)
2	Gen 2 Baseline	Gen 2 Baseline	Gen 2 Baseline	0.37 **	xxx	400
17	Gen 2 Baseline	Gen 2 Baseline	Gen 2 Baseline	500	124	300
24	Gen 2 Baseline	Gen 2 Baseline	Gen 2 Baseline	0.132	5.4	140
25	Gen 2 Baseline	Gen 2 Baseline	Gen 2 + 2% VEC	64	184	350
28	Gen 2 Baseline	Gen 2 Baseline	Gen 2 + 2% VEC	26	70	290
37	Gen 2 Baseline	Gen 2 Baseline	Gen 2 + 2% VEC	0.03	2.6	130
1	Gen 2 Baseline	Gen 2 Baseline	Gen 2 + 2% VEC + 5% TPP	0.15	242	400
3	Gen 2 Baseline	Gen 2 Baseline	Gen 2 + 2% VEC + 5% TPP	0.95	238	400
4	Gen 2 Baseline	Gen 2 Baseline	Gen 2 + 2% VEC + 5% TPP			
6	Gen 2 Baseline	Gen 2 Baseline	Gen 2 + 2% VEC + 5% TPP			
7	Gen 2 Baseline	Gen 2 Baseline	Gen 2 + 2% VEC + 5% TPP			
61	Gen 2 Baseline	6% GDR	Gen 2 Baseline	3.3	156	350
63	Gen 2 Baseline	6% GDR	Gen 2 Baseline	0.06	100	400
64	Gen 2 Baseline	6% GDR	Gen 2 Baseline			
87	Gen 2 Baseline	6% GDR	EC:PC:EMC + 2% VEC	1.1	244	400
88	Gen 2 Baseline	6% GDR	EC:PC:EMC + 2% VEC			
89	Gen 2 Baseline	6% GDR	EC:PC:EMC + 2% VEC			
				* punctured	** leak	

Three baseline cells were measured and showed a certain degree of variability in heat rate. In general, the cells showed a high peak heating rate (500°C/min) at approximately 250°C. This thermal response (for the 100 mAh cells) occurs at a higher temperature than that for the 18650 cells. The volume of gas generated was 124ml (STP) at a temperature of 300°C (see Figure III-19). The gas composition was primarily CO_2 with a small amount of CO and H_2 as in the 18650 cells.

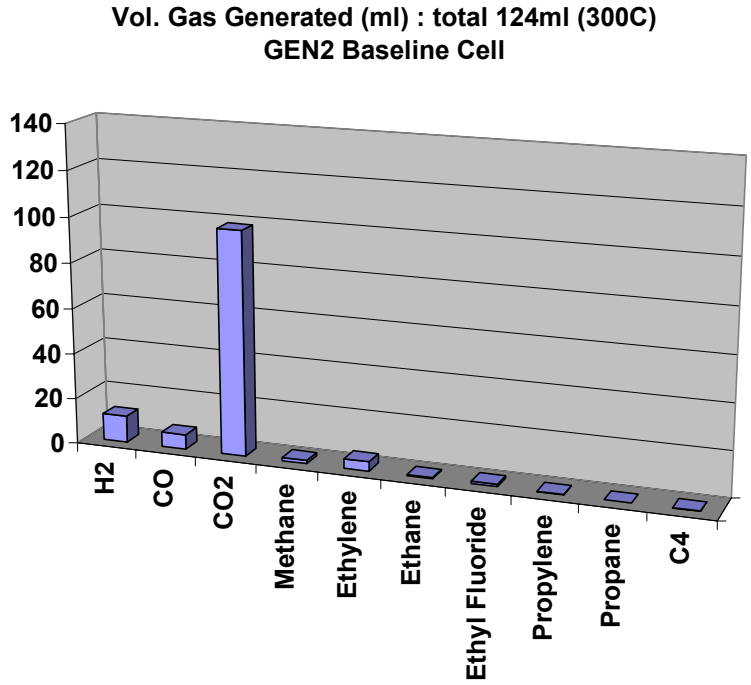

Figure III-19 Calculated volumes of each gas species from ARC run of Gen 2 baseline thermal mitigation cell.

Electrolyte Additives

The addition of 2%VEC to the Gen 2 electrolyte resulted in a significant reduction in the peak heating rate (60°C/min) which also occurred at 250°C. The volume of gas generated was 184 ml at 325°C, similar to that of the Gen 2 baseline cell. The most significant difference in gas composition was a strong increase in the amount of ethylene with a smaller increase in ethane and C4 species. The VEC itself is most likely the source of these gas species.

The addition of 5% TPP along with the 2%VEC resulted in even a greater reduction in peak heating rate (1°C/min) but the peak reaction temperature decreased to around 210°C. The cell generated 238 ml of gas at 400°C (220 ml at 300°C) and was still increasing at that temperature. The gas composition showed a marked increase in the level of methane along with the previous gas species of CO_2, CO, H_2, ethylene, and ethane.

Anode Modification

A cell with the Gen 2 cathode and electrolyte but with a 6% GDR anode resulted in a more stable anode material with a peak heating rate of 3°C/min around 225°C which was much less than the Gen 2 baseline cells with MAG10 graphite anodes. The two cells generated gas volumes of 100 ml and 160 ml at 300°C. Variations in gas evolution may result from differences in mass loadings in these small cells. The 6% GDR anode emitted much less CO_2 and more of other gas species than was observed for the Gen 2 baseline cell, which primarily emitted CO_2.

Anode and Electrolyte Modification

The final cell composition consisted of the Gen 2 cathode, the 6% GDR anode, and a new electrolyte consisting of EC:PC:EMC+2%VEC. There were two peaks in the heating rate at 200°C (0.6°C/min) and 240°C (1°C/min). Gas evolution reached a plateau at 325°C with a volume of 243ml while the second cell measured 238ml. The gas composition was mostly CO_2 with smaller but measurable amounts of H_2, CO, methane, ethane and propane.

VEC reduces the peak heating rates but the two measured cells showed some variability. Figure III-20 shows the effects of the various materials and additives by focusing on the onset of thermal runaway below 200°C. The two Gen 2 baseline cells showed onset at temperatures near 50°C. The cells with improved carbon and/or additives all showed onset at temperatures near 100°C. The rates varied in magnitude (the 6%GDR/EC:PC:EMC+2%VEC showed the lowest rate) but all cells showed similar accelerating rates by 180°C.

The volume of gas generation is compared for all cells in Figure III-21. Most noticeable is that the amount of gas generated was similar for all cells up to 250°C. Above this temperature, the greatest gas evolution was associated with the cells with VEC additive. All cells vented in the 140°C-160°C range indicating similar initial gas generation levels. Mitigation additives and advanced materials are showing that more stable cells can be designed but that further testing, especially in larger cell configurations, is required.

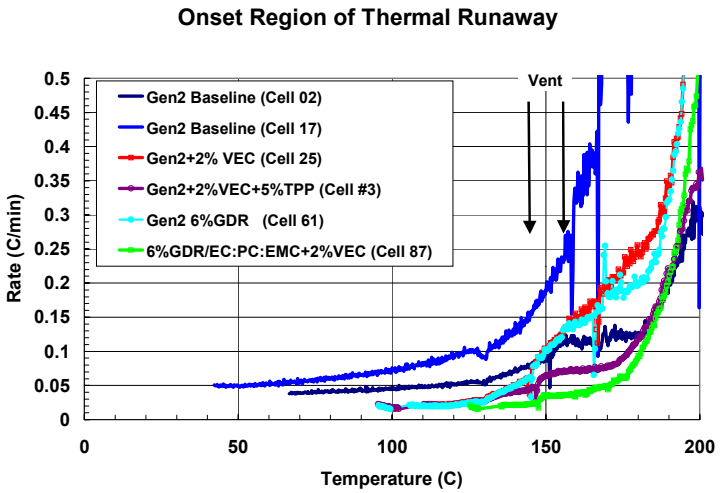

Figure III-20. Heating rate in the thermal runaway onset region for all mitigation cells.

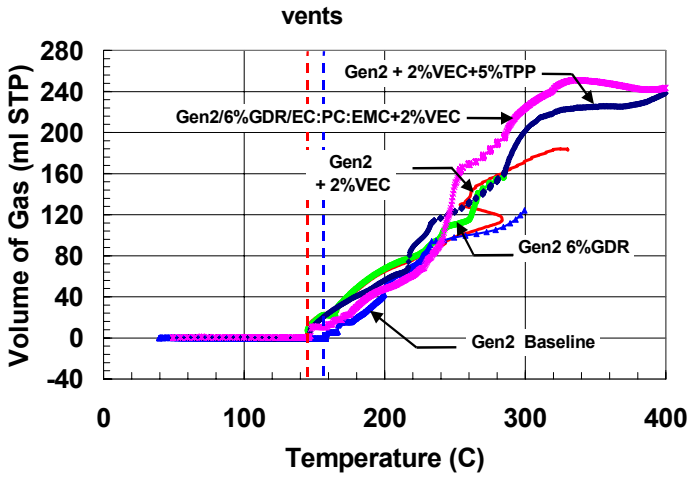

Figure III-21. Gas generation in thermal runaway region for all mitigation cells.

Electrolyte Decomposition Study – Impact of LiBETI Salt

The individual gas species generated during ARC runs of electrolytes consisting of EC:EMC with increasing $LiPF_6$ molarities (0.2M to 1.8M were previously measured in this activity. EMC is the major source of gas generation, and both $LiPF_6$ and EC serve to increase the rate of EMC decomposition. Gas generation is a major concern during thermal abuse since gas generation can result in cell rupture and the high-pressure release of flammable solvents.

$LiPF_6$ catalytically reacts with the solvents leading to poor thermal abuse response. An alternative salt that does not contain the highly reactive PF_6 ion was investigated. LiBETI ($LiN(SO_2C_2F_5)_2$) salt has been shown to have good thermal stability and conductivity. Two electrolyte solutions of 0.6M and 1.2M LiBETI in EC:EMC (3:7) were prepared. ARC bomb runs were performed to determine the thermal and gas generating properties up to 400°C. Figure III-22 shows the heating rate of these compositions compared to 0.6M and 1.2M $LiPF_6$ electrolytes. The LiBETI salts both showed much greater thermal stability, showing exothermic decomposition only around 380°C. The gas generating properties of these electrolytes are shown in Figure III-23. These results are promising in that the higher molarity did not result in increased gas generation above 0.6M.

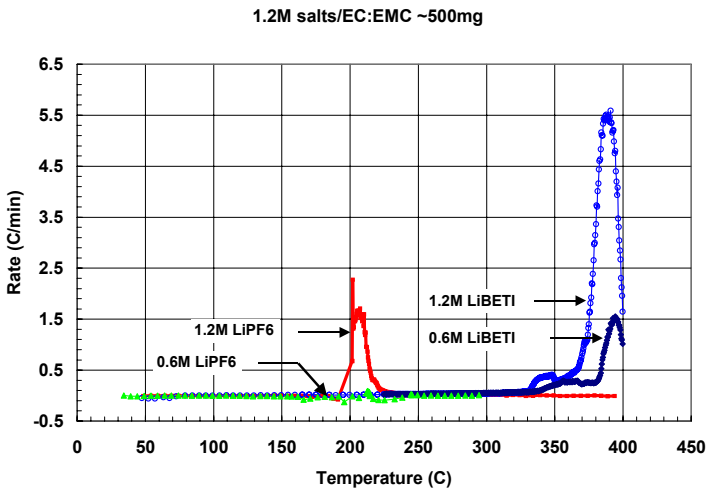

Figure III-22. ARC bomb run of Li BETI salt in EC:EMC (3:7) solvent compared to $LiPF_6$ salt at 0.6M and 1.2M.

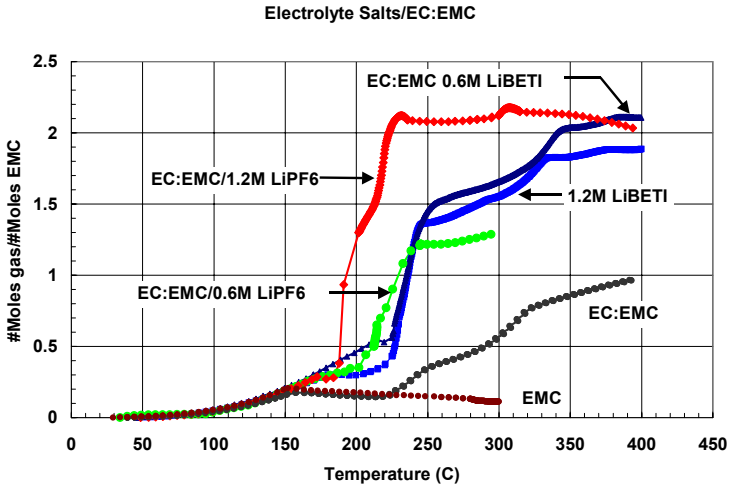

Figure III-23. Ratio of moles of gas per mole of EMC for ARC bomb runs of Li BETI and $LiPF_6$ salts.

Comparative measurements of $LiPF_6$ based electrolytes with other linear carbonate constituents, including electrolytes with EC:DEC and EC:DMC solvents, were also performed. Figure III-24 shows ARC data for the electrolytes compared to the Gen 2 electrolyte. The EC:DMC showed greater thermal stability, having a decomposition reaction temperature of 225°C compared to 190°C for the EC:EMC. The EC:DEC electrolyte only showed a very small exothermal reaction in this region. The ARC bomb pressures showed that the EC:DMC resulted in the lowest level of gas generation followed by EC:EMC and then EC:DEC.

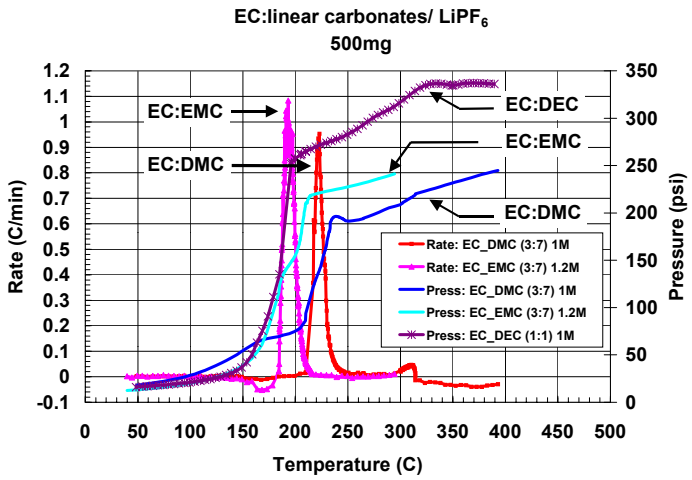

Figure III-24. ARC bomb runs of $LiPF_6$ with different linear carbonate components: EC:DMC, EC:EMC, EC:DEC.

A number of additional cathode and electrolyte additives, including flame retardants, have been investigated recently. Highlights of this work are summarized below.

- 0.7M LiBOB in EC:DEC(50/50) electrolyte is very stable up to 360°C.
- Exothermic reactions were observed for all cathodes around 260°C, with the spinel cathodes showing much lower heat generation than the lithium nickel cobalt manganese oxide cathodes.

III.C.2.2 Overcharge Study

The goal of this work is to determine the relative effects of electrochemical overcharge and thermal decomposition on cell thermal runaway. A system that permits the measurement of both the thermal output and generated gas species in real time during cell overcharge has been developed. The system is designed to minimize the temperature rise during the overcharge while allowing an accurate measurement of the heat generation by the cells. The desire is to determine if and how runaway reactions can initiate at different charge rates apart from thermal reactions.

The initial overcharge measurements showed that the cell response was determined largely by the shutdown separator. Charging at rates above 1C resulted in an increasing cell potential up to a peak voltage of 5.1V-5.3V, the peak potential increasing with increasing charge rate. The potential then began to drop while the cell temperature continued to increase, the temperature increase is shown in Figure III-25.

Separator melt occurred at an external cell temperature of approximately 110°C. A separate measurement with an internal thermocouple showed that the inner cell temperature was 15°C higher than the outer surface temperature. The inner temperature was thus approximately 125°C, which corresponds to the beginning of separator melt. At the melt temperature of the separator the cell impedance increases sharply with a resulting increase in the cell overpotential.

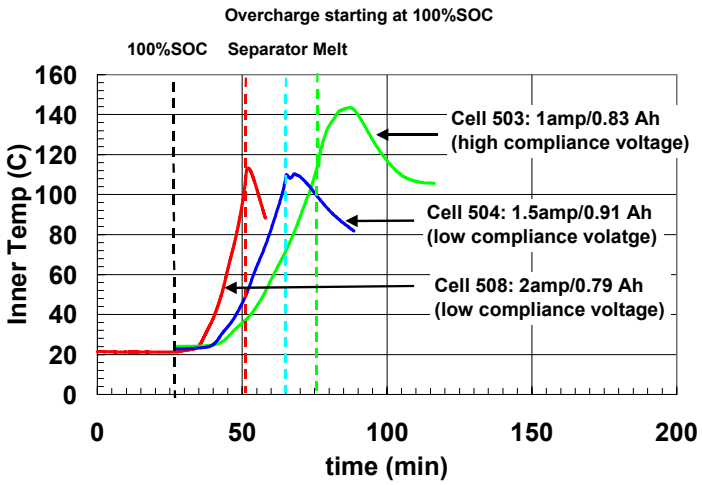

Figure III-25. Cell temperatures during overcharge at increasing charge rate.

The subsequent response of the cell depends on the maximum compliance voltage of the power supply. At high voltages (~45V) the melted separator breaks down and allows a current path to be established. This current drives an initial thermal impulse to the system while the potential is still high. The power supply voltage drops after the lower resistance current path is established and the thermal input to the cell drops. At lower compliance voltages (~12V) the separator remains at high impedance and the current drops to a very low value.

One cell did continue to increase up to a temperature of 140°C (which is very close to thermal runaway) before dropping to a lower temperature. If the cells had been more highly insulated the cells may have reached thermal runaway. Figure III-26 shows the heat outputs calculated from the measured temperature differentials. The cells all showed an increase in heat output at 125% SOC. The heat output increased during overcharge, reaching a peak around 4W-5W at the separator melt temperature which occurred near 175%-200% SOC.

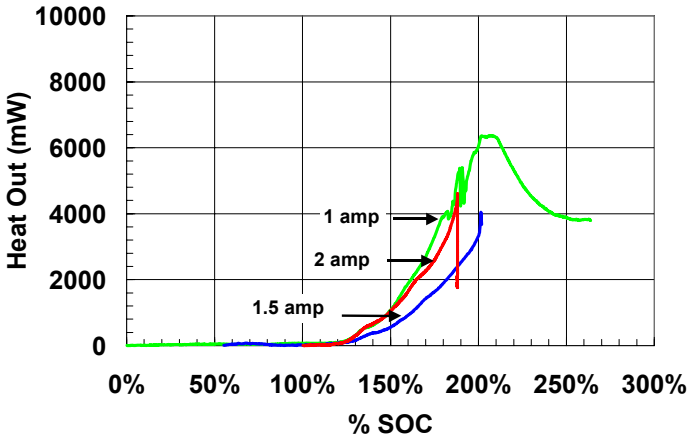

Figure III-26. Heat output during overcharge at increasing charge rates.

Another cell was charged at an initial low rate (0.45amp) for an extended period up to approximately 250% SOC. The cell voltage/current profiles are shown in Figure III-27 and the cell temperatures in Figure III-28. The cell underwent a small pinhole vent near 40°C as was seen in many of the cells. The cell reached a peak voltage of 5.3V and then maintained a voltage between 5.0V-5.2V. The cell temperature remained constant at 50°C for a period of three hours and showed no sign of thermal runaway. The charge rate was then increased to 0.9amp. The cell voltage again showed a peak (5.6V) followed by a return to a steady 5.2V and a cell temperature of 79°C. Again, no sign of thermal runaway was observed. The cell was charged to a nominal 300% SOC and then the charge rate increased to 2.7 amps. The voltage peaked and dropped as before but then began to increase as the cell temperature approached the separator melt temperature. The heat output increased steadily and then the cell went into thermal runaway at the separator melt temperature even though the compliance voltage was held at 12V. These measurements indicate that overcharged cells can be less stable after long periods of low-rate overcharge. A comparative response of the cells is shown in Figure III-29.

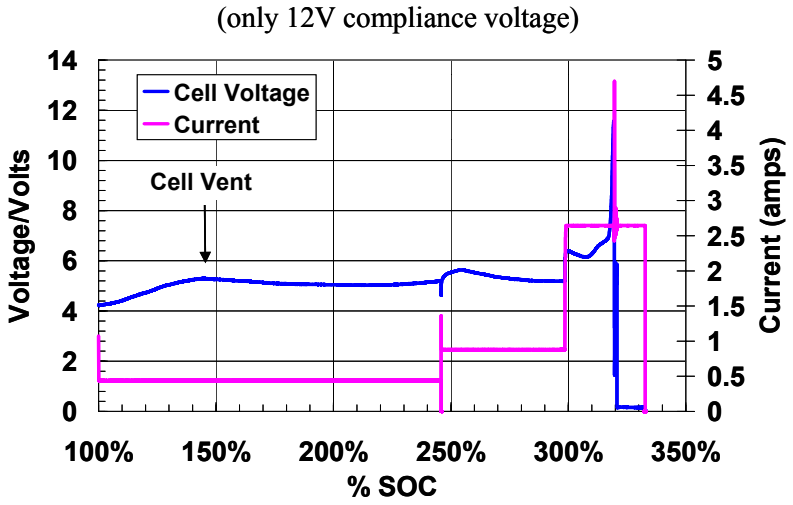

Figure III-27. Initial low-current overcharge followed by increasing charge rates.

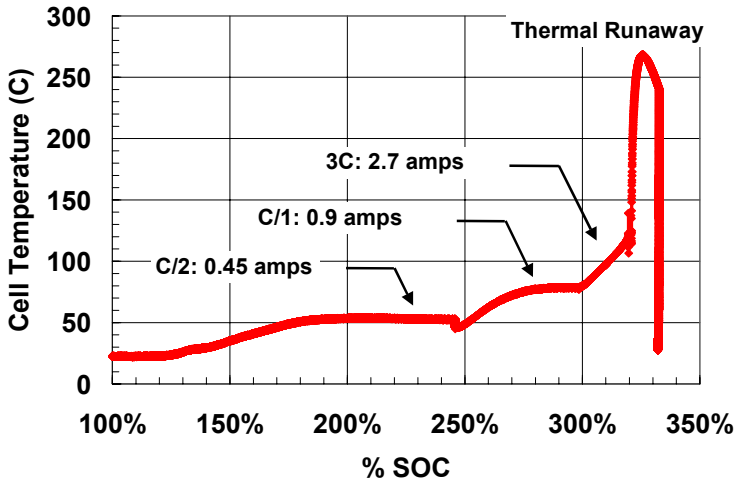

Figure III-28. Cell temperatures during low-current overcharge with subsequent higher rates.

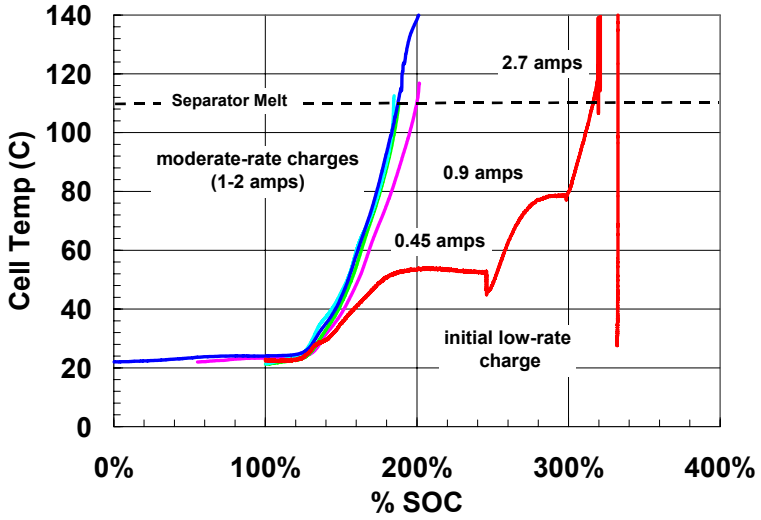

Figure III-29. Comparison of cell temperatures during high-rate and low-rate overcharges.

III.D Cost

Objectives

- Identify and secure advanced low-cost cell materials from international material suppliers and evaluate samples for their suitability in high-power HEV applications. Provide feedback to material suppliers on the capabilities and limitations of their materials.
- Develop lower-cost high-power cell chemistries--using the most promising materials--and conduct preliminary performance, life, and safety evaluations to establish their viability.
- Assess viability of gel electrolyte lithium-ion systems for use in high-power HEV applications.
- Conduct post test analyses of gel electrolyte cells to understand performance decay mechanisms and delamination problems.
- Explore novel approaches for reducing the cost of cell packaging.

Approach

- Secure samples of the most advanced materials from material suppliers.
- Develop and refine rapid screening test protocols to assess the suitability of novel materials. Employ protocols to evaluate material capabilities, provide feedback to the material suppliers.
- Produce cells from the most promising low-cost materials and conduct preliminary evaluations on their performance, life, and safety characteristics, using sealed prismatic cells.
- Collaborate with developers of gel electrolytes to evaluate their technologies.
- Thoroughly examine aged/tested cells for adhesion, wetting, and gassing problems.
- Develop a flexible cell containment system using laminates that provide good barriers to air, moisture, and electrolyte.
- Develop a new class of organoclay nanocomposite materials that improve the barrier properties of the sealant layer and the adhesion of the sealant layer to the aluminum foil layer.
- Develop a new flexible pouch design that limits permeation of electrolyte and moisture from the seal edges.

Accomplishments

- Established and maintained contacts with material suppliers in Japan, Korea, and Europe.
- Obtained samples of advanced natural and synthetic graphite materials, advanced layered and 3D spinel cathode materials, electrolyte salts, separators, and binder materials for evaluation.
- Conducted screening tests on advanced materials and provided feedback to suppliers. One notable accomplishment was the development of a more optimal form of GDR carbon-coated round-edge natural graphite by Mitsui Mining, based on recommendations from this program.
- Fabricated and evaluated PVdF-based PLI and gel electrolyte cells for ASI, gas evolution, adhesion, and delamination issues.
- Evaluated the power and aging characteristics of cells employing Daiso and DKS gel electrolytes.
- Evaluated thermal safety of Daiso pre-gelled (liquid) electrolyte cell chemistry.

- Showed that VEC added to the Daiso electrolyte reduces cell capacity fade.
- Collaborated with Sumitomo Electric Industries (SEI) to develop HEV-sized flexible battery packaging. Evaluated their laminate in pouch tests with water, solvent, and electrolyte at various temperatures.
- Produced an initial organoclay nanocomposite material with the new extruder and created a laminate for pouch testing.

Future Studies

- Solicit samples of separator materials from the industrial firms that are developing low-cost separators under the FreedomCAR Partnership.
- Continue conducting screening tests of new materials and providing feedback to the suppliers.
- Determine best tie-layer adhesives and identify candidate aluminum pretreatments.
- Continue working with Showa Denko and Quallion to evaluate the Showa Denko technology.
- Continue the evaluation of $LiBF_4$/EC/GBL as an advanced PEO gel electrolyte and develop additives to stabilize the cell ASI.
- Continue development of materials for use with gel electrolytes (lithium salts, electrodes, etc.)
- Continue collaboration with SEI to develop and evaluate their HEV-sized flexible battery packaging under abuse conditions.
- Develop organoclay nanocomposite films for evaluation as a barrier/sealant layer and possible use as an adhesive material.

III.D.1 Introduction

As described above, there are three major barriers to the use of high-power lithium-ion batteries in automotive applications: calendar life, abuse tolerance, and cost. The efforts described in this section address all three of these barriers, but the overall emphasis is on low-cost advanced materials. The cost target for a FreedomCAR HEV energy storage device is $20/kW. This activity is addressing this cost target via three approaches: (1) screening and developing advanced low-cost cell materials, (2) evaluating advanced gel-polymer electrolyte systems, and (3) developing low-cost flexible cell packaging technology.

III.D.2 Material Screening & Development

The Applied Battery Research activity continues to search for and evaluate low-cost cell components that are promising for use in the next generation of high-power lithium-ion cells. One such cell chemistry is based on a new low-cost layered cathode material (one-third) and a second is based on the use of $LiMn_2O_4$ spinel cathode materials.

A cost model developed in this activity was used to analyze the costs of the Gen 2 chemistry, a next generation cell comprised of the one-third cathode plus GDR anode, and finally an advanced chemistry cell comprised of $LiMn_2O_4$ and GDR natural graphite. The material costs associated with those three cells, in a 25 kW configuration, is shown in Table III-6. It should be noted that the costs shown in Table III-6 are material costs only. If it is assumed that the full battery cost, including

manufacturing cost and profit for the manufacturer, will be approximately 100% of the material cost, then only the spinel material appears capable of meeting the USABC cost target of $20/kW for a high-power battery.

Table III-6. Materials Costs for Three HEV Lithium ion Cells

	Cost/kW
Gen 2 Chemistry	$16
Next Generation (one-third cathode plus GDR anode)	$12
Advanced Chemistry (spinel plus GDR anode)	$9

Advanced Cathode Materials

$Li(Ni_{1/3}Co_{1/3}Mn_{1/3})O_2$ ("one third") Cathode Material: Among a list of layered oxide materials having α-$NaFeO_2$ structure type, the one third material [$Li(Ni^{2+/3+}_{1/3}Co^{3+}_{1/3}Mn^{4+}_{1/3})O_2$] is a very promising cathode for use in HEV applications. As an example, the predominant oxidation states of Ni, Co and Mn in this material mean that the capacity of 160 Ah/kg delivered in the range 3.0 to 4.3V is provided by the oxidation of Ni^{2+} to Ni^{3+} with limited Ni^{4+} generation at that cutoff voltage. Thus, there is no generation of highly oxidizing and unstable Ni^{4+}, which appear to play a role in the capacity and power fade process, as well as in limiting the safety of the Gen 1 and Gen 2 cell chemistries.

This research activity has received three lithium nickel cobalt manganese oxide layered materials from Tanaka Chemical Corp., Toda Corp., and Seimi Chemical Corp. These materials were evaluated for use in HEV applications and show good uniformity of particle size and morphology. SEM photographs indicate that the Seimi material has a compact dense spherical morphology. The other two appear to have a less dense, but spherical morphology.

Typical charge/discharge curves have been obtained for Seimi's one third cathode material vs. lithium metal between 3 and 4.3 V using 1.2 M $LiPF_6$ in (EC:PC:DMC) (1:1:3). At C/12, 156 Ah/kg capacity can be achieved with good retention during cycling (Figure III-30).

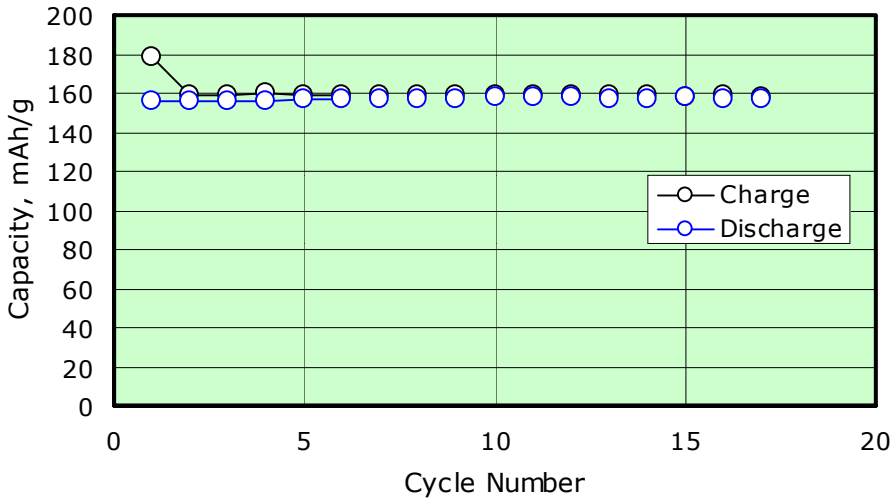

Figure III-30. Capacity vs. cycle number for $Li(Ni_{1/3}Co_{1/3}Mn_{1/3})O_2$ (Seimi) vs. lithium metal at C/12.

The high power capabilities of the one third materials were evaluated by performing HPPC tests. These tests were carried out on GDR/$Li(Ni_{1/3}Co_{1/3}Mn_{1/3})O_2$ cells using a 10C pulse rate. The ASI values obtained are slightly higher than the target values, which are 35 $\Omega.cm^2$ for an 18-s discharge and 25 $\Omega.cm^2$ for a 2-s charge pulse. This research effort will continue to evaluate cell chemistries based the one third cathode and we anticipate that this material will meet and exceed the performance requirements for the HEV application.

Spinel Cathode Materials

This research effort has evaluated two lithium rich manganese oxide spinels from Toda Kogyo Corp. for their potential use in HEV applications. These materials appear to be of high quality with unique features, such as homogenous particle size and low specific surface area (one sample is 0.36m^2/g), as shown Figure III-31. Half cell tests show that cathodes made from these spinels exhibit stable capacities when tested between room temperature and 50 °C.

Surface Area (m2/g)	0.36
Tap Density (g/ml)	2.04
Particle Size Distribution by Laser Diffraction	
D-10 (μm)	6.3
D-50 (μm)	8.8
D-90 (μm)	12.6

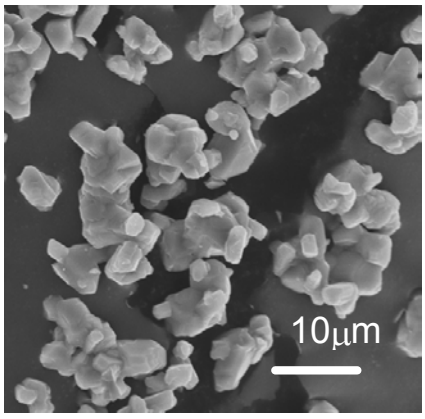

Figure III-31. SEM image of TODA lithium-rich manganese spinel and its physical properties.

This research activity continues to test the TODA spinel cathode in a full cell that employs a GDR graphite anode and 0.7 M LiBOB electrolyte. The capacity fade of the cathode is less than 10 % after 60 cycles. Using the same electrolyte, full cells were tested at 55°C. Two cells with TODA cathodes and GDR graphite anodes exhibit appreciable capacity fade. It has been found that the stabilized spinel is very stable at 50°C against a metallic lithium anode. This indicates that something at the graphite anode is causing the capacity fade observed in full cells.

The ASI data from the cell that was cycled at 55°C shows that its ASI value increased approximately 75% during cycling. The reasons for this ASI increase are currently being studied. Some potential contributions include:

- Electrolyte impurities
- Mn dissolution from spinel
- Unstable SEI layer

The use of an additive in the electrolyte and a reference electrode to determine if the SEI layer on the surface of the anode is causing the impedance rise is currently being studied.

Spinel materials from Japan Metals & Chemicals Co., Ltd. (JMC) have been evaluated. One spinel sample had a surface area of 0.74 m^2/g and a mean particle size of 13.9 μm. The SEM image of the sample shows rough edge and flaky type morphology and a large range of particle sizes. HPPC tests on this spinel vs. the Gen 1 anode shows ASI values that meet the requirements for high-power HEV applications.

Another JMC spinel sample, with a relatively low surface area and a mean particle size of 14.2 μm was evaluated. The spinel has a discharge capacity density of ~110 Ah/kg and exhibits very good cycle performance vs. lithium anode at room temperature.

Mitsubishi Chemical supplied spinel samples that possess unique spherical shaped particles. The sample has a low surface area of 0.8 m^2/g, a mean particle size of 15 μm, and a discharge capacity of 100 Ah/kg. HPPC tests on this spinel vs. GDR graphite anode in 1M $LiPF_6$ EC/DEC(1:1) electrolyte, show ASI values that meet the requirement of high power for HEV application.

Advanced Anode Materials

A composite material from Petoca Co., a mixture of carbon fiber and graphite, was evaluated. This type of anode material, possessing a very low surface area and low irreversible loss, should enhance the inherent safety of the cell. HPPC tests on this material demonstrate that it meets the ASI requirements. A full cell employing a spinel cathode and the GMCF carbon fiber composite anode, in 0.7M LiBOB electrolyte, was cycled at room temperature. The capacity fade is small even after 90 cycles at C/2 rate, as shown in Figure III-32.

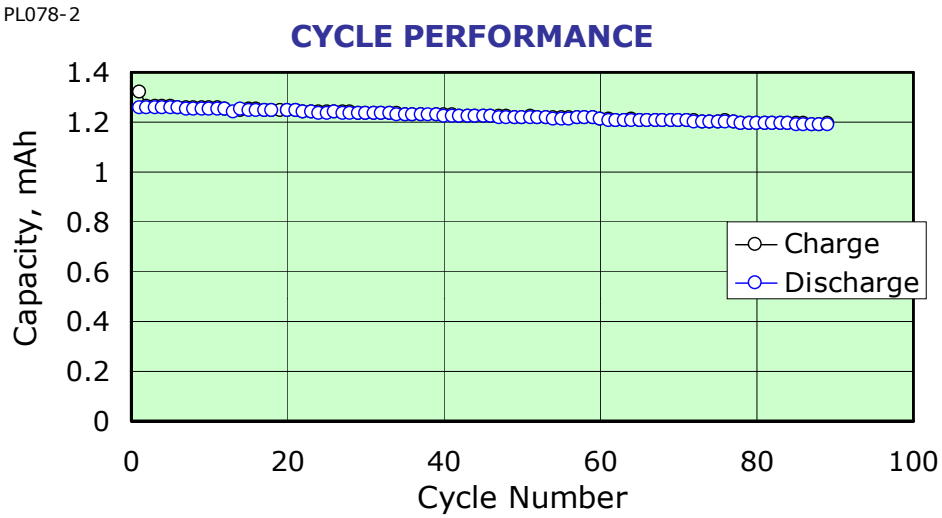

Figure III-32. Spinel vs. GMCF composite anode in 0.7M LiBOB electrolyte at room temperature.

Low-Temperature Performance

The influence of low temperature on cell performance is being studied. Gen 2 cells were built with electrode areas of 32 cm^2. Three constant current charges and discharges were performed at each current level, after which an HPPC test was performed. The rate capability of this cell is shown in Figure III-33 in a plot of discharge capacity versus discharge time. It is apparent that the performance falls off considerably below -15ºC. It was also found that the capacity at -30ºC could be doubled by using a constant voltage charge (with extra time given for the tapering current). However, the constant voltage charge did not improve the ASI. Reference electrode studies are planned with various electrode materials and electrolytes to determine if the performance loss is due to the active material, SEI layer, or electrolyte conductivity.

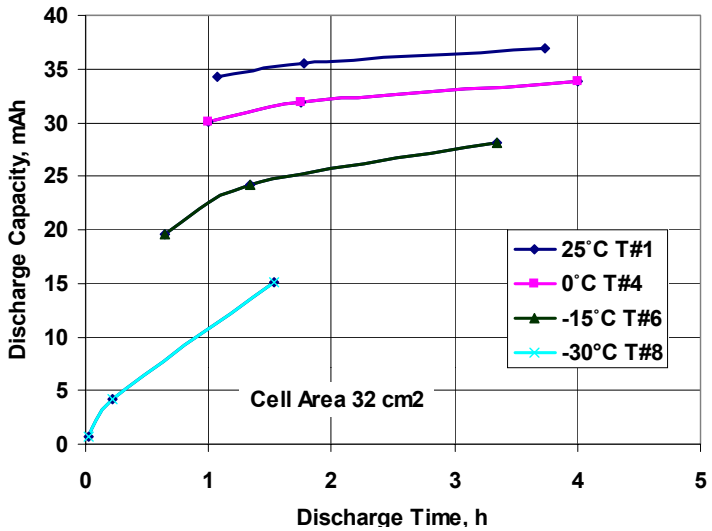

Figure III-33. Discharge capacity vs. discharge time with temperature as a parameter for the Gen 2 cell system.

III.D.3 Gel-Polymer Technologies

The potential advantages of gel polymer electrolytes compared to liquid electrolytes are safety (thermal stability) and low swelling at temperature above 80°C in a plastic/metal package form. Also, vapor pressures of the organic solvents are generally lower when gel polymer electrolytes are used. Finally, gel polymer electrolytes immobilize and thereby retard the leakage of liquid electrolyte. However, there are several issues to be addressed, including reduction of the ASI to meet the performance required for high-power applications.

In 2003, LiBOB/macromonomer gel polymer electrolyte cells were fabricated and evaluated. Also, preliminary tests were conducted on cells that employed the Tosoh $LiMn_2O_4$ spinel in the positive electrode, GDR graphite in the negative electrode, and the DKS macromonomer gel polymer electrolyte.

This research effort conducted an evaluation of modified gel polymer cells from Kokam which employ a $LiCoO_2$ positive electrode. Feedback has been provided to Kokam to improve their technology for use in high-power applications. Also, Gen 2 positive electrode material was shipped to Kokam to fabricate Gen 2 type cells that employ their gel polymer electrolyte. Interactions with LG Chemical were also initiated in order to evaluate their gel polymer electrolyte.

Dai-ichi Kogyo (DKS) cells

Gelation by thermal curing of DKS macromonomer precursor solutions with LiBOB salt was investigated. A 0.7M LiBOB EC/PC/DMC (2/2/6 by wt%) liquid electrolyte was mixed with the DKS macromonomer in different weight ratios. Gelation was successful with the LiBOB based electrolyte when more than 5 wt% of the macromonomer in the precursor solutions was used. However, the ionic conductivity of the electrolyte decreased proportionally as the content of the macromonomer was increased. It is thought that the macromonomer caused hardening of the gel polymer electrolyte and reduced the free volume available for lithium ion transport. No leakage of LiBOB electrolyte was observed.

A 10 wt% macromonomer gel polymer electrolyte caused a 25% reduction in the ionic conductivity of pristine LiBOB. Thus, the polymer content has a significant impact on the conductivity. The effect of temperature on ionic conductivity of the gel electrolyte is shown in **Figure III-34**. Further gelation experiments will be conducted with a focus on those that contain less than 5 wt % macromonomer in order to maximize the conductivity and retain a soft gel.

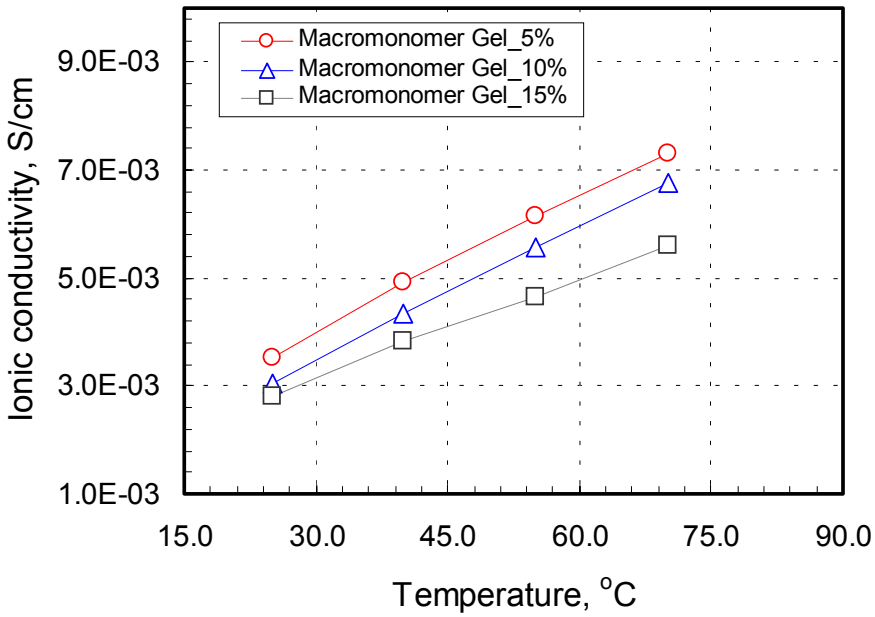

Figure III-34. Ionic conductivities of DKS macromonomer gel electrolytes with 0.7M LiBOB in EC/PC/DMC (2/2/6 by wt.).

Early on, the EC/γBL solvent system was selected for gelling tests due to its high boiling point. However, γBL is known to cause poor cycle performance in cells that use graphite anodes. Later, the EC/PC/DMC solvent system was used for evaluation of the macromonomer gels. PC is a good solvent for the gel polymer electrolyte because of its high boiling point. Figure III-35 shows the initial charge/discharge cycle on a cell that employs the Gen 2 negative electrode (MAG-10 graphite). No exfoliation of the MAG-10 graphite was observed and the cell could be cycled using this electrolyte.

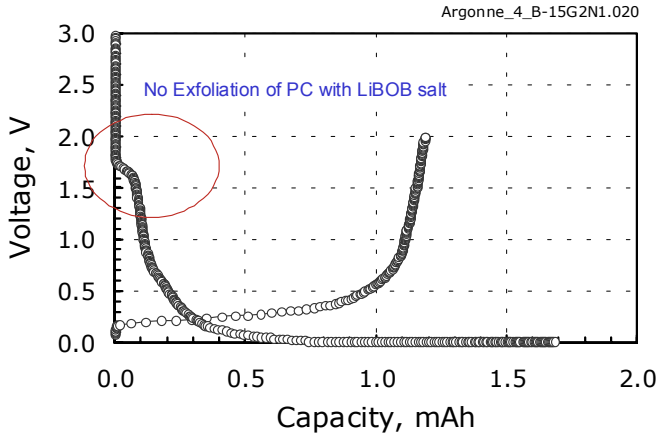

Although macromonomer gel electrolytes employing 0.7M LiBOB in EC/PC/DMC showed similar ionic conductivities to those of 2M $LiBF_4$ in EC/γBL, the cell ASI values are slightly higher than those obtained with $LiBF_4$ (see Figure III-36). The reasons for the increased ASI with the gel electrolytes are being analyzed and improvements in ASI are expected by adjusting the content of

macromonomer as low as possible and by adding other compounds to provide more free volume inside the gel polymer network.

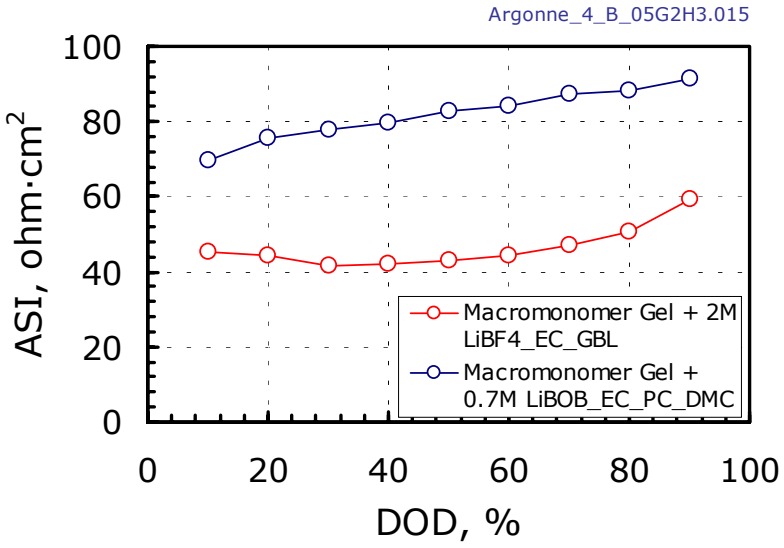

Figure III-36. Comparison of ASIs of macromonomer gel polymer cell from 5C based HPPC test measured at room temperature.

A preliminary investigation was conducted on a cell that employed a Tosoh $LiMn_2O_4$ spinel cathode, GDR anode, and macromonomer gel polymer electrolyte. A slight decrease in discharge capacity was observed after gelation, as shown in Figure III-37. Longer term cycle tests and ASI studies are continuing.

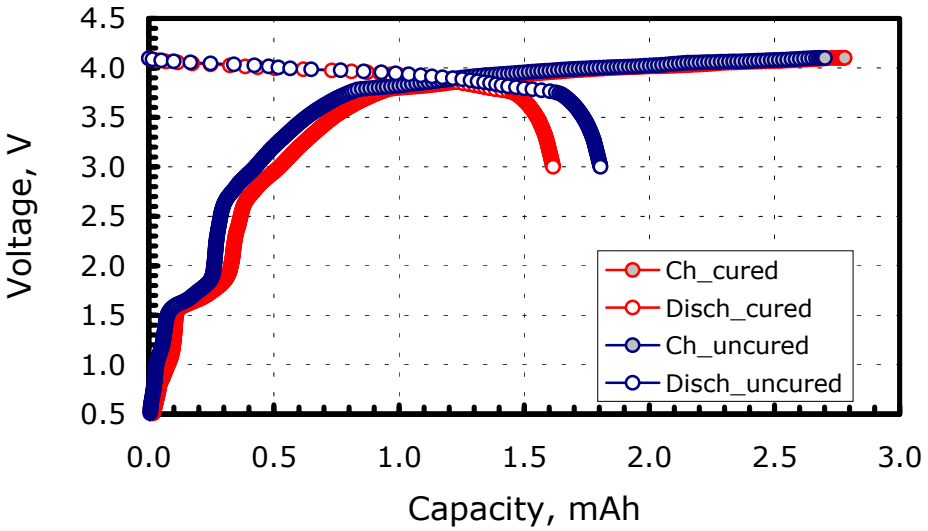

Figure III-37. Initial charge/discharge profiles for cells that employ Tosoh $LiMn_2O_4$ and GDR graphite, with the DKS macromonomer gel electrolyte. This gel electrolyte was made with 2M $LiBF_4$ in EC/γBL(1/3 by vol.).

Novel Electrolytes

The Applied Battery Research activity has also continued to investigate a relatively new class of LiBOB based electrolytes, see Figure III-38. The advantages of these materials are that they:

- Cycle at high temperatures (70°C) with good stability.
- Stabilize graphite in PC-based electrolytes.

However, their low temperature performance is less than ideal and they exhibit solubility limits.

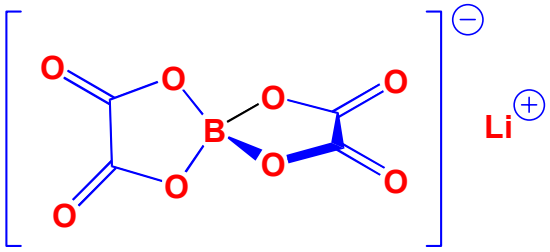

Figure III-38. Structure of the LiBoB electrolyte

Recently, a large number of LiBOB-based electrolyte systems have been investigated, including those with the following solvents: PC, γBL, PC-EC, PC-DEC, PC-EA, γBL-DMC (3:7), (4:6), (5:5), γBL-EA, EC-EMC (3:7), (5:5), PC-EC-EMC (1:1:3), EC-DMC-γBL-EA (2:1:1:6), (2:1:2:5), (3:1:1:5), and PC-EMC-γBL-EA (2:1:1:6), (2:1:2:5), (3:1:1:5).

It has been found that solvents such as γBL and EA result in much better capacity and conductivity for LiBoB based electrolytes. This is shown in Table III-7, that shows the relative capacity of Lithium-ion cells based on LiBOB in γBL vs. an $LiPF_6$-based electrolyte provided as a benchmark.

Table III-7. Relative capacity of Lithium-ion Cells with LiBOB-based Electrolyte

T(°C)	$LiPF_6$ EC/PC/EMC (1:1:3)	LiBOB - γBL	LiBOB/ γBL/DMC (5:5)
25	1.0	1.0	1.0
0	1.0	1.0	0.95
-10	1.0	1.0	0.95
-20	0.86	1.0	0.47
-30	0.82	0.84	0.43
-40			0.06

The results of these studies indicate that

- LiBOB based electrolytes provide much improved conductivity when blended with esters such as γBL and EA.
- Both γBL and EA do not provide sufficient stability for Lithium-ion cells to operate at high temperatures and high voltages.
- Carbonyl linked carbon in SEI formed on graphite in LiBOB based electrolytes provides high temperature stability.

III.D.4 Low-Cost Flexible Packaging

Commercial pouches for HEV-sized cells from Sumitomo Electric Industries (SEI) are undergoing accelerated thermal-aging profiles to test their thermal abuse response. These 30 pouches were filled with an electrolyte blend with two electrode feed-throughs, included during fabrication at SEI. There are no electrodes or active materials in these pouches. Thirteen of these pouches are being stored at 55°C and ~95% relative humidity (RH), ten are undergoing rapid thermal cycling, and seven are undergoing summer/winter thermal cycling. The weight and integrity of these pouches are monitored and periodically one is opened and analyzed for HF, H_2O, and solvent degradation.

The results to date for the pouches undergoing rapid thermal cycling between -40°C and 60°C indicate that the electrolyte loss rate is approximately 1.4 μg per thermal cycle per centimeter of perimeter. The majority of the pouches have reached over 1500 thermal cycles without any signs of rupturing, delamination, or seam splitting. Two pouches were removed because they developed a pinhole leak at the bottom corner where the pocket is formed (see Figure III-39). Even for these pouches, no signs of delamination or seam splitting were observed. This defect was not due to failure of the packaging material itself, but is rather due to the sharp radius of curvature at the pocket corners. Sumitomo was informed of this problem and is working on a solution.

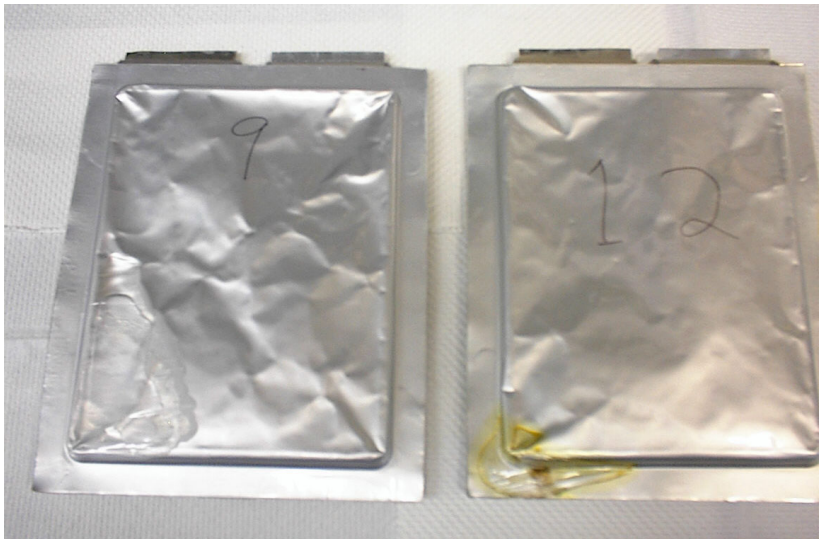

Figure III-39. Typical examples of a pinhole leak at the pocket corner.

The majority of the 13 pouches stored at 55°C and 95% RH have now reached over 275 days without any signs of rupturing, delaminating, or seam splitting. A slight weight loss is observed for these pouches. From the slope of the weight loss curves, the electrolyte loss rate was estimated to be 8 milligrams per year per centimeter of perimeter.

The seven pouches undergoing summer/winter thermal cycling achieved 620 summer cycles and 200 winter cycles. One of the pouches developed a leak at the pocket corner and lost its entire electrolyte.

Adhesion Investigation

Results of the ongoing test of promising tie layer materials are shown in Table III-8. Several of these samples are holding tightly to the aluminum foil after 21 weeks of being immersed in a blended electrolyte. These tests are performed at 55ºC in a dry box oven to minimize the influence of moisture. The EVOH samples appear to be the best, in particular, LC-L101A.

Table III-8. Update of tie layer materials

Adhesive	Manufacturer	Time to delamination, color
Tymor 1N05 (Mod. Polyolefin)	Rohm & Haas	2 weeks, colorless
Tymor 1221E (PE-based)	Rohm & Haas	4 weeks, colorless
Tymor 1258B (PE-based)	Rohm & Haas	6 weeks, colorless
EVOH LC-E105B	EVAL Co.	~ 10 weeks, tan
EVOH LC-E105B & clay	EVAL/ANL	~ 15 weeks, black
EVOH EP-F104BW	EVAL Co.	~ 15 weeks, light beige
EVOH LC-L101A	EVAL Co.	> 21 weeks, light beige
EVOH GC-156B	EVAL Co.	~ 15 weeks, dark bonze
SEI Laminate from 12/01	Sumitomo	> 21 weeks, colorless

A summary of non-chromium (VI) commercial pretreatments of aluminum that are undergoing electrolyte soak tests is listed in Table III-9. The test consists of applying the pretreatment to aluminum foil, followed by hot pressing polypropylene film onto the foil, and then immersing the laminate sample in blended electrolyte at 55ºC. All of the samples delaminated within a few days except for the Alodine 5200, which is still holding after 13 weeks. This is especially remarkable considering that the electrolyte is contained in a Nalgene bottle that is exposed to ambient humidity (not in a dry box). The electrolyte was recently replaced with fresh electrolyte because it had turned completely brown (due to moisture attack). It is hoped that the combination of this aluminum pretreatment and the corona discharge treatment of the polyolefin film could provide the best adhesion method to date.

Table III-9. Commercial pretreatments of aluminum under test.

Product Name	Manufacturer	Chemical Basis
Alodine 5200	Henkel Surface Tech.	Ti-based flourorefractory
Z-100	Dovey Corp. (Natural Coating Sys.)	Zirconia based
Z-168	Dovey Corp. (Natural Coating Sys.)	Zirconia based
Oxsilane AL-0500	Chemetall Oakite (Brent Chemcoat)	Silane-based, fluotitanic acid
Oxsilane MM-0705	Chemetall Oakite (Brent Chemcoat)	Silane-based
Garobond X 4591	Chemetall Oakite (Brent Chemcoat)	Zirconium, fluoride based
Garobond X 4650	Chemetall Oakite (Brent Chemcoat)	Zirconium, fluoride based
Prekote (X-IT)	Pantheon Chemical	Biodegradable, polar/non-polar molecule

Organoclay Technology

The calendar life goal of 15 years poses a significant challenge to the conventional flexible packaging approach. With this in mind, the activity is investigating a novel organoclay nanocomposite barrier material that was already being developed at ANL under a separate activity. This material is based on a method of combining natural clays with organic polymers to form organoclays. The organoclays are then compounded with traditional polymers to form barrier films.

The film die for making extruded nanocomposite film was installed on an extruder and is functional. Test film (low density polyethylene) has been produced. Production of the surfactant used to prepare polyolefin nanocomposites has been scaled up to enable production of kgs per batch. A range of surfactants have been synthesized - all have melting points of at least 110°C, with some as high as 120-130°C.

The new surfactants were used to prepare small batches of LDPE, HDPE, and EVOH nanocomposites. The LDPE nanocomposites display a significant increase in crystallinity, and with only 0.4 vol.% clay loading the oxygen barrier was increased by 30-35%. In EVOH, the presence of less than 1 vol.% organoclay strongly affected crystallinity and produced a clear nanocomposite which displayed no small-angle light scattering. This is an indication that the organoclay is nucleating the polymer and reducing the polymer crystallite size to diameters that are below the wavelength of light. This effect should increase the modulus and impact strength of the polymer.

IV. LONG-TERM BATTERY RESEARCH

The Long-Term Research Activity is supported by the DOE's FreedomCAR and Vehicle Technologies Program (DOE-FCVT) to research and analyze high-performance rechargeable batteries and new materials for high-performance rechargeable batteries for use in EVs and HEVs.

Background and Program Context

The development of an advanced battery for automotive applications is a complex process. There is a strong need to identify and understand performance and lifetime limitations to help guide the search for new battery materials. The Long-Term Research activity addresses fundamental issues of chemistries and materials that face all lithium battery candidates for EV and HEV applications. It emphasizes synthesis of components into battery cells with determination of failure modes, coupled with strong efforts in materials synthesis and evaluation, advanced diagnostics, and improved electrochemical models. Battery chemistries are monitored continuously with periodic substitution of more-promising components. This is done with advice from within, from outside experts, and from assessments of world-wide battery R&D.

The work is carried out by the Lawrence Berkeley National Laboratory (LBNL) and several other organizations, and is organized into six research tasks: (1) Cell Development, (2) Anodes, (3) Electrolytes, (4) Cathodes, (5) Diagnostics, and (6) Modeling. Task 1 comprises cell fabrication, testing and characterization, Tasks 2-4 are aimed at identifying new materials, and Tasks 5-6 support all Long-Term Research work. Brief descriptions of each task follow.

1. The ***Cell Development*** task aims to understand the failure and degradation modes in the baseline systems, investigate self-actuating overcharge protection mechanisms, synthesize and evaluate alternative electrode materials, and support cell development. To date, three "baseline" rechargeable Li cell chemistries have been identified:
   - The polymer-electrolyte chemistry with a Li metal anode, $Li(CF_3SO_2)_2N$ + cross-linked PEO-based polymer electrolyte, and a V_6O_{13} or tunnel-structure Li_xMnO_2 cathode.
   - The gel-electrolyte cell chemistry with a natural graphite anode, $LiBF_4$ + cross-linked gel electrolyte, and a $LiFePO_4$ or $Li_{1.02}Al_{0.25}Mn_{1.75}O_{3.92}S_{0.03}$ cathode.
   - The baseline Lithium-ion chemistry is based on the ATD Gen 2 chemistry: a graphite-based anode, a $LiPF_6$ + EC-EMC electrolyte, and a $LiAl_{0.05}Ni_{0.80}Co_{0.15}O_2$-based cathode.

1. The ***Anodes*** task seeks to overcome the two major problems associated with the carbon-based anodes used in commercial Lithium-ion batteries: poor safety characteristics and short lifetimes. Therefore, either improved anode structures or non-carbonaceous anodes must be developed. Low-cost metal alloys with acceptable capacity, rate, cyclability, and calendar life are under investigation.

2. ***Polymer Electrolyte*** research aims to understand performance characteristics by studies of the transport properties of the electrolyte as a function of polymer and salt structure, polymer structural changes with temperature, and interactions at the electrode/electrolyte interface related

to transport and chemical/mechanical stability. A multi-pronged approach involving chemical synthesis, advanced diagnostic tools, and coordinated modeling is being used.

3. The identification and development of novel ***Cathodes*** are critical because of the cost and environmental limitations of cobalt- and vanadium-based materials used in current Li batteries. The focus of this effort is to develop a high-rate and stable MnO_2 cathode. Although manganese is a low-cost constituent, MnO_2 cathodes tend to lose capacity quickly. Research is directed at understanding the reasons for the fade and developing methods to stabilize this material, as well as evaluating novel forms of MnO_2 cathodes.

4. ***Advanced Diagnostics*** are essential to investigate life-limiting and performance-limiting processes in batteries. We use post-test analyses and spectroscopic and microscopic techniques to investigate morphology, structure, and compositional changes of electrode materials. These provide better understanding of electrode surface processes, and permit detailed investigation of the Li/polymer interface.

5. Sophisticated ***Modeling*** is required to support Tasks 1-5. This effort brings physical understanding to complex interactions through the development of comprehensive phenomenological models. Models are being advanced to elucidate the failure mechanisms of Li battery components and to understand the mechanisms for thermal runaway.

The Long-Term Battery Research activity is now in the process of redefining its baseline systems, and leading candidates are (See Figure IV-1):

1. A high-energy cell with a $LiNi_{1/3}Mn_{1/3}Co_{1/3}O_2$ cathode (called 123 or one third), $LiPF_6$/PC-EC-DMC electrolyte, and a carbon-coated graphite anode. This is regarded as the next generation of the existing baseline system. It contains a cathode that is less expensive and can also provide higher energy than the Gen 2 cathode, the lower-cost PC-containing electrolyte is possible due to the amorphous carbon coating that prevents anode exfoliation.

2. Continued work on the $LiFePO_4$ system, but focused on PC-EC-DMC instead of a gel electrolyte. It is believed that significantly improved materials can be developed through the use of a liquid electrolyte, without the complications of a gel. This could be regarded as a moderate-energy, low-voltage system that is inherently stable and low cost.

3. A high-rate liquid-electrolyte/spinel system paralleling work in the Applied Battery Research activity to develop a low-cost high-power battery.

A website for the Long-Term Research activity is located at http://berc.lbl.gov/BATT/BATT.html.

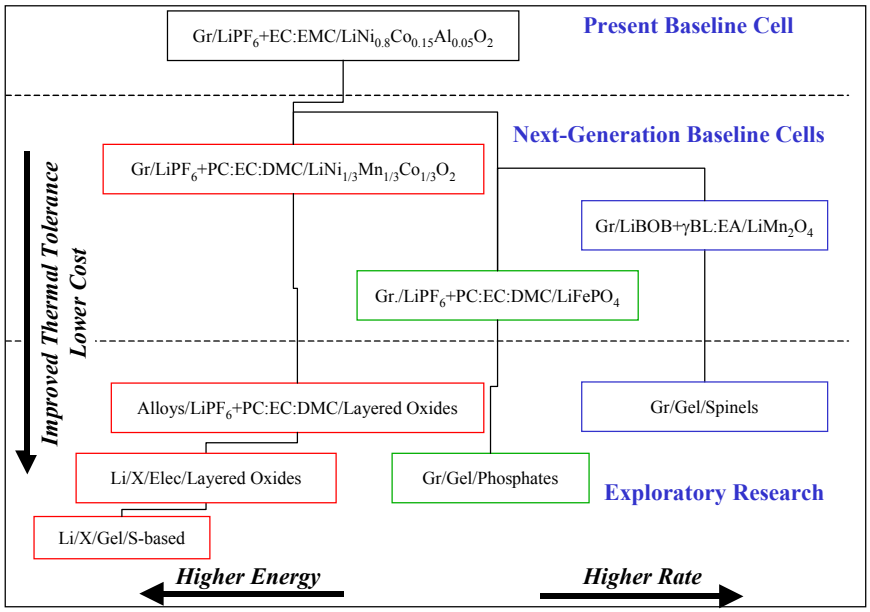

Figure IV-1. Overview of BATT Chemistries

IV.A Task 1 – Cell Development

Objectives

- Understand the failure and degradation modes in the baseline systems.
- Synthesize and evaluate alternative electrode materials and support cell development through structural characterization of electrode components before, during, and after cycling. Specifically, synthesize low-cost graphite anodes and $LiFePO_4$ cathode materials for Lithium-ion polymer cells.
- Investigate inexpensive, self-actuating overcharge protection mechanisms.
- Determine the cycle life and self-discharge rates of Lithium-ion polymer cells from 0°C to 55°C and investigate interfacial phenomena at the anode/separator and cathode/separator interfaces in polymer cells.

Approach

The testing of novel materials in a standard cell with preset protocols provides the ability to associate new battery components and additives with the diagnostic evaluation of failure modes. Components developed in Tasks 2, 3, and 4 are incorporated into a standardized cell and tested to determine cell capacity, energy, power, and lifetime characteristics. Cell components are then delivered to the diagnostics team.

Some of this task's specific activities include synthesizing and coating electrodes (both anode and cathode) with low-cost materials, and using these materials in prismatic cells. Additional work is focused on gel polymers, as well as studies of pressure effects and interfacial phenomena at the polymer/electrode interfaces.

Another activity during the past year was to determine the primary causes of capacity and power fading by correlating them with changes in the composition and structure of electrode materials. Techniques employed include XRD, vibrational spectroscopy, and electroanalytical testing.

Finally, work was done on developing an internal overcharge protection mechanism based on an electrolyte or separator component that internally shorts an overcharged cell.

All of the activities within this task are focused on the USABC goals of achieving a specific power of 300 W/kg, and a 10 year life with less than 20% capacity fade.

Accomplishments

Development of the Natural Graphite / $LiFePO_4$ Cell: A considerable investment in $LiCoO_2$ cathodes has been made over the past 10 years. However, lower-cost cathode materials are required for many applications, including EVs and HEVs. Recently, $LiFePO_4$ (Figure IV-2) was investigated intensively as a potential cathode material for Lithium-ion batteries because of its low cost, stability, and the associated safety. In FY2003, the performance and failure modes of the low-cost baseline

cell containing natural graphite and $LiFePO_4$ electrodes were studied and several avenues for improving the cycle life and power capability were investigated.

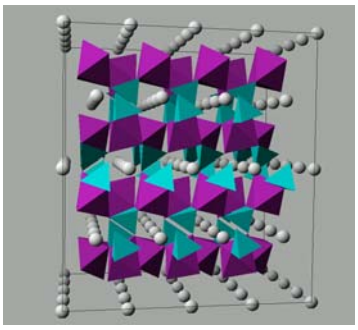

Figure IV-2. $LiFePO_4$ structure

Early testing of cells with both gel and liquid electrolytes revealed several issues with capacity fade during 100% DOD cycling at C/2. In addition, the power capability of this cell was low, in large part due to the low conductivity of $LiFePO_4$. Diagnostics from disassembled cells revealed that capacity fade was due to increases in the impedance of both electrodes (Figure IV-3), anode structural degradation, and a larger-than-expected loss of cyclable Li, due to instability of the anode SEI. The degradation of the Mag-10 anode was worse in pouch cells containing $LiFePO_4$ cathodes than in those containing $LiNi_{0.8}Co_{0.15}Al_{0.05}O_2$ suggesting a negative influence of the $LiFePO_4$.

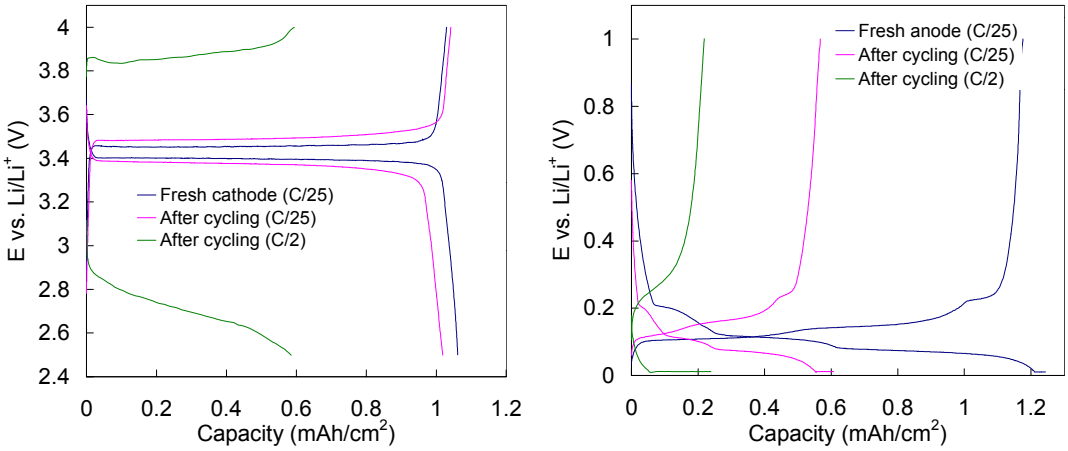

Figure IV-3. Cathode (left) and anode (right) half cell cycling

Several avenues for improvement of the capacity retention of this cell were evaluated, including the addition of vinylene carbonate (VC), the improvement of anode conductivity and the oxidative treatment of the natural graphite. The addition of VC was successful in improving both the coulombic efficiency and capacity retention (Figure IV-4). In addition, VC added to PC-based electrolytes was found to prevent graphite exfoliation that normally occurs.

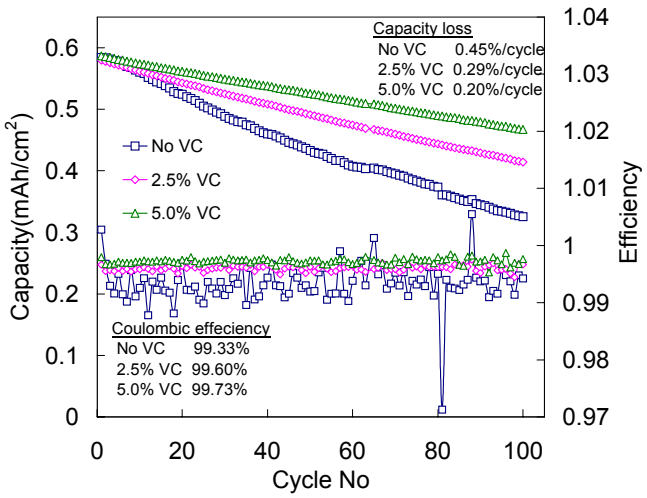

Figure IV-4. Addition of VC Improves both cyclability and coulombic efficiency.

The dependence of the impedance and high-rate utilization of the $LiFePO_4$ cathode on the nature and content of the conductive carbon added to the cathode was examined with a series of cathodes supplied by Hydro-Québec. Utilizing an optimal carbon content and a carbon-coated current collector, the impedance of the cathode was lowered by an order of magnitude to values close to those required for a high-power application. Specifically, the results indicated that 6% carbon provides a good compromise for energy and power, while still achieving a reversible capacity of 65% at 2C rate and 62% at 3C rate, Figure IV-5.

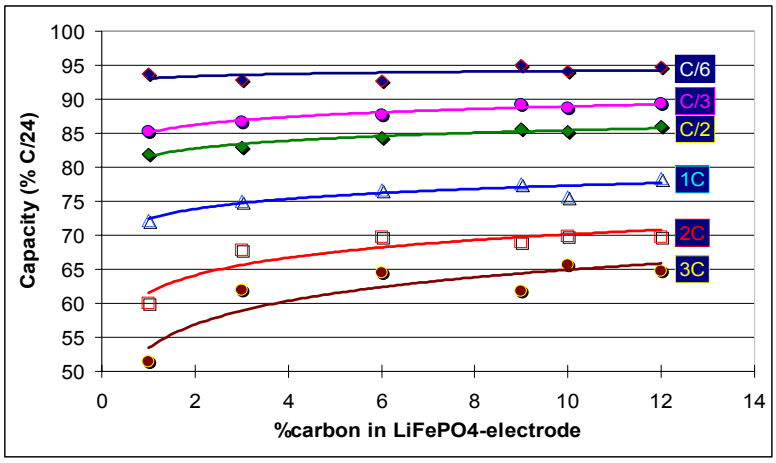

Figure IV-5. Affect of carbon content on iron phosphate electrode performance

In addition, the carbon-coated current collector showed much improved cell cyclability, as seen in Figure IV-6.

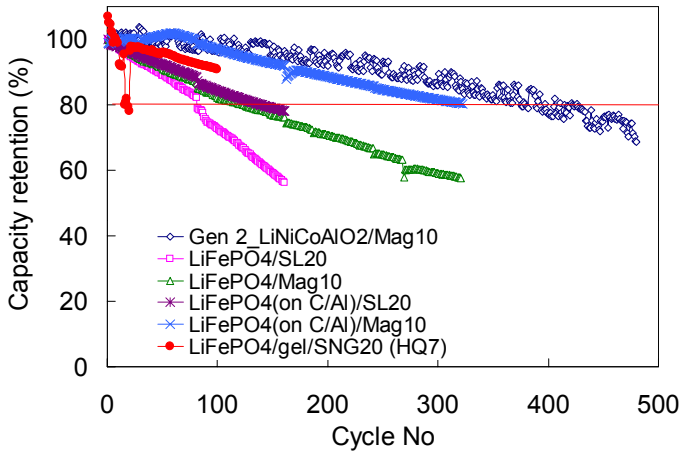

Figure IV-6. $LiFePF_4$ with carbon coated aluminum

The room-temperature performance and cycle life of two $LiFePO_4$ cathode/natural graphite anode cells have been benchmarked against the USABC goals as shown in Table IV-1. The first cell contains an SL-20 (Superior Graphite) anode, a Celgard separator, and a liquid electrolyte (1M $LiPF_6$/EC-DEC). The second cell contains a Hydro-Quebec (HQ) purified spherical natural graphite (SNG20) anode and a gel separator with 1.5M $LiBF_4$- EC:γBL (1:3). One common issue with gel polymer electrolytes is their relatively poor low-temperature performance. Figure IV-7 shows that the performance of this cell decreases significantly below room temperature.

Table IV-1. Comparisons of LiFePO4/NG Low-Cost Baseline Cells

	Units	USABC Mid-Term	USABC Long-Term	HQ Gel	LBNL Liq.
Power Density[13]	W/l	250	600	523	2852
Specific Power, Dischg	W/kg	150	400	282	1018
Specific Power, Regen[14]	W/kg	75	200	576	1788
Energy Density	Wh/l	135	300	89	150
Specific Energy	Wh/kg	80	200	48	54
Cycle Life[15]	cycle	600	1000	222	200
Cell Weight	mg/cm^2			27	44
Theor. Capacity	mAh/cm^2			0.82	1.3

[13] 18s, at 80% DOD
[14] 10s at 20% DOD, 3. cycles to 20% capacity loss during C/2 (100%DOD) cycling
[15] Cycles to 20% capacity loss during C/2 (100%DOD) cycling

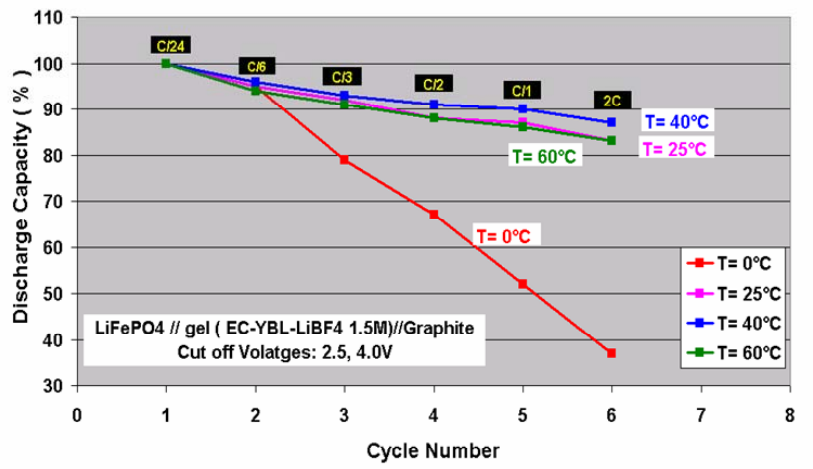

Figure IV-7. Performance vs temperature, low-temperature limitations

The ASI of the liquid cell was approximately 44 Ω-cm^2 compared to 250 Ω-cm^2 for the gel cell. Both cathodes contain carbon-coated current collectors, however, the LBNL current collector is significantly rougher than that used by HQ. This appears to yield much lower contact resistances between the active layer and the Al. The ASI in the liquid cell is also lower because of the higher conductivity of both the separator and the electrolyte.

The cycle-life of both cells is approximately 200 cycles. Electrochemical diagnostics reveal that this fade is due to a side-reaction in the cell, possibly the dissolution and reformation of the SEI layer on the surface of the graphite. For the different sources of natural graphite, this reaction was found to increase in the order Mag-10 (Hitachi) < SNG20 (HQ) < SL-20 (Superior Graphite). More diagnostic analyses of the anodes will be necessary to further understand the source of the instability.

Comparison of $LiFePO_4$ from Different Labs: A comparison was carried out on six different sources of $LiFePO_4$ with the aid of a computer model to help account for the differences in active material loading and cathode porosity. Fitting of the variable-rate discharge data to determine the two most appropriate particle sizes and conductivity for each cathode revealed that the HQ cathode showed the best high-power performance due to the high solid-phase conductivity. It has been shown that poor utilization results when the mean $LiFEPO_4$ particle size is greater than 20 μm, (Figure IV-8).

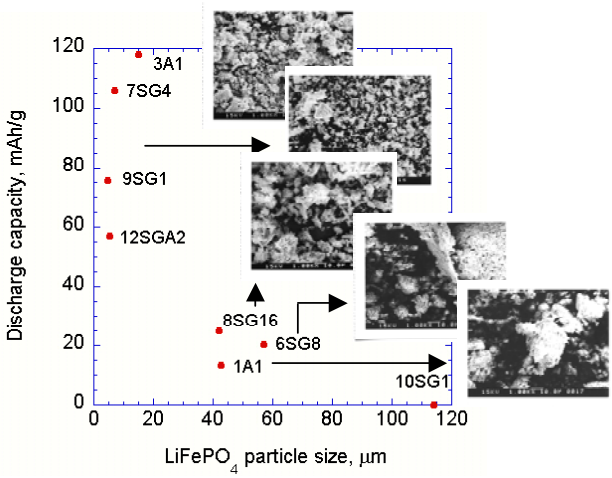

Figure IV-8. Capacity of $LiFePF_4$ as a function of particle size

Moderate-rate utilization of the active materials was best for the MIT cathode, due to its extremely small and narrow particle size distribution. All of the $LiFePO_4$ cathodes showed excellent capacity stability when cycled at C/2 against a Li counter electrode. See Table IV-2 for a summary of the results on these cathodes.

Table IV-2. Comparison of Different $LiFePF_4$ Cathodes

Cathode[16]	Source	Carbon (%)	Loading (mg/cm^2)	Ohmic R (Ω-cm^2)	Capacity (C/25)	5C ret
LFP_6	U.d'Montreal (Al)	8	7.1	195	147	13
LFP13a	U.d'Montreal (c-Al)	8	7.1	34	167	66
LFP10	SUNY, ground w/ C	8	7.3	120	107	10
LFP-M1[17]	MIT, Zr-LiFePO4	10	3.5	62	151	70
LFP14a	U. Waterloo	13	8.2	82	137[18]	30

Overcharge Protection: This work addresses inexpensive, effective overcharge protection that does not compromise the energy and power density. Effective overcharge protection becomes increasingly indispensable as the use of Li battery cell stacks in vehicles approaches reality.

It has been shown that electroactive polymers whose conductivity depends upon their state of charge can provide excellent overcharge protection in Li batteries. Using thin films of these polymers, we are able to visualize the potential profile across a separator containing the polymer. The result is a reversible, self-actuating, low-resistance internal shunt that allows overcharge currents to pass through a cell without damaging the components, maintaining the discharge capacity and allowing the rest of the cell stack to operate normally.

[16] All electrodes have approximately 10% PVdF and 77-82% active material.
[17] Electrode prepared at MIT, all others prepared at LBNL.
[18] Waterloo sample may perform better with less binder.

The initial proof of concept used Li-TiS_2 cells containing separators modified by poly-3-butylthiophene. The potential of an unprotected cell rose rapidly at the end of charge to more than 4V, and the subsequent discharge capacity was severely reduced. In a protected cell, the cell potential rose to approximately 3.2V and held at this value indefinitely due to the shunting effect of the polymer. As a result, the discharge capacity of the protected cell was preserved, and its behavior under normal cycling conditions was largely unaffected by the polymer. We have recently extended the onset potential for the internal short to 4.0 V through the use of Poly (3-butylthiophene) (P3BT) polymers and structural modifications, Figure IV-9. This has allowed demonstrating overcharge protection for 3 V $LiMnO_2$ and 3.5 V $LiFePO_4$ cells. It is expected that further improvements will lead to protection for 4 V $LiCoO_2$ and $LiNiO_2$ cells.

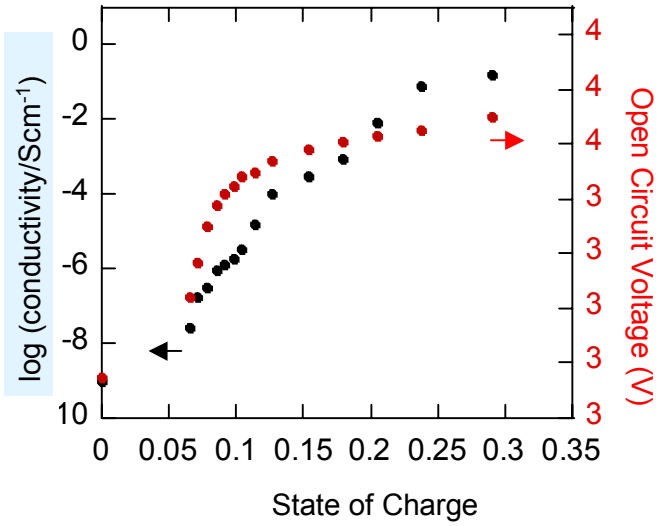

Figure IV-9. Conductivity vs SOC of P3BT

A model has been developed to understand how this overcharge protection works. Essentially, the cell is transformed from a battery into a resistor whose resistivity varies with position across the separator. The resistor is then transformed back into a battery after the charging current is turned off. Figure IV-10 shows the affect of the polymer on the cell voltage during an overcharge condition. The simulations show that the polymer's degree of oxidation varies across the separator, being more oxidized (and thus more conducting) closer to the positive electrode, and confined to the neutral (insulating) state in a submicrometer-thick region adjacent to the negative electrode. The result is that the cell voltage is constant during overcharge, and this voltage depends *only* on the properties of the polymer short and is independent of the positive electrode chemistry. The model matches experimentally observed trends of the effects of polymer conductivity and current density. The model has helped to identify which parameters control the behavior of the short, to allow rational design and selection of materials.

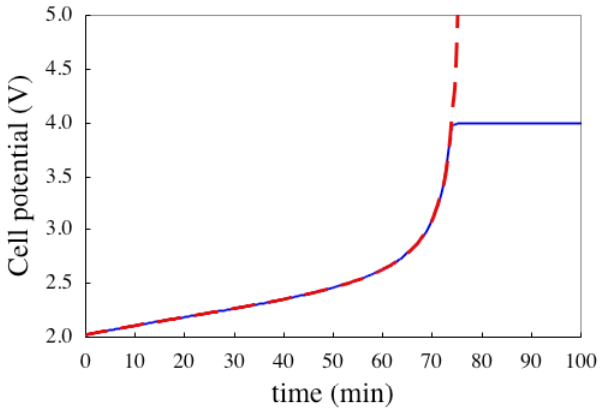

Figure IV-10. Cell voltage during simulated overcharge

Gel Electrolyte Characterization: Polymer and gel-polymer electrolytes are potential candidates for use in EV and HEV applications due to improved mechanical stability and safety. Despite significant improvement of transport properties however, the ionic conductivity and transference numbers of the current polymers are still too low for viable Li batteries.

A recent study conducted on the effect of the one polymer used to develop a gel electrolyte, x% polymer-(1-x)%EC-γBL-1.5M LiTFSI. Figure IV-11 shows that the vapor pressure is lower when the amount of γBL is reduced. At high temperature (100-125°C), the vapor pressure decreases when the polymer content increases. This effect helps improve the safety of the battery.

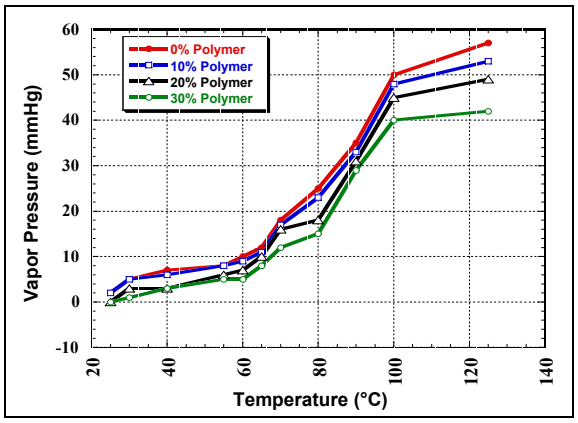

Figure IV-11. Vapor pressure of the gel polymer as function of temperature.

TGA was used to investigate the weight loss with different polymer ratios in the gel. The polymer ratios selected were 100%, 30, 20 and 10% by weight. The results in Figure IV-12 show the weight loss as a function of polymer content. An increase in the polymer content resulted in a decrease in the weight loss of the gel.

In the second set of experiments, the gel samples were held at a fixed temperature (60°C) for 3 hours. After that time, the weight loss of the different gel compositions (10, 20, 30 weight %) was comparable (17.3%) independent of the polymer ratio.

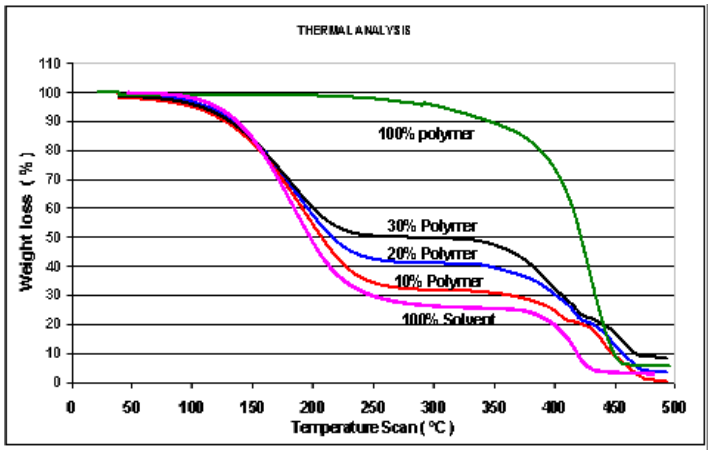

Figure IV-12. TGA of the gel polymer as function of temperature.

Optimization studies of the new HQ gel electrolyte indicated that good mechanical properties are obtained at a 10/90 polymer/liquid weight ratio.

IV.B Task 2 – Anodes: Non-Carbonaceous Materials

Objectives

- Replace carbon with an inexpensive anode material that will be compatible, in particular, with low-cost manganese oxide cathodes.
- Develop a low-cost and safe composite anode plate with no intrinsic irreversible capacity loss (ICL) and with higher energy density than the current carbonaceous anodes. Improve the kinetics of the Li insertion-extraction process in the composite anodes.
- Design a program to identify, understand, and mitigate the capacity loss upon cycling of simple alloy systems. This will result in the ability to understand the cause of capacity fade in pure tin and to propose a means of remediating that fade.

Approach

The approach for this task is to search for and develop inexpensive intermetallic electrodes that provide an electrochemical potential a few hundred mV above that of metallic Li, with capacities of 300 Ah/kg and ~2000 Ah/l (graphite theoretical capacities are 372 Ah/kg and 818 Ah/l). The approach includes investigations of standard $Li_4Ti_5O_{12}$ and electronically-conducting Li-, Mg-, and Al-doped $Li_4Ti_5O_{12}$ anodes against high-voltage layered and spinel cathodes.

Specifically, composite anodes have been prepared *via* reactive mechano-milling to eliminate large ICLs of metal-oxide anodes. Vanadium and manganese oxides, pure Al, and tin-containing materials, such as $MnSn_2$ have been investigated. Pure Sn anodes appear to cycle better than $MnSn_2$.

All of the activities in this area are geared towards exceeding the 10-year life goal, low capacity loss (< 20%), good safety and high reliability (no toxic and flammable gas formation).

Accomplishments

During FY 2003, efforts were made to improve the electrochemical capacity and cycle life of Sn- and Sb-based intermetallic electrodes that operate by Li insertion/metal displacement reactions. Although the capacity goal could be achieved, the long-term cycling stability of the electrodes was strongly dependent on the voltage window selected for the electrochemical experiments. Although antimony-based electrodes can meet the capacity goal (MnSb and Ag_3Sb systems), the capacity fade after approximately 40-50 cycles and the ICL severely limits the cycle life of these electrodes (Figure IV-13). Si- and Sn-based electrodes are now being investigated because they offer a lower potential compared to Sb and show promise when combined with graphite.

Preliminary experiments of composite systems such as Si-Sb and Si-C have demonstrated superior performance when graphite acts as a buffer for the volume expansion of the metal/Si component. Figure IV-14 shows the excellent cycling stability that was achieved from a Li/Si-2C (i.e. the Si:graphite ratio = 1:2) cell when the capacity of the electrode was limited to 500 Ah/kg during cycling between 0.5 and 0.0 V vs. Li^0. (This cell failed abruptly at 52 cycles, the reason for which is unknown.) Li/Si-2C cells that were cycled between these voltage limits without imposing a capacity

restriction decayed rapidly. Because of the promising data shown in Figure IV-14, a major effort will be made during FY2004 to exploit and optimize Si-graphite and metal-graphite composite electrode systems.

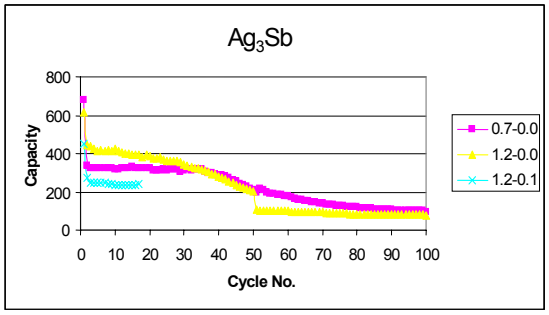

Figure IV-13. Capacity vs. Cycle No: Li/Ag_3Sb

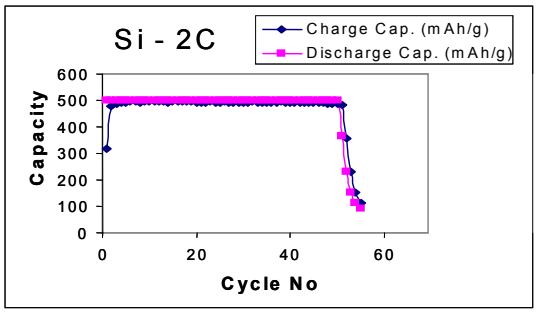

Figure IV-14. Capacity vs. Cycle No: Li/Si-2C

The cycling and structural stability of $LiCu_2Sb$ anodes have also been investigated. The cycling behavior is shown in Figure IV-15, the electrode delivers a capacity close to the theoretical value (323 Ah/kg). The ICL on initial cycle is common to many metal/intermetallic electrodes

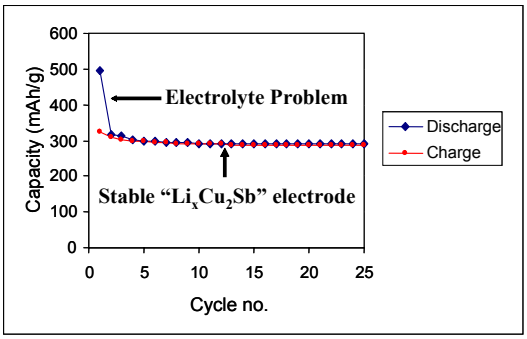

Figure IV-15. Cycling behavior of $LiCu_2Sb$ anode

Metal oxides are also being explored as alterative negative electrodes to graphite. These include the electronically conducting Mg- and Al-substituted Li spinels that are being evaluated against high-potential (>4.5 V) spinel and layered lithium-manganese-nickel-oxide electrodes. We have initiated

a theoretical study of low-potential Li_2MO_2 systems to explore the possibility of using lithiated $LiMO_2$ compounds, notably lithiated $LiVO_2$, as insertion electrodes. First principles density-functional-theory calculations are being performed to determine the voltage of such reactions and to predict which of the following possible reactions would be most favorable:

1) $Li + LiMO_2 \rightarrow Li_2MO_2$
2) $Li + LiMO_2 \rightarrow Li_2O + MO$
3) $3\ Li + LiMO_2 \rightarrow 2\ Li_2O + M$

Tin-Based Anodes. The behavior of bulk tin foil is being studied, where there is no need for conductive diluent or binder, and therefore minimum likelihood of side reactions. This will allow a better understanding of what causes capacity fade in metal anodes. The electrochemical cycling of the tin foil has been compared with electrodeposited Sn and Sn_2Mn. The Sn foil shows equivalent or better behavior than the other electrodes. The Sn foil, even at cycling rates of $3mA/cm^2$ is comparable to Cu_6Sn_5, formed *in situ* by heating a tin film electrodeposited on copper.[19] The phases formed, their grain size, and the cell impedance have been measured.

An analysis of recent data, shown in Figure IV-16, shows that after a break-in period, the amount of lithium inserted into the tin foil is equal to the amount of lithium removed in the previous cycle. This indicates that freshly formed tin is essentially inert in the electrolyte used. Capacity fade therefore must be associated with the lithium-tin phase after lithium insertion. Two possible options are: (1) some of the lithium in the tin reacts irreversibly with the electrolyte, thus becoming unavailable for subsequent use, and (2) some of the Li_xSn alloy becomes physically and electronically detached from the electrode so it can no longer participate.

To help determine the impact of the electrolyte salt on the capacity fade, the tin foil in a LiBOB EC/DMC electrolyte cell has also been cycled. The results are shown in Figure IV-17. Tin appears to cycle well in this electrolyte; the smaller measured capacity may be associated with the rate used, $1\ mA/cm^2$, which is high for this relatively low-conductivity salt.

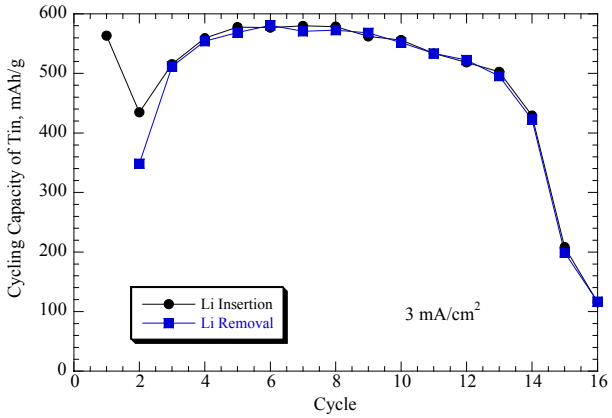

Figure IV-16. Cycling capacity of tin foil in $LiPF_6$, EC/DMC electrolyte

[19] N. Tamura et al, *J. Power Sources*, 2002, 107:48.

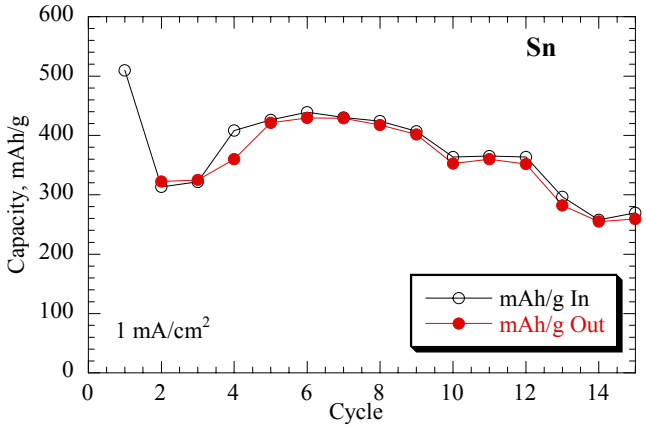

Figure IV-17. Cycling capacity of tin foil in LiBOB, EC/DMC electrolyte.

Anode Safety Studies: The safety of a lithiated graphite anode has been revisited. One of the common causes of cell failure is gas evolution from the graphite anode during Li intercalation. Figure IV-18 shows a correlation between this gas evolution and the mean particular size in the anode.

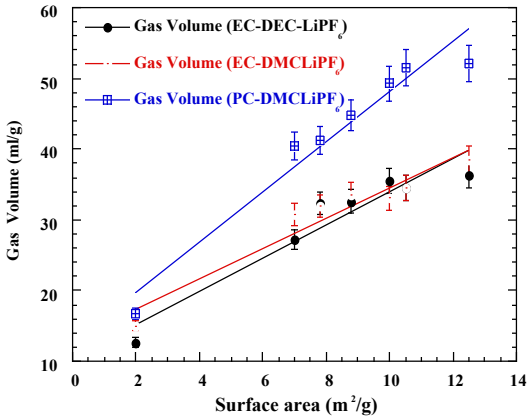

Figure IV-18. Correlation between gas generation and anode surface area

Recently, we have found that the lithiated graphite anode (LiC_6) reacts violently with electrolyte when the SEI layers are destroyed at temperatures >120°C. Therefore, the development of a safer composite anode is being focused on. Based on previous success on prelithiation of inorganic compounds we have investigated a transition metal phosphide-halide compound as a new anode material. The most practical system is based on copper phosphides iodide with a theoretical reversible capacity of 665Ah/kg. The charge-discharge process for the compound is shown immediately below.

$$CuP_aI_b + (3a + b)Li \longrightarrow [aLi_3P + bLiI + Cu]_{composite}$$

$$\Downarrow\Uparrow$$

$$Li_bI_bCuP + 3aLi^+ + 3a(e)^-$$

The ICL of copper phosphohalide is reduced to less than 5% by mechanochemistry. In addition, the large hysteresis usually observed for oxides and nitrides is reduced due to the good ionic and electronic conductivity of the composite matrix anode.

It is commonly observed that the first charge cycles of anodes and cathodes in Lithium-ion cells are different from their subsequent cycles. In some cases, it requires several cycles to stabilize the electrodes. Therefore, construction of a balanced cell based on the initial capacity of electrode materials becomes more complicated. In addition, during initial cycles, parasitic reactions occur which may reduce the cell's cycle life and cause safety problems. The focus has been on the development of a process to stabilize composite anodes to provide a safer electrode with no ICL and no electrolyte decomposition.

The process involves mechanomilling of anode materials with Li or Li-containing precursors, according to the following formulations:

$$MO_x + 2xLi \xrightarrow{\text{Mechanomilling}} [xL_2O + M]_{composite} \underset{y(-Li^+ - e^-)_{discharge}}{\overset{y(+Li^+ + e^-)_{charge}}{\rightleftharpoons}} (Li_yM)_{active\ phase}$$

$$MN + 3Li \xrightarrow{\text{Mechanomilling}} [Li_3N + M]_{composite} \underset{Y(-Li^+ - e^-)_{discharge}}{\overset{Y(+Li^+ + e^-)_{charge}}{\rightleftharpoons}} (Li_yM)_{active\ phase}$$

This process allows different degrees of lithiation of anode materials. The prelithiation can proceed to eliminate only the first cycle irreversibility or can include excess Li for stabilization of the cathode plate as well.

Several oxides and nitrides have been studied, using the mechanomilling process. Anode plates were made from the above composites and tested in a conventional but optimized multi-blend carbonate based electrolyte, (EC-DMC-PC, 50:30:20, containing 0.8M $LiPF_6$). Recent results for the electrochemical charge discharge cycles for stabilized SnO, SnO_2, Sb_2O_3, CoO, CuO, Ge_3N_4 and Cu_3N indicate that the lithium oxide coating provides a more protective film than the lithium nitride films.

Publications and Presentations

- S. Yang, P. Y. Zavalij and M. Stanley Whittingham: "Anodes for Lithium Batteries: Tin Revisited**,"** *Electrochem. Commun*. 2003, **5**: 587-590.
- P. Y. Zavalij, S. Yang and M. Stanley Whittingham: "Structures of potassium, sodium and lithium bis(oxalato)borate salts from powder diffraction data," *Acta. Cryst*. **B59**, in press (2003).
- S. Yang, P. Y. Zavalij and M. Stanley Whittingham: "Anodes for Lithium Batteries: Tin Revisited,**"** presented at Solid State Ionics Meeting, Monterey, California, July 2003 and at Arcachon, France, September 2003.

IV.C Task 3 – Electrolytes

Objectives

- Determine the feasibility of using Li metal electrodes with organic electrolytes and investigate operating conditions that prevent dendrite growth.
- Determine the limitations on Lithium-ion transport in polymer electrolytes and composite electrodes, develop new materials capable of ambient-temperature operation with Li metal, and study the influence of polymer structure on ion complexation, dynamics and transport properties of polyether-based polymer electrolytes.
- Determine the stability limits of organic electrolytes in high-voltage cathode materials (*e.g.*, 4 V) and develop materials and methods to increase stability.
- Develop composite polymer electrolytes that are low-cost, have high conductivities, impart electrode-electrolyte interfacial stability, and yield long cycle life.

Approach

Lithium solid polymer electrolytes (SPE) are potential candidates for use in EV and HEV applications due to processing ease, mechanical stability and safety. Despite significant improvement of transport properties of SPEs over the last two decades, ionic conductivity and transference numbers are still too low for high-power Li batteries.

In this task, solid polymers that show promise as electrolytes have been characterized by methods such as neutron scattering, dielectric relaxation spectroscopy, and light scattering to obtain new insights into the rate-limiting transport processes. The purpose of this diagnostics work is to obtain a fundamental understanding of charge transport in polymers through in-depth characterization.

Surface-functionalized fumed silica fillers have also been used to determine the effects of filler type and concentration on interfacial stability and cell cycling. These electrochemical characteristics with mechanical properties and materials chemistry (*e.g.*, silica-type or PEO-type). Data collected include elastic and viscous moduli, ionic conductivity, transference number, Li cycling efficiency, Li-electrolyte interfacial resistance, and full-cell cycling capacity using 3-V cathodes.

Also, new salts have been synthesized using methodologies developed over the last 15 years.[20] SPEs were prepared from crosslinked low-MW polyethylene glycol (PEG) and also non-crosslinked PEG for comparison. Transport properties were measured using EIS combined with restricted diffusion, DC polarization, and concentration cell techniques.

This task has also employed ab-initio quantum-chemistry calculations to develop classical force fields for polyether/$LiBF_4$. Next, molecular dynamics simulations were used to investigate the influence of polyether structure, strength of the polyether-Li and Li-anion interactions, and the barriers to conformational isomerization reactions, and their impact on ion transport.

[20] D. DesMarteau, *J. Fluorine Chem*. 1995, **72**, 203-208.

The goals that these activities are aiming to satisfy include 10 year life, <20% capacity fade over a 10-year period, 1000 cycles, operating environment –40 to 65°C, specific energy >170 Wh/kg, specific power >300 W/kg, <$150/kWh @ 20K/year.

Accomplishments

The limitations of PEO as a polymer electrolyte in Li ion batteries are well-established. In an attempt to combine the positive attributes of PEO (which include the ease of manufacture, and good mechanical properties) and overcome its limitations (primarily low conductivity), studies have begun for nanostructured polymer electrolytes obtained from PEO-PI block copolymers.

A diblock copolymer system has been synthesized with the goal of increasing the efficiency of ion transport in the polymer system. It is possible to change parameters such as the chain length (i.e. molecular weight) of either block and the volume fraction of one block relative to the other. It has been shown, using DSC, that the PEO chains are stable at room temperature up to three months and that the crystallization temperature is reduced from 50°C to approximately -30°C (Figure IV-19). This is a major milestone because the confinement of the PEO chains and lack of crystallization at ambient temperatures will result in better ionic conductivity.

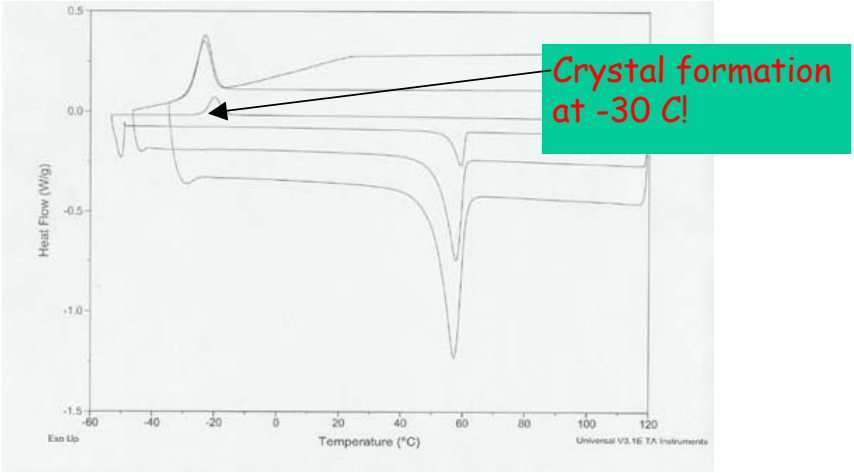

Figure IV-19. DSC of diblock copolymer

Small Angle X-ray Scattering (SAXS) has been used to confirm the presence of PEO cylinders in our system. The existence of cylinders in the polymer electrolyte is a necessary but not sufficient condition to achieving the required goals. It is crucial that these cylinders be aligned orthogonal to the electrodes to obtain the enhanced conductivity. Next, AFM was used (Figure IV-20) to show that the cylinders of spin-coated IEO when doped with salt do align perpendicular to the surface.

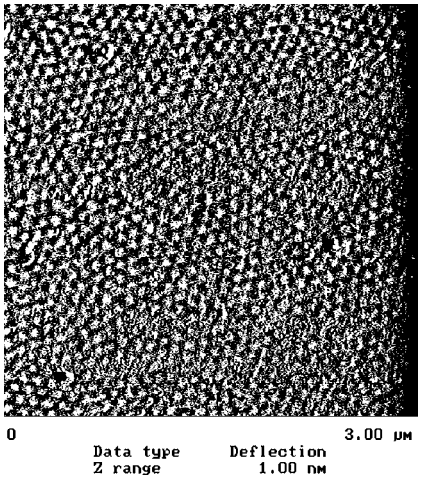

Figure IV-20. Structure of spin-coated IEO[27-9] with salt

Polymer Electrolyte Interface Findings, Control of Dendrite Formation: Experiments are continuing with the collaboration of the modeling group to determine the factors that control dendrite growth. Both transport and mechanical properties, and concentration gradients at both electrodes have been found to be important. Interfacial impedances influence the rate of dendrite initiation, and therefore, the factors which influence this parameter have been investigated.

The interfacial impedance of polymer electrolytes at electrodes increases rapidly as the temperature is decreased. With Li/Li cells, PEO-LiTFSI has the following interfacial impedances: 85°C, 50 Ωcm^2; 60°C, 300 Ωcm^2; 40°C, 3000 Ωcm^2. Similar trends are observed with PEGDME250 and PEGDME500-LiTFSI but the magnitude of the interfacial impedance is ten times lower. These effects can be understood by the interaction of the electrolytes with the electrode surfaces. The high interfacial impedance of high molecular weight polymers at lower temperatures significantly increases the cell polarization to untenable levels. The interfacial impedances may be altered by modifications of the lithium and cathode surfaces.

Polymer electrolytes require an elastic shear modulus of at least 10^6 Pa and a Poisson Ratio of 0.5 to inhibit dendrite growth. Such properties may be obtained by cross-linking the polymer and by the addition of nano-particle fillers. However, the transport properties of the lithium salts are degraded by the addition of fillers and also by dense cross-linking. Since the transport properties of the unmodified polymer electrolytes barely meet the requirements for high-power batteries, the addition of fillers and cross-linking can result in severe concentration polarization. It has been found that fillers with modified surfaces and comb-branch polymer architectures with appropriate cross-linking can provide the desired mechanical strength without a severe impact on the transport properties

It is likely that dendrite suppression at lithium metal electrodes can only be achieved through the use of single-ion conductor electrolytes that remove concentration polarization, are mechanically strong, and do not exhibit high interfacial impedances at electrodes.

TMO Polymer Electrolyte Findings: Linear polymers containing trimethylene oxide (TMO) solvation units, i.e.–O-$CH_2CH_2CH_2$-O, have much higher salt diffusion coefficients than those with

EO solvation units and can sustain current densities of >0.5 mA/cm^2. *A cross-linkable form of linear TMO polymers that has the required mechanical properties has not yet been prepared.*

Comb-branch polymer electrolytes containing TMO units in the side chains but PPO or polyacrylate backbones have lower D_s values than the linear TMO polymers at higher temperatures (60^o and 85^o C) and higher D_s values at low temperatures (25^{o}C). These materials can be cross-linked to give the required mechanical properties but cannot sustain the desired current densities. The propylene oxide and acrylate units in the backbones act as traps for the lithium ions and slow the diffusion rates. *A new backbone is required in order to achieve the full benefits of the TMO solvation units in this architecture.*

Ionene based electrolytes: Members of the ionene series of structure $CF_3SO_2N(Li)[SO_2(CF_2)_xSO_2N(Li)]_nSO_2CF_3$ with x=4 and 6 and n=0,1,3,5, and 17 have been synthesized. Each new salt has been used to prepare solid-polymer electrolytes using high-molecular-weight PEO as host. A complete study focusing on salt structure effects on ionic conductivity has been completed. Salt diffusion coefficients for a series of ionenes with n = 0, 1, 3, 5, 17, and 225 are shown in Table IV-3.

Table IV-3. Salt diffusion coefficients and ionic conductivities for PEO-based SPEs prepared using ionene salts with x=4. EO/Li = 30/1, T = 90^{o}C.

Salt Type	$(D_s \pm \sigma)\cdot 10^{-8}$ (cm^2/sec)	$\kappa \cdot 10^{-3}$ (cm^2/sec)	Li Salt Conc. (wt%)
n = 0 (LiTFSI)	4.2 ± 0.8	1.33	17.9
n = 1	1.9 ± 0.7	0.20	19.4
n = 3	1.6 ± 0.3	0.24	20.2
n = 5	1.3 ± 0.3	0.34	20.5
n = 17	0.5 ± 0.06	0.58	20.8
n = 225	0.4 ± 0.08	0.04	20.8

The observed systematic reduction of diffusion coefficient with increasing anion chain length is consistent with the expectation that the anion contribution to ionic transport will be diminished as the anions become larger. These measurements will be used together with concentration-cell measurements to calculate Lithium-ion transference numbers for each SPE.

Fumed Silica Doped Polymers: Studies of the effects of ceramic nanoparticle filler material (silica, alumina and carbon black) on the transport and mechanical properties of composite electrolytes have shown that the fillers reduce the conductivity and diffusion coefficient while increasing the mechanical moduli. The behavior is consistent with restriction of the segmental motion of the polymer by the filler (which also increases the electrolyte impedance at the electrode interface). The magnitude of the effects depends on the nature of the polymer-particle interaction. Exposure of the composites to atmosphere results in increases in conductivity, which strongly suggests that the improvements are due to water bound to the filler particles.

However, this research activity has also established that fumed silica-based composite electrolytes with low-molecular weight (MW) PEOs exhibit conductivities exceeding 10^{-3} S/cm at 25ºC (Figure IV-21), appear to stabilize the Li/electrolyte interface, and may suppress Li dendrite growth. It has

also been found that the addition of fumed silicas into low-MW PEOs significantly improves charge-discharge cycle performance, coulombic and energy efficiencies, rate capabilities, and self-discharge performance of Li/V_6O_{13} cells. Finally, fumed silica improves the rheological properties of high-MW polymer electrolytes.

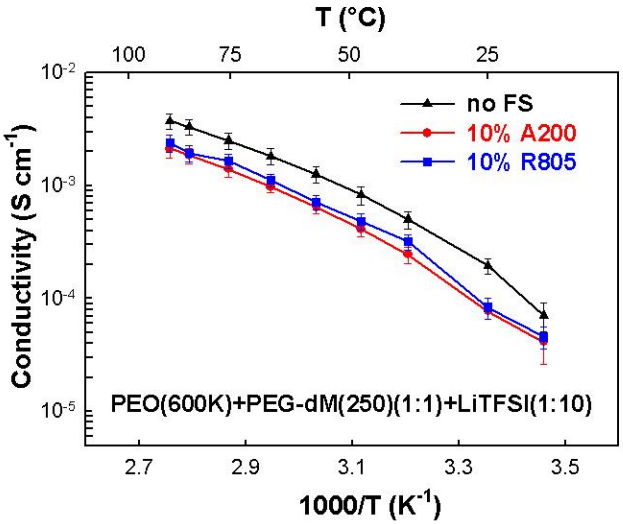

Figure IV-21. Conductivity vs 1/T of $P(EO)_{10}LiTFSI$

Dynamic rheological results of mixed-MW polymer electrolytes, which were measured between 80 and 25°C, have been obtained. The addition of fumed silica to the electrolyte changes its rheological response under shear in that the material becomes more elastic at all temperatures. These trends show the reinforcing effect of the nanoparticles, even at high temperatures where the polymer is in the melted state. As expected, the conductivity increases considerably in the same temperature range where a decrease in the elastic modulus is observed.

Half-cell and full-cell cycling results have been collected at 65°C for mixed-MW polymer electrolytes. The cell voltage increases considerably for the electrolyte without fumed silica, whereas the cell voltage is more stable for the one containing fumed silica. This result suggests that adding fumed silica into mixed-MW polymer electrolytes attenuates lithium dendrite formation and improves the lithium/electrolyte interfacial stability, Figure IV-22. These effects have also been demonstrated for full-cell cycling of $Li/electrolyte/V_6O_{13}$.

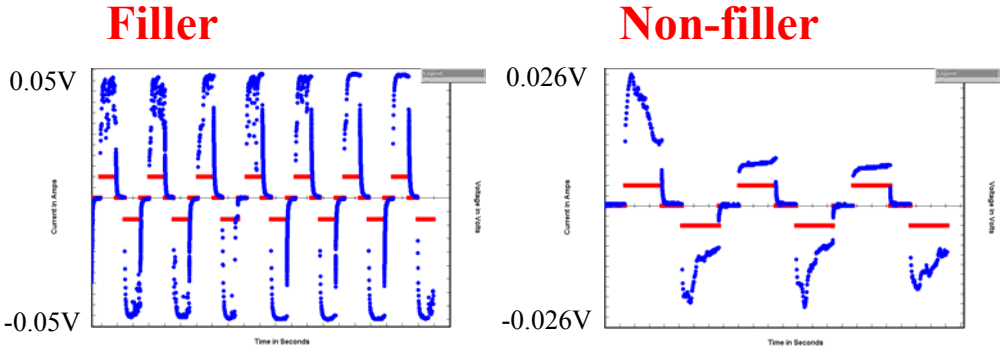

Figure IV-22. Cycling of Li/P(EO)$_{20}$LiTFSI/Li cells, filler inhibits dendrite growth

The effect of fumed silica on aluminum corrosion has been studied as well. Li/electrolyte/Al cells and two types of Al foil (one from Fisher and the other from Celgard) were tested at room temperature. The open-circuit voltage for cells with fumed silica-based gel electrolytes was more stable than that for baseline liquid electrolyte; the current density for gel electrolytes was lower and changed less with increasing potential than that for baseline liquid electrolyte; and the impedance for gel electrolytes was more stable, Figure IV-23. Three possible explanations may exist for the enhanced aluminum corrosion resistance: covering a defect site in the oxide film, scavenging moisture from the electrolyte, and increasing adhesion of salt films on the aluminum surface.

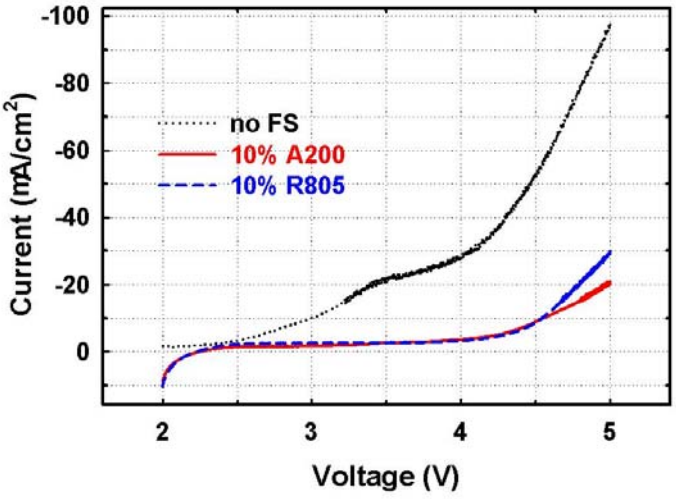

Figure IV-23. Electrolytes with fumed silicas are stable to approximately 4.5 V

Modeling of Advanced Electrolytes: MD simulations of linear PEO(M_w=2380)/LiTFSI, Li:ether oxygen have been performed in order to validate previously developed quantum chemistry based force fields and their ability to predict the Li^+ cation environment, anion and cation self-diffusion coefficients, and ionic conductivity. The Li^+ cation environment was consistent with the results of

neutron scattering experiments.[21] Next, the ion self-diffusion coefficients from MD simulations are compared against the results of pulsed magnetic field gradient NMR experiments, see Figure IV-24. MD simulations predictions are within 25% of the experimental results, indicating that the quantum chemistry based force field is accurate.

Next, the PEO/Li^+/$TFSI^-$ force field was extended to describe the relative conformational energies and barriers between the most stable conformers for the side group termination of the single-ion conductor shown in Figure IV-25. MD simulations have been performed on single ion conductors and gel electrolytes, using the polymer shown in Figure IV-25, similar to the PEPE5 comb-branch polymer used by Dr. Kerr's group, as a matrix. The Li^+ cations and EC molecules were added to the polymer matrix to create a gel electrolyte. Approximately 70% of the Li ions are found to be disassociated in the gel electrolyte. Each Li^+ cation was complexed by approximately 1.8 EC molecules, 1.8 ether oxygen groups, and 0.4 oxygen atoms from the $TFSI^-$ anion. Simulation results indicate that the PEO-based polymer matrix is involved in Li^+ complexation and transport. Because of the complexation of the $TFSI^-$ end groups and PEO-side chains, the Li^+ self-diffusion coefficient is approximately two times smaller than that of the ethylene carbonate molecules. It was found that the conductivity of the gel electrolyte was $8x10^{-3}$ S/cm, which is sufficiently high for use in electric vehicles.

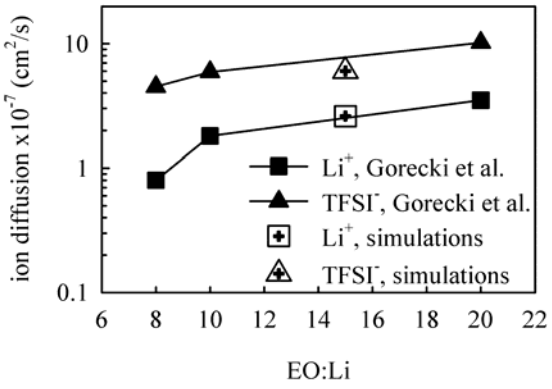

Figure IV-24. The Li+ and TFSI- ion self-diffusion coefficients from MD simulations and experiments.[22]

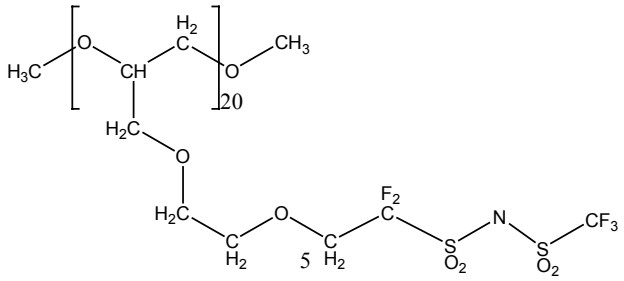

Figure IV-25. Polymer chain used in simulations of single-ion conductor and gel electrolytes.

[21] Mao et al., *Phys. Rev. Lett*., *84*, 5536, 2000
[22] Gorecki et al., J. Phys.: Condens. Matter, 7, 6823, 1997

Five polymers have been investigated as potential hosts for SPE's: PEO, POM, PPO, PTMO, and a copolymer of PEO-TMO. Quantum chemistry based force fields have been developed for all these polymers and their interactions with $LiBF_4$. MD simulations of these polymers doped with $LiBF_4$ were performed at EO:Li=15:1, 393 K

POM melts had the slowest dynamics and lowest binding energies resulting in $LiBF_4$ salting out. The fractions of the uncomplexed or "free" Li^+ were predicted in the following order PEO-TMO/$LiBF_4$ > PEO/$LiBF_4$ > PTMO/$LiBF_4$ > PPO/$LiBF_4$, while polymer dynamics was predicted in the order of PEO ≈ PEO-TMO ≈ PEO ≈ PTMO > PPO which, as expected, mirrors the Li conductivity data. In accord with the parametric studies, the ionic conductivities were predicted in the order: PEO-TMO/$LiBF_4$ > PEO/$LiBF_4$ > PTMO/$LiBF_4$ > PPO/$LiBF_4$, with the difference between PEO-TMO/$LiBF_4$ and PTMO/$LiBF_4$ being similar to the simulation's error bars, *i.e.*, a factor of two. It is concluded that the investigated structural changes of linear polyethers doped with $LiBF_4$ do not result in significant improvements of SPE transport properties suggesting that alternative strategies for design of novel SPEs be investigated.

IV.D Task 4 – Cathodes: Novel Materials

Objectives

- Develop low-cost manganese oxide cathodes to replace $LiCoO_2$.
- Find lower-cost and higher-capacity cathodes, exceeding 200Ah/kg, that are based on benign materials (*e.g.,* manganese oxides, lithium iron phosphates) having electrochemical properties consistent with the USABC goals.
- Evaluate alternative layered oxides as cathode materials for a Lithium-ion battery that operates between Ni(II) and Ni(IV).

Approach

The approach for this task is to search for, characterize, and develop low-cost novel cathodes for Lithium-ion cells. We have focused on composite layered lithium-manganese oxide structures that are represented by the general formula $xLi_2M'O_3(1-x)LiMO_2$ in which M′= Mn, Ti, Zr, Ru and M = Li, Mn, Ni, Co, which are showing excellent promise to replace $LiCoO_2$ as the cathode in Lithium-ion cells. We explore the electrochemical properties of high-potential layered and spinel electrodes against $Li_4Ti_5O_{12}$ and substituted, electronically-conducting $Li_4Ti_5O_{12}$ anodes in 3 V Lithium-ion cells that is expected to be inherently safe.

A second approach is to place emphasis on manganese dioxides, both pure and modified with other transition metals. Cathode materials are synthesized using both conventional solid-state techniques and solution methods. The microstructures and atomic structures of the materials are determined, and electrochemical analysis is carried out in a variety of cell configurations.

The USABC goals being pursued in this work is to achieve a 10-year life with less than 20% fade over that period.

Accomplishments

Composite Cathodes: Preliminary investigations of $xLi_2M'O_3(1-x)LiMO_2$ composite electrodes in which the $Li_2M'O_3$ component (M′=Mn, Ti, Zr) was used to stabilize layered $LiMO_2$ electrode structures, particularly $LiMn_{0.5}Ni_{0.5}O_2$, were undertaken. These electrodes tend to show a relatively large ICL during the initial cycles, but thereafter cycle with good reversibility, and provide a rechargeable capacity of approximately 140 Ah/kg between 4.6 and 2.5 V at room temperature and 160-170 Ah/kg at 50°C. These electrodes can accommodate extra Li to form Li_2MO_2 compounds with remarkable reversibility and without destroying the integrity of the layered structure; this finding has implications for using the surplus Li in Li_2MO_2 structures to combat the ICL at graphite and intermetallic negative electrodes.

Efforts have continued to stabilize $xLi_2M'O_3(1-x)LiMO_2$ electrodes and to reach the targeted capacity of 190 Ah/kg at 50°C. This goal has almost been reached with a Li-$[0.3]Li_2MnO_3$-$[0.7]LiMn_{0.5}Ni_{0.5}O_2$ cell, which delivered 175 Ah/kg at 50°C between cycles 50 and 100 (Figure IV-26). The first 50 cycles were conducted at room temperature yielding a cathode capacity

of 120 Ah/kg. Because of the promise that lithium-manganese-nickel oxides hold, efforts will continue in FY2004 to increase the room-temperature capacity and to reduce the ICL that occurs when cells are initially charged above 4.3 V. By lowering the voltage of these cells to 1.45 V to access a Li_2MO_2-type structure, electrode capacities well in excess of 200 Ah/kg have been achieved.

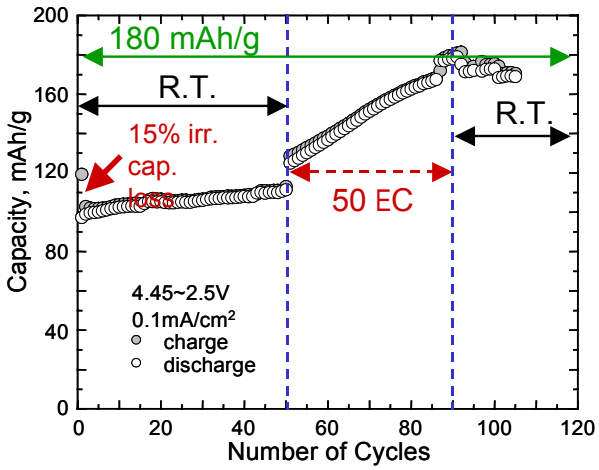

Figure IV-26. Capacity vs cycle number for $0.70LiMn_{0.5}Ni_{0.5}O_2/0.30Li_2MnO_3$

Other Cathodes: It has been determined that layered manganese dioxides can be structurally stabilized, and that their electronic conductivity and cycling can be significantly enhanced by the addition of other transition metals or by the addition of coatings, including Al and Zr. Figure IV-27 shows the effectiveness of conductive coatings for enhancement of capacity at room temperature. However, these cathodes still show unacceptable capacity fade at elevated (50°C) temperatures.

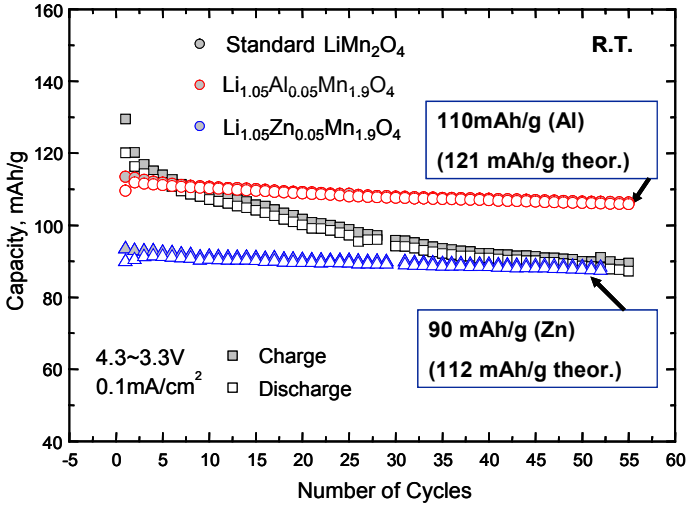

Figure IV-27. Electrochemical Performance of Al- and Zn-doped Spinel Electrodes at room temperature

An evaluation of $LiFePO_4$ as a low cost cathode has been completed, and it has been shown that hydrothermal synthesis is not a viable approach. It has also been shown that vanadium oxides can be stabilized by the addition of manganese ions to attain capacities greater than 200 Ah/kg. In summary:

- $LiFePO_4$: > 120 Ah/kg for 100 cycles at 1 mA/cm^2.
- Layered $Li_xCo_zNi_yMn_{1-y-z}O_2$: 180-200 Ah/kg for 5 cycles
- Layered $A_zMn_{0.1}V_2O_5$ (A= NH_4 or TMA): ≥ 200 Ah/kg for 6 cycles.

Recently studies were initiated of 4.7 V spinel cathodes against 1.5 V Mg- and Al-substituted $Li_4Ti_5O_{12}$ anodes which, when coupled together, provide 3.2 V cells. These studies are being undertaken against the more stable 2.5 V $Li_4Ti_5O_{12}$(Al-substituted)/$Li_{1+x}Mn_{2-x}Al_xO_4$ system as a reference. Figure IV-28 and Figure IV-29 show capacity vs. cycle number for two such cells. Although both 3.2 V and 2.5 V cells show excellent cycling stability after the first cycle, the ICL on the first cycle of the 3.2 V cell is significantly worse than it is for the 2.5 V cell. This finding is consistent with the electrochemical behavior of the layered lithium-manganese-nickel-oxide composite electrodes, described above, if charged above 4.3 V (vs. Li^0). A previously tried approach is being followed to stabilize the surface of both high-potential layered and spinel lithium-manganese-nickel-oxide cathodes by applying protective coatings and by introducing H_2O and HF scavengers to minimize the initial capacity loss of these electrodes.

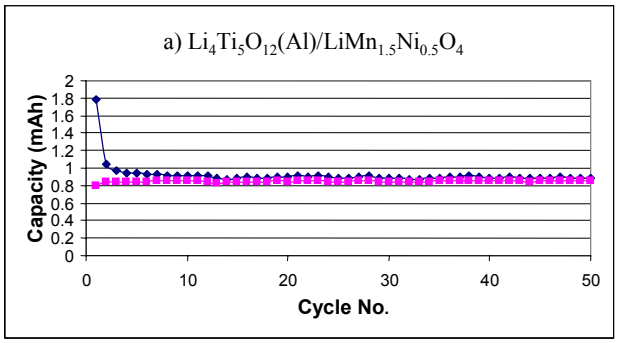

Figure IV-28. Cell capacity vs. cycle no. plots for 3.2 V Li/$Li_4Ti_5O_{12}$ (Al-substituted)/$LiMn_{1.5}Ni_{0.5}O_4$ (top curve=charge capacity; lower curve=discharge capacity).

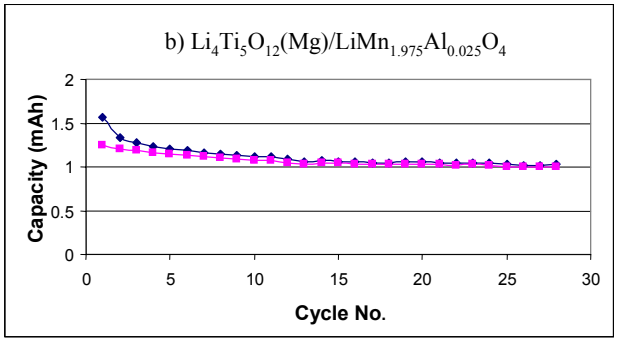

Figure IV-29. Cell capacity vs. cycle no. for 2.5 V Li/$Li_4Ti_5O_{12}$ (Mg-substituted)/$LiMn_{1.975}Al_{0.025}O_4$ cells (top curve=charge capacity; lower curve=discharge capacity)

NMR experiments, conducted in collaboration with C. Grey, confirm that these structures are domain-like in character. Very high reversible capacities (~300 Ah/kg) can be achieved from the electrodes if discharged from 4.6 V to low potentials (1.5 – 1.0 V); their reversible capacity, which is composition dependent, can exceed 200 Ah/kg over the high-voltage range (4.6 to 2.0 V). The performance of these electrodes is compromised by a highly oxidizing surface above 4.3 V which results in a large ICL. Attempts to pre-reduce the surface of the electrode particles with a mild reducing agent have indicated that it may be possible to increase the capacity and stability of these electrodes. A parallel investigation of highly lithiated Li_2MO_2 phases that form at 1.5-1.0 V has shown that their high reactivity in air compromises their possible use as "overdischarged" electrodes for offsetting the irreversible capacity loss that occurs at the negative electrodes of Li cells.

Electronic Stabilization of Manganese Oxide: The layered nickel/manganese system, $LiNi_yMn_yCo_{1-2y}O_2$ has been studied for $0.33 \leq y \leq 0.5$ to determine the optimum composition, the nature of the electrochemically active specie, the role of cobalt, and to compare its capabilities against $LiFePO_4$. Physical and electrochemical characterization of these materials shows that they may best be described as stabilized nickel oxides. They are all significantly better electrical conductors than $LiFePO_4$, and as showed earlier for $LiMnO_2$ itself,[23] the conductivity is enhanced by the addition of cobalt. In addition, their higher discharge potentials and density leads to much higher gravimetric and volumetric energy densities.

The characterization of the 442 composition $Li_xNi_{0.4}Mn_{0.4}Co_{0.2}O_2$, which shows optimum behavior with very little polarization on cycling, has continued. However, the synthesis temperature has a marked impact on the first cycle ICL and on the subsequent cycling capacity. Thus, this work is restricted to compounds made between 800 and 900°C. It is found that this compound, even without any special conductive coatings, supports a higher capacity at all discharge rates than carbon-coated $LiFePO_4$, as shown in Figure IV-30. It is expected that carbon coatings formed *in situ* from carbon gels will have a positive impact on the rate capability of these layered nickelates. The impact of such coatings on this 442 composition will be explored.

The compounds formed as lithium is removed from the 442 composition have been characterized. X-ray analysis indicates that these materials are single phase from x=1 to $x \leq 0.1$, where some evidence appears for the formation of a second phase. The lattice parameters as a function of lithium content are shown in Figure IV-31. The volume increases by just 4% as the lithium content increases from 0.05 to 1.

[23] P.Sharma et al, *Elec. SS. Lett.* 1999, 2:494.

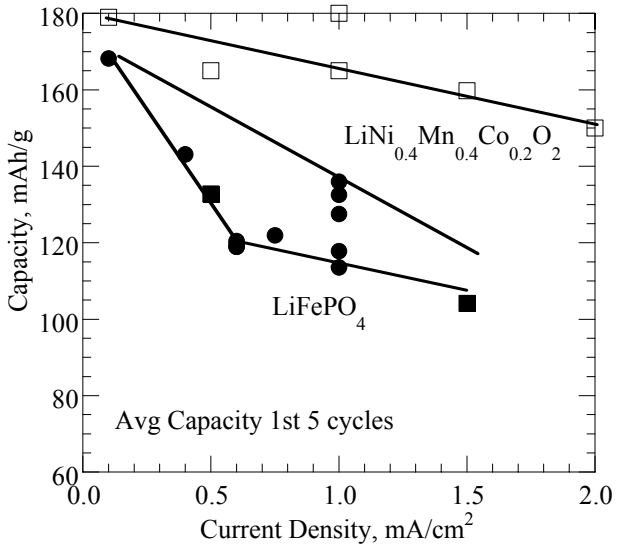

Figure IV-30. Cycling capacity of $LiNi_{0.4}Mn_{0.4}Co_{0.2}O_2$ as a function of cycling rate compared with $LiFePO_4$.

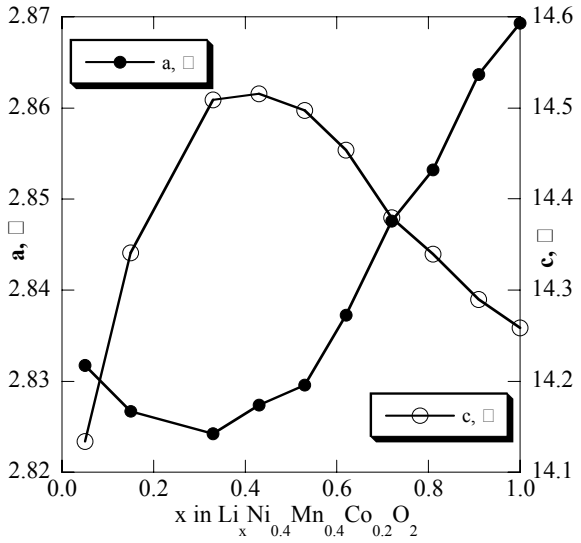

Figure IV-31. Change of the lattice parameters of $Li_xNi_{0.4}Mn_{0.4}Co_{0.2}O_2$ as a function of lithium content.

Iron Phosphate Cathodes: The role of elemental carbon additives has been studied with special emphasis on $LiFePO_4$ electrodes because of their intrinsically low electronic conductivity. Samples of raw $LiFePO_4$ powders were analyzed before they were mixed with carbon, and it was concluded that all of them contain significant amounts of residual carbon (0.5-1.5% wt.). The structure of this residual carbon is highly amorphous. It was also determined that the electronic resistivity of amorphous carbons produced by pyrolysis of organic precursors decreases by 4 orders of magnitude for pyrolysis temperatures between 600 and 800^{o}C, as shown in Figure IV-32.

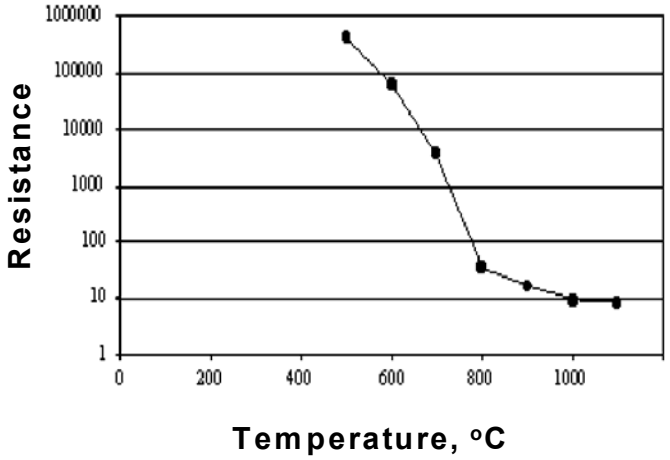

Figure IV-32. Electronic Resistance of Pyrolyzed Carbons

$LiFePO_4$ raw powders were then analyzed in search of a correlation between carbon structure/ conductivity and cathode electrochemical performance, in collaboration with Dr. Doeff who provided raw samples of $LiFePO_4$ synthesized under different conditions. It was concluded that the electrochemical behavior of $LiFePO_4$ is highly dependent upon the details of processing and that the properties of residual carbon determine the $LiFePO_4$ electrochemical performance. Further mixing of $LiFePO_4$ with carbon does not appear to have a significant effect on the electrode performance.

Work continued on sol-gel $LiFePO_4$ for the purpose of studying the effect of carbon coatings on performance. The synthesis method results in high-purity materials with well-controlled particle sizes, allowing straightforward analysis of the effect of carbon coatings without complications from impurities common to other preparations. During the past year, it was discovered that $LiFePO_4$ electrochemical performance was strongly correlated to the structure of surface carbon on the particles, as determined by Raman microprobe spectroscopy. Coatings with lower D/G (disordered/graphene) and higher sp^2/sp^3 ratios have higher electronic conductivities, and allow better utilization of the $LiFePO_4$ electrode. By incorporating organic or polymeric additives during synthesis, it is possible to manipulate the D/G and sp^2/sp^3 ratios in the carbon coating. Best results are obtained when small amounts of pyromellitic acid are used. TGA shows that this compound decomposes rapidly at low temperatures compared to polymeric or polyaromatic compounds (Figure IV-33). $LiFePO_4$ samples processed with the latter two also contain residual hydrogen or nitrogen suggesting incomplete decomposition. This is likely to reduce electronic conductivity of carbon significantly.

It is interesting to note that increasing the amount of carbon from pyromellitic acid in the samples does not necessarily result in better performance; best results are obtained when the carbon content is about 1 wt% (Figure IV-34). Elemental analysis on the sample with 1.66% C indicates some residual hydrogen is present, suggesting that the decomposition rate is dependent upon the amount of pyromellitic acid in the sample. Further work will be directed towards understanding the decomposition pathways of this additive so that coatings can be further optimized.

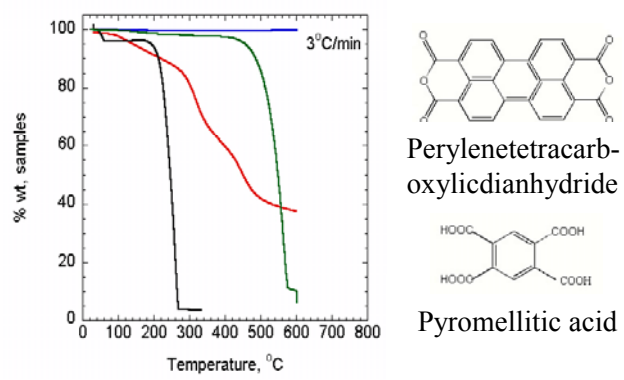

Figure IV-33. TGA traces of $LiFePO_4$ (blue), perylenetetracarboxylicdianhydride (green), photoresist polymer (red), and pyromellitic acid (black). Samples were heated at 3ºC/min under N2

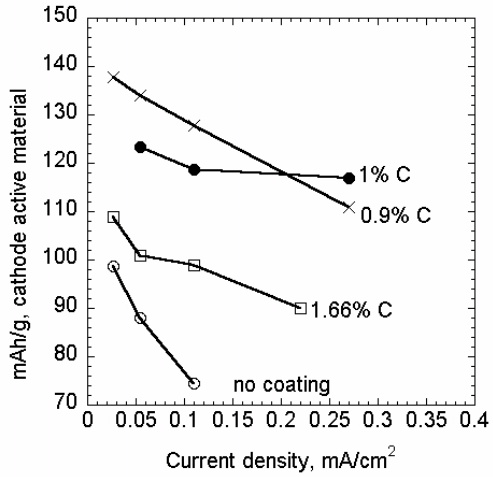

Figure IV-34. Capacity as a function of current density for $LiFePO_4$ cathodes coated with carbon from pyromellitic acid. An uncoated sample (which contains residual carbon) is shown for comparison.

Investigation of Substitution with M^{4+} other than Mn^{4+} in $LiNi_{1-x}M_xO_2$: Initial investigations into these materials have been centered on Ti^{4+}. Central to obtaining a composition with good electrochemical characteristics is the cation order, which is more difficult in the Ti^{4+} system than in the Mn^{4+} system due to the former's larger ionic radii. Matters are further complicated by a very limited number of Ti^{4+} precursors that are water solvable and thus suitable for co-precipitation. However, initial attempts using a modified version of the method used in the Li_2MnNiO_4 system have yielded material with intimate mixing of the transition metal cations, a prerequisite for cation ordering at a low temperature. Experiments to deduce the optimal sintering temperature are therefore underway.

The Ti in $LiNi_{1-x}Ti_xO_2$ is present as Ti^{4+} and the Mn in the same material is also expected to be present as Mn^{4+}. A 4 V average voltage *vs.* Li/Li^+ at $0.1mA/cm^2$ has been reported[24] for

[24] Ohzuku T, Makimura Y, *Chem Lett*. (8): 744

$Li_{1-x}Ni_{0.5}Mn_{0.5}O_2$ with a capacity of ~150 Ah/kg. This would correspond to operation on the Ni^{3+}/Ni^{2+} couple if Mn is present as Mn^{4+}. In an initial study of this system,[25] it was shown that coating the particles with carbon increased the performance at higher current densities, but careful examination of the XRD patterns showed that the capacity was limited by the presence of transition-metal ions in the Li layers.

Publications and Presentations

- S. Yang, Y. Song, K. Ngala, P. Y. Zavalij and M. Stanley Whittingham: "Performance of $LiFePO_4$ as lithium as lithium battery cathode and comparison with manganese and vanadium oxides," *J. Power Sources*. 2003, 119-121: 239-246.
- Y. Song, N. Chernova, P. Y. Zavalij, and M. Stanley Whittingham: "Iron phosphate and related phases as cathodes for lithium batteries," presented at the Solid State Ionics Meeting in Monterey, July 2003, and in Arcachon, France, September 2003.
- "Effect of Surface Carbon Structure on the Electrochemical Performance of $LiFePO_4$," M. Doeff, Y. Hu, F. McLarnon and R. Kostecki, Electrochemical and Solid State Letters, 6, A207 (2003).
- "Evaluation of Sulfur-Doped Aluminum-substituted Manganese Oxide Spinels for Lithium Ion Battery Applications", M. Doeff, J. Hollingsworth, J. Shim, Y.J. Lee, K. Striebel, J.A. Reimer and E.J. Cairns, J. Electrochem. Soc., 150, A1060 (2003).
- "A Study of Layered Lithium Manganese Oxide Cathode Materials", T.A. Eriksson and M. Doeff, J. Power Sources, 119-120C, 145 (2003).
- "Effect of Surface Carbon Structure on Electrochemical Performance of LiFePO4", M. Doeff, R. Kostecki, F. McLarnon, and Y. Hu, 14th International Conference on Solid State Ionics, Monterey, CA, June 2003, Abstract II O T 02, p.88.
- "Investigation of Layered Intergrowth LixMn1-yO2 (M=Ni, Co, Al) Compounds as Positive Electrodes for Li-ion Batteries," M. Dollé, J. Hollingsworth, T. J. Richardson, and M. Doeff, 14th International Conference on Solid State Ionics, Monterey, CA, June 2003, Abstract II O T 13, p. 100.

[25] Cushing BL, Goodenough JB, *Solid State Sciences*, **4**(11-12):1487

IV.E Task 5 – Diagnostics

Objectives

- Establish direct correlations between electrode surface changes, interfacial phenomena, electrolyte decomposition, materials changes and cell capacity/power decline.
- Directly observe Li in cathode materials, characterize the Li atomic and electronic local environment, determine changes in this environment with cycling, and use this information to identify causes of capacity loss and propose improved electrode materials.
- Engineer high-capacity, stable cathode materials by working with redox-active metal ions that can exchange multiple electrons in a narrow voltage range, focusing initially on the Ni^{2+}/Ni^{4+} couple. Determine the effect of structure and cation doping on the Li deintercalation/intercalation mechanisms and the Ni^{2+}/Ni^{4+} couple.
- Characterize the long-term corrosion performance of Al current collectors in Gen 2 chemistry baseline cells. Determine the mechanism of passivation in Gen 2 electrolyte and identify the passive film responsible for the corrosion resistance of Al current collectors in Gen 2 cells. Identify electrolytes of multi-component salts that are optimized for battery service and that are noncorrosive to Al current collectors.

Approach

The approach includes using Raman microscopy, scanning probe microscopy (SPM), ellipsometry, and standard electrochemical methods to characterize cell components taken from baseline cells, fresh electrode materials, and thin-film model electrodes. Data collected include electrode surface morphology and structure, electrode surface chemistry, and SEI thickness and composition, all of which change during cell cycle-life tests.

Also, a combination of *in situ* and *ex situ* synchrotron techniques (XAS) are used to characterize electrodes. Exploratory work has been done on other techniques such as non-resonant inelastic x-ray scattering (NRIXS). Another technique involves *in situ* Fourier transform infrared (FTIR) spectroscopy to study the interfacial chemistry in model systems. *In situ* differential electrochemical mass spectrometry (DEMS) has been added as a technique for studying gas generation from electrolyte decomposition reactions.

^{7}Li MAS-NMR was also employed to characterize electrodes before and after cycling. Data collected are isotropic chemical shift, linewidth, and relaxation times for each species of Li which provides structural and local environment information to improve our ability to design new electrode materials.

Raman microscopy and current-sensing atomic force microscopy (CSAFM) were used to characterize surface phenomena in baseline cells. By combining these methods, one can evaluate the surface and near-surface changes in electrode morphology, and SEI thickness and composition

that may arise during cell aging. The goal is to understand the mechanisms of surface phenomena and determine their impact on performance and life of Lithium-ion cells.

Finally, a combination of electrochemical tests (anodic and cathodic polarization and concurrent measurement of mass change using electrochemical quartz crystal microbalance) and surface analytical techniques was used to investigate the mechanism of Al corrosion and passivation in baseline electrolytes relevant to Lithium-ion batteries.

The goals being pursued through these activities are 15 year life, and less than 20% capacity fade over the 10-year period.

Accomplishments

Surface Studies: In order to determine a possible impact of carbon recession on the cathode performance, $LiAl_{0.05}Ni_{0.8}Co_{0.15}O_2$ was investigated using color-coded Raman maps of Gen-2 composite cathodes from tested cells. A typical Raman spectrum of a fully discharged $LiNi_{0.8}Co_{0.15}Al_{0.05}O_2$ cathode is dominated by a broad band centered at ~500 cm^{-1} with a small shoulder at 558 cm^{-1}. On the other hand, Raman spectra of $Li_{1-x}Ni_{0.8}Co_{0.15}Al_{0.05}O_2$ display two peaks at 480 and 550 cm^{-1}. By deconvoluting the Raman spectra and integrating the bands characteristic of this material, it was possible to determine the state of charge (SOC) of individual grains of the active material.

Interestingly, the cathodes from room temperature cells, which were assembled and tested by K. Striebel (Task 1), displayed spectral variations with location on the cathode surface, which indicate the presence of at least partially charged $Li_{1-x}Ni_{0.8}Co_{0.2}O_2$. The cathode surface SOC showed individual grains of fully charged material at some locations, even though the cell was slowly discharged (C/25) to 3.0 V. Figure IV-35 shows Raman images of a cathode, which suffered 16% irreversible capacity loss at the end of the test. It is clear that some particles of $LiNi_{0.8}Co_{0.15}Al_{0.05}O_2$ became electrically disconnected from the active cathode due to mechanical stress and poor intergranular electronic contact

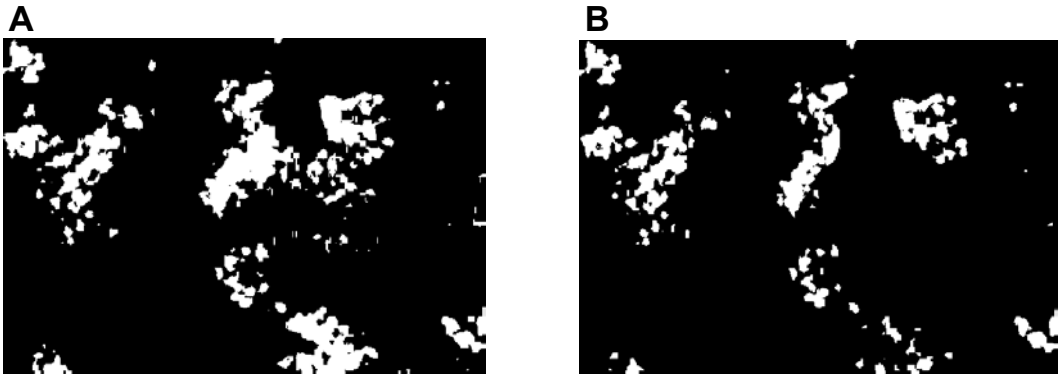

Figure IV-35. Raman microscopy 50 x 80 μm surface images of $LiNi_{0.8}Co_{0.15}Al_{40.05}O_2$ composite cathode from a cell surface. The bright areas show (A) charged and discharged active material, (B) charged active material

Moreover, microprobe Raman spectra from the surface of the tested cathodes displayed spectra characteristic of lithium pyrophosphates. There were also areas on the surface of the tested cathodes which showed very broad and featureless maxima centered near ~550 and 1050 cm^{-1}. Their origin is most likely phosphate-type compounds that are products of $LiPF_6$ decomposition.

The analysis of power fade mechanisms of $LiAl_{0.05}Ni_{0.8}Co_{0.15}O_2$ cathodes at elevated temperatures was completed. Based on Raman microscopy data analysis and CSAFM imaging results, it was concluded that carbon recession and/or rearrangement results in poor intergranular electronic contact within $LiAl_{0.05}Ni_{0.8}Co_{0.15}O_2$ agglomerates, which is correlated with the observed power and capacity loss. The mechanism of carbon retreat within the composite cathodes requires further understanding and will be the subject of further work.

Battery Materials, Structure and Characterization via Spectroscopy: X-ray absorption spectroscopy (XAS) in both the transmission and electron yield modes does not support the uniform two phase moving boundary mechanism that has been proposed for the charge/discharge process in $LiFePO_4$ particles. Figure IV-36 shows that the internal and surface structures of the electrode are essentially identical throughout the charging process. Other possibilities are localized extraction/insertion of Li on the surface of $LiFePO_4$ particles or progressive nucleation of the charged/discharge phase.

In situ XRD on $LiMn_2O_4$ in the 4.1 V region was completed. The work showed that electrolyte composition had major effects on the stability of $LiMn_2O_4$ at elevated temperatures.

In situ XRD and a combination of *in situ* and *ex situ* XAS was used to study the phase changes and the redox processes in $LiNi_xMn_{1-x}O_2$ and $LiNi_{1/3}Co_{1/3}Mn_{1/3}O_2$. The results indicate that Ni exists initially as Ni(II) and Mn as Mn(IV) in $LiNi_xMn_{1-x}O_2$. When Li is extracted during charge, Ni(II) is oxidized to Ni(IV) and there is no change in the Mn oxidation state. In $LiNi_{1/3}Co_{1/3}Mn_{1/3}O_2$, Ni(II) is also oxidized to Ni(IV) during charge and Mn remains as Mn(IV). The Co exists as Co(III) in the initial material and does not change during charge. However, the O K edge XAS indicates that charge compensation occurs on the O that is associated with Co.

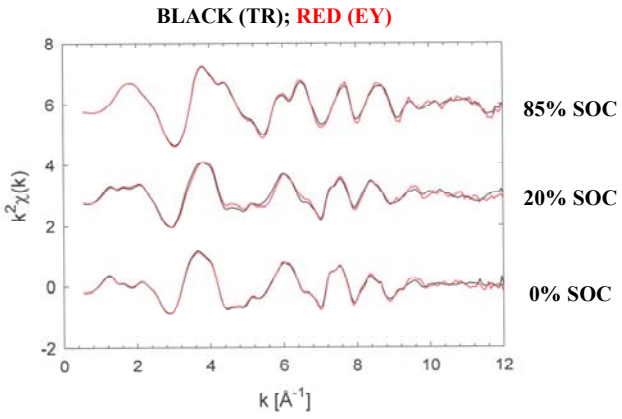

Figure IV-36. Fe K edge XAFS during charge of $LiFePO_4$

The surface films formed on ATD Gen 2 cathodes charged to 3.75V and 4.2V vs. Li/Li^+ in EC:DEC - 1M $LiPF_6$ were analyzed using *ex situ* FTIR with the attenuated total reflection (ATR) technique. A surface layer of Li_2CO_3 is present on the virgin cathode, probably from reaction of the active material with air during the cathode's preparation. The Li_2CO_3 layer disappeared after simple soaking in the electrolyte, indicating that the layer dissolved into the electrolyte possibly even before cycling. IR features from the binder (PVdF) and a trace of polyamide from the Al current collector were observed on the surfaces of cathodes charged to below 4.2 V, and no surface species from electrolyte oxidation were found.

The formation of the SEI layer on graphite anodes cycled in PC/LiBOB electrolyte using *ex situ* FTIR analysis in the ATR mode, was also studied. The spectra clearly show that electrochemical reduction of the BOB anion is a part of the SEI formation chemistry. Based on the combination of electrochemical and FTIR data, it is concluded that the preferential reduction of the BOB anion versus the PC solvent molecule prevents solvent co-intercalation, and is the mechanism responsible for the cyclability of graphite anodes in purely PC-based electrolyte.

Cathode Material Studies Using NMR: ^{7}Li MAS NMR spectroscopy has proven to be very useful in determining the local structure of $L_y[M_{0.11}Mn_{0.89}]O_{2.05}$ layered compounds. This new probe allows us to obtain higher resolution NMR spectra than was previously possible. The compounds can be categorized into three classes:

1. Al, Fe, Co, and Ni-substituted compounds contain both O2 and O3 type environments.
2. Cu-doped material contains both O2 and T2 environments and
3. Zn-doped material contains only O2 type environment.

For example, ^{7}Li NMR spectra were obtained for $L_y[Al_{0.11}Mn_{0.89}]O_{2.05}$ during and after cycling. No change in the spectrum was observed, indicating that there is no phase transition during the charging/discharging process.

Olivine $LiMPO_4$: ^{7}Li and ^{31}P NMR spectra were obtained for various $LiMPO_4$ compounds. A single ^{7}Li resonance of –92 to 57 ppm was observed depending on the transition metal. In contrast, a large ^{31}P hyperfine shift was seen, ranging from 1700 to 7300 ppm. The P NMR appears to be very informative in probing the local environment of the $LiMPO_4$ compounds, since the P atoms remain in the structure during the deintercalation process and ^{31}P NMR is more sensitive to the local environment than Li.

$LiFePO_4$: ^{7}Li and ^{31}P NMR spectra were obtained for $LiFePO_4$ during the charging cycle. A single Li resonance without a significant change in the peak position was seen for all the states of charge, indicating that the Li cations in the compound have the same local environment at all states of charge, consistent with the flat potential profile of this material. In contrast, an additional P resonance at higher shift than the original peak position was observed during the charging cycle. The former was assigned to P in the $FePO_4$ phase and the latter to P in the $LiFePO_4$ phase. The two ^{31}P resonances are consistent with the two-phase behavior during cycling.

$LiAl_{0.05}Co_{0.15}Ni_{0.8}O_2$: ^{7}Li NMR spectra of the Gen 2 cathode material show two dominant resonances which have been assigned to Li with Co/Al-neighbors and to Li with Ni-neighbors. The

spectra suggest that the oxidation of Ni occurs during the entire charging range, whereas the oxidation of Co occurs only at high potentials (above 4.2 V). An electrode with large capacity fading showed a significant decrease in intensity of the resonance due to Li with Ni-neighbors, suggesting that the capacity fading is mainly caused by the changes relating to the Ni-sites.

First-Principles Calculations and NMR Spectroscopy of Cathode Materials: Results from a detailed investigation of the structures of $Li[Ni_xMn_{(2-x)/3}Li_{(1-2x)/3}]O_2$, with NMR and first principles calculations, are described. The double redox couple Ni^{2+}/Ni^{4+} in these materials makes them of interest as high capacity electrodes. Analysis of the ^6Li resonances in the Ni/Mn layers demonstrate that Li preferentially occupies sites near Mn^{4+} ions and avoids the Ni^{2+} ions, leading to configurations that are far from random. Calculations for $Li(Ni_{0.5}Mn_{0.5})O_2$ show that the Ni^{2+} and Mn^{4+} ions form alternating zig-zag rows, see Figure IV-37.

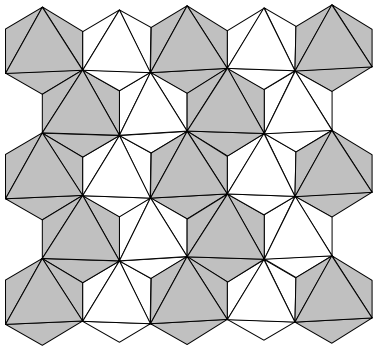

Figure IV-37. Ordering of Ni^{2+} and Mn^{4+} cations

NMR results demonstrate that the Li is removed from both the Li layers and the transition metal layers on cycling, as shown in **Figure IV-38**. Calculations were performed in order to understand this phenomenon in more detail. Voltages for Li removal from different Li sites created by different ordering schemes were calculated, which showed that Li is removed from the Li and transition metal layers at similar potentials. The latter process is facilitated by Li vacancies in the transition metal layers. As the number of vacancies in the Li layers increase, the Li site in the transition metal layers becomes increasingly less stable. Furthermore, at high concentrations of Lithium-ion vacancies, the activation energy for the octahedral to tetrahedral site migration is essentially zero. The Li ions in the tetrahedral sites may then participate in the electrochemical process or remain pinned in the tetrahedral sites (depending on the local environments surrounding the sites). Li NMR showed that the Li ions return to the transition metal layers on discharge and that the process is reversible. Computations simulating the effect of overcharge indicate that the creation of Mn^{3+} may significantly reduce the stability of this material.

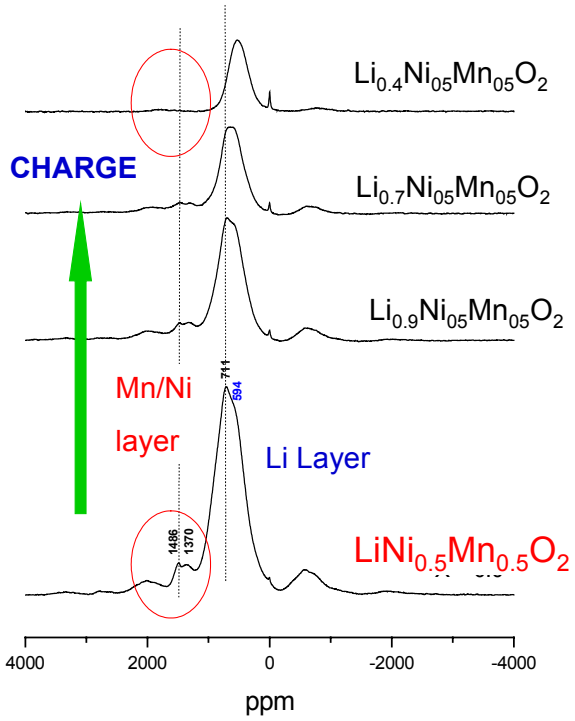

Figure IV-38. NMR results showing Li is removed from the Li layers *and* the Ni/Mn layers

Corrosion of Aluminum Current Collectors in Lithium Ion Batteries: Our research is focused on predicting the corrosion-related lifetime of aluminum current collectors. Towards that end, the extent of corrosion in batteries that were assembled and tested within this activity was measured. Specifically, aluminum current collectors were removed from Li-ion batteries coin cells and analyzed for corrosion.[26] Corrosion of the current collectors was detected by a combination of optical and scanning electron microscopies. In all instances, the form of corrosion was pitting corrosion, a sample of which is shown in Figure IV-39.

Two different cathodes, $LiFePO_4$ and $LiMn_2O_4$, were used in the coin cells, which employed a lithium anode and an electrolyte of 1M $LiPF_6$ in EC+DMC. A total of 36 current collectors from coin cells were inspected, in which corrosion was detected in 33. The cells were tested by cyclically charging and discharging at one of three different current densities, although the same amount of charge was passed during each cycle for the different current densities. In cells with $LiFePO_4$ cathodes, the amount of corrosion varied directly with the time of charging. For cells with $LiMn_2O_4$ cathodes, the opposite was true, the amount of corrosion varied inversely with the time of charge.

These results suggest that different corrosion mechanisms operate on current collectors covered with $LiMn_2O_4$ and with $LiFePO_4$. The most severe corrosion occurred in collectors covered by $LiMn_2O_4$ that were subjected to a total of 80 charge/discharge cycles. However, the highest rate of corrosion

[26] Unfortunately, significant mechanical damage occurred during the assembly of the ATD batteries that is indistinguishable from pitting corrosion. As a result, lifetime predictions are based on the corrosion behavior of the current collectors of the coin cells.

damage in collectors with $LiFePO_4$ occurred in cathodes subjected to 10 charge/discharge cycles. The results predict that corrosion of current collectors with $LiMn_2O_4$ cathodes would cause a 20% capacity decrease after 1,000 cycles at 0.1 mA/cm^2.

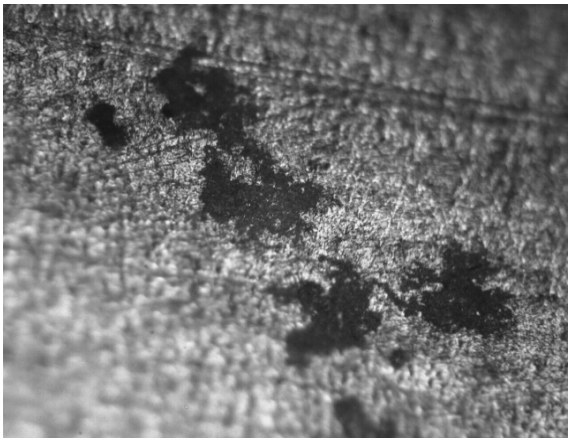

Figure IV-39. Aluminum corrosion

To determine the mechanism of aluminum passivation in battery electrolytes, two types of experiments were conducted: electrochemical anodic polarization tests in which the corrosion rate of aluminum is measured as a function of potential, and IR and Raman spectroscopies of the solid corrosion products formed on samples of anodically polarized aluminum. Most interestingly, the results of the anodic polarization tests indicate that the corrosion of aluminum is related to the compositional purity of the aluminum and the solvent. High-purity aluminum is very resistant to pitting corrosion in EC+DMC, but low-purity aluminum undergoes severe pitting corrosion. If the purity of the EC is lowered from 99.9% to 99.0%, high-purity aluminum is susceptible to pitting corrosion. Finally, far IR spectroscopy of the surface of aluminum anodically polarized in 1.2 M $LiPF_6$ with a solvent of EC + DMC indicates the corrosion resistance of aluminum is most likely due to the formation of a protective film that consists, in part, of AlF_3.

Publications and Presentations

- W.S. Yoon, M.Balasubramanian, X.Q. Yang, Z. Fu, D. A. Fischer, and J. McBreen "*Soft* X-ray Absorption Spectroscopic Study on the $LiNi_{0.5}Mn_{0.5}O_2$ Cathode Material during charge" *Journal of the Electrochemical Society*, accepted.

- W.S. Yoon, C.P. Grey, M. Balasubramanian, X.Q. Yang, D. A. Fischer, and J. McBreen "A Combined NMR and XAS Study on the Local Environments and Electronic Structures of the Electrochemically Li-ion deintercalated $LiCo_{1/3}Ni_{1/3}Mn_{1/3}O_2$ electrode System" *Electrochemical and Solid-State Letters*, accepted.

- N. Pereira, M. Balasubramanian, L. Dupont, J. McBreen, L. C. Klein, and G. G. Amatucci, The Electrochemistry of Germanium Nitride with Lithium, *J. Electrochem. Soc*. **150**, A1118 (2003).

- X. Q. Yang, J. McBreen, W.S. Yoon, M. Yoshio, H. Wang, F. Fukuda, T. Umeno, "Structural studies of the new carbon-coated silicon anode materials using synchrotron-based *in situ* XRD", *Electrochemistry Communication*, **4** 893 (2002).

IV.F Task 6 – Modeling

Objectives

- Develop experimental and computational methods for measuring and predicting transport, kinetic, and thermodynamic properties. Model electrochemical systems to optimize performance, identify limiting factors, and mitigate failure mechanisms.
- Predict the role of conductive and mechanical failures on reduced performance in the baseline systems through tightly coupled experimental and simulation studies of microscale transport and mechanics phenomena.

Approach

- Develop a model of dendrite formation on Li metal. Use simulations to improve understanding of the SEI layer. Use simulations to understand performance limitations of baseline chemistries and to identify promising design options.
- Use simulations to design combinations of conductive additives to improve battery performance, and to reduce irreversible capacity losses. Perform complete studies of electrode conduction with cell testing to confirm the materials' effect on battery performance. Show improvement in the performance of baseline materials with additives, as determined by simulation.
- The USABC goals pursued by this activity are specific power of 300 W/kg, with a 10 year life, and less than 20% capacity fade.

Accomplishments

Modeling $LiFePO_4$: Recently, developed a model has been developed for the phase change and diffusion in the iron phosphate electrode, and compared to experimental data, Figure IV-40, identifying the performance-limiting factors. While the graphite electrode model has previously been developed in the group, a model for the phase change and diffusion in iron phosphate was completed using a shrinking-core approach. Experiments were performed to extract the equilibrium potential of the iron phosphate electrode and used with the model to predict discharge curves at various rates in a half-cell configuration. Ohmic drops due to the poor conductivity of the active material and transport limitations in the solid phase were identified to be the cause for the low rate capability of this chemistry. The cathode model was integrated into a cell model with a natural graphite anode to simulate the baseline and identify the optimum design in order to maximize the specific energy of the battery. The specific energy maximization was conducted for a wide range of discharge times, ranging from 2 minutes to 10 hours, in order to simulate both EV and HEV needs. This resulted in a map of the maximum performance of this baseline chemistry, allowing us to gauge its ability to achieve the DOE goals, Figure IV-41. Simulations suggest that while the present cell design shows performance (80 Wh/kg) far below the DOE specific energy goals (150 Wh/kg), significant improvements can be achieved by changing the balancing of the cell and increasing the electrode thickness.

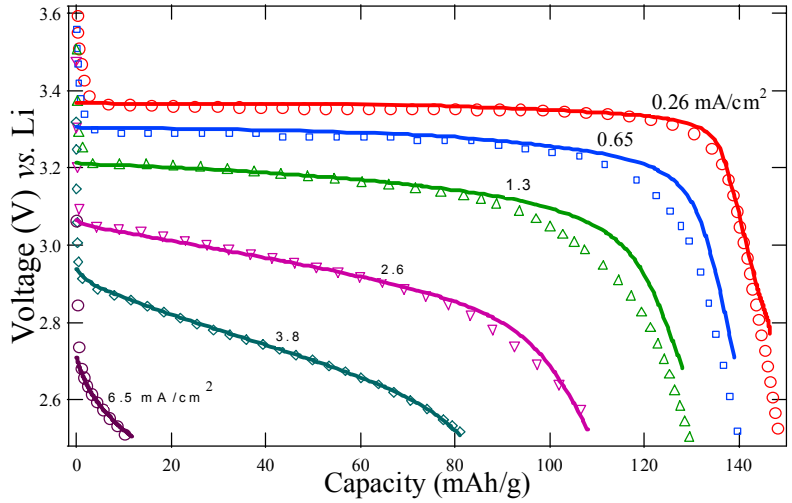

Figure IV-40. Comparison of model and experimental data for iron phosphate cathode

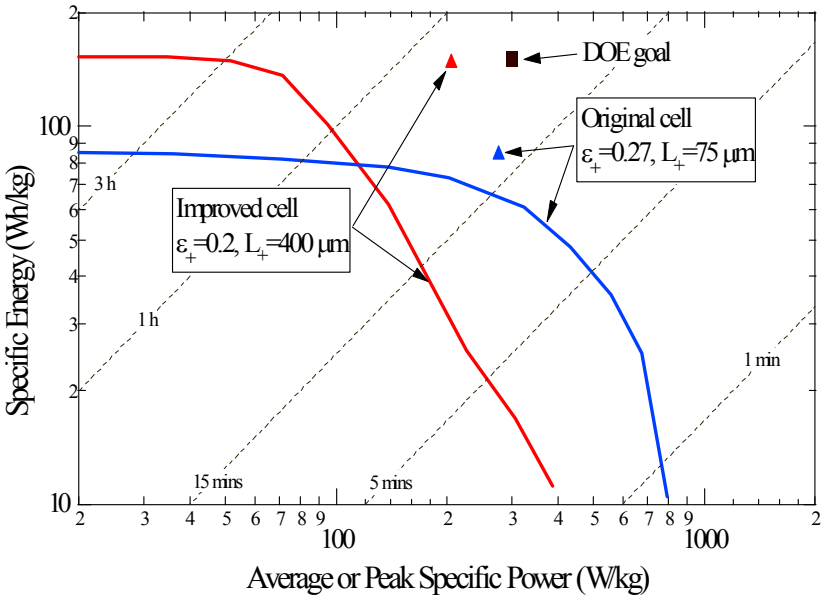

Figure IV-41. Optimum cell configuration

In order to address the problem of dendrite growth in Li-polymer cells, a theory has been developed to correlate surface roughness to measurable mechanical properties. This theory extends those previously developed in the literature to include properties like the elastic modulus and viscosity, in addition to the surface tension. The theory has shown that materials with higher values of shear modulus *G* are more likely to inhibit dendrites.

Conduction Models, Anodes and Cathodes: Thin, multilayered electrodes were fabricated with carbon additives to reduce resistive losses between current collector and active materials (Striebel), in order to verify new experimental techniques and analytical models for conduction. Progress has been made on development of an analytical solution to conduction in multilayered sheets; it appears likely that an analytical solution may be derived, to obviate the need for direct, finite element simulations.

In order to generate simulation data, extensive image analysis was performed on as-received anodes and cathodes. Data on particle size and shape was used to predict electrical resistance in the active layers of electrodes, and contact resistance between layers. Conduction experiments were performed and analyzed using a protocol and closed-form theoretical approach developed in the last year. It was found that the coating shape has a significant effect on conduction, both experimentally and through our simulations, and that simulations were able to quite satisfactorily predict top-layer resistance in anodes. Also, we investigated use of 3D models and found that 3D packing effects play a significant role in all of the electrochemistries being investigated in this activity due to the size of the particles relative to electrode thickness.

Contact resistance was reduced for SL20 with increasing compression of the anode (Figure IV-42); however, the contact resistance increased with compression of the GDR6 and GDR14 anodes. This finding is consistent with cracking observed in SEM imaging of compressed particles. The close match with simulations verifies that these simulations can be used by other teams to design electrodes for conductivity.

Testing of cathodes resulted in generation of data sent to LBNL for use in electrochemical simulations. Results on conductivities suggest that volume fractions of conductive additives (carbons) can be maintained for thicker electrodes required for DOE specific energy goals with predictable, stable conductivities. Finally, volume fractions of conductive additives can be significantly reduced, in all probability, using higher-aspect ratio particles, thus reducing electrode mass.

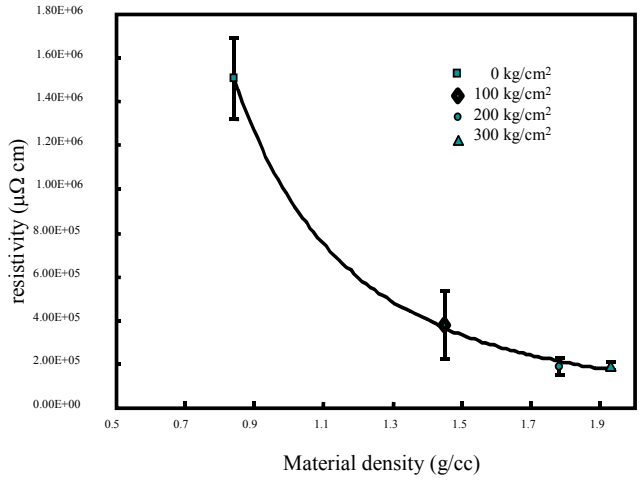

Figure IV-42. Electrical resistivity of SL-20 matrix vs density (pressure)

Appendix A

Contributors

V. Battery Technology Development	
J. Barnes	Naval Surface Warfare Center West Bethesda, MD 20817-5700
A. Pesaran	National Renewable Energy Laboratory 1617 Cole Boulevard Golden, CO 80401-3393

Applied Battery Research	
Calendar and Cycle Life	
J. Christophersen, D. Glenn, Chinh Ho, C. Motloch, T. Murphy, and R. Wright	Idaho National Engineering and Environmental Laboratory Idaho Falls, ID 83415-3830
D. Abraham, K. Amine, V. Battaglia, I. Bloom, D. Dees, G. Henriksen, Y.E. Hyung, S. Jones, and J. Liu	Argonne National Laboratory Argonne, IL 60439-4837
H. Case, D. Doughty, G. Nagasubramanian, P. Roth, and E. Thomas	Sandia National Laboratories Albuquerque, NM 87185-0613
M. Balasubramanian, James McBreen, X. Sun, and X. Q. Yang	Brookhaven National Laboratory P.O. Box 5000, MSD Bldg. 555, Upton, NY 11973-5000
J. Kerr, R. Kostecki, F. McLarnon, K. McCarthy, L. Norin, T. Richardson, P. Ross, X. Song, S. Zhang, and V. Zhuang	Lawrence Berkeley National Laboratory Berkeley CA 94720-8168
R. Haasch, S. Maclaren, I. Petrov, E. Sammann, and R. Twesten	Center for Microanalysis of Materials University of Illinois at Urbana-Champaign
Abuse Tolerance	
C. Crafts, D. Doughty, P. Roth	Sandia National Laboratory Mail Stop 0613 Albuquerque, NM 87185
K. Amine, G. Henriksen, Y.E. Hyung, and D. Vissers	Argonne National Laboratory Argonne, IL 60439
J. Prakash	Illinois Institute of Technology Department of Chemical and Environmental Engineering, Chicago, IL 60616
Cost Reduction	
K. Amine, D. Chaiko, C. Chen, G. Henriksen, Y.E. Hyung, A. Jansen, A. Kahaian, J. Liu, A.L. Bookeun Oh, S. Oliver, D. Vissers, and S. Y. Yoon	Argonne National Laboratory Argonne, IL 60439
J. Prakash	Illinois Institute of Technology Department of Chemical and Environmental Engineering, Chicago, IL 60616
S. W. Cornell	Plastic Technology Partners Naperville, IL 60540

Long-Term Battery Research	
Cell Development	
M. Doeff, R. Kostecki, Y. J. Lee, T. Richardson , J. Shim, A. Sierra, V. Srinivasan, V. Zhuang, and X. Zhang	Lawrence Berkeley National Laboratory Berkeley CA 94720-8168
M. Thackeray	Argonne National Laboratory Chemical Technology Division Argonne IL 60439
A. M. Sastry	The University of Michigan Department of Mechanical Engineering and Applied Mechanics, Ann Arbor, MI 48109-2125
S. Whittingham	Chemistry and Materials Research Center State University of New York at Binghamton Binghamton, NY 13902-6000
P. Charest, E. Dupuis, P. Hovington, R. Veilleux, and K. Zaghib	Hydro-Québec, IREQ Varennes, QC, J3X 1S1
Y.M. Chiang	Massachusetts Institute of Technology Department of Materials Science and Engineering Cambridge, MA
L. Nazar	U. Waterloo
M. Armond	UDM
M. Gauthier	Phostech
M. Petitclerc	LTEE
Modeling	
J. Christensen, J. Kerr, C. Monroe, T. Richardson J. Shim, V. Srinivasan, S. Stewart, K. Striebel, and K. Thomas	Lawrence Berkeley National Laboratory Berkeley CA 94720-8168
K. Cook, A.M. Sastry, C.W. Wang, and Y.B. Yi	The University of Michigan Department of Mechanical Engineering and Applied Mechanics, Ann Arbor, MI 48109-2125
Diagnostics	
E. J. Cairns, T.M. Devine, M. Doeff, J.W. Evans, Y. J. Lee, J. Lei, K. McCarthy, F. R. McLarnon, R. Muller, J. A. Reimer, P. N. Ross, Jr., S.W. Song, K. Striebel, X. Zhang and V. Zhuang	Lawrence Berkeley National Laboratory Berkeley CA 94720-8168

Long-Term Battery Research	
K. Amine, D. Abraham, C. S. Johnson, J.S. Kim and M. Thackeray	Argonne National Laboratory Chemical Technology Division Argonne IL 60439
S. Whittingham	Chemistry and Materials Research Center State University of New York at Binghamton Binghamton, NY 13902-6000
D. Carlier, G. Ceder, J. Gorman, Y. S. Horn, K. Kang, S. Meng, and J. Reed	Massachusetts Institute of Technology Cambridge, MA 02139-4307
C. P. Grey	State University of New York at Stony Brook, Department of Chemistry Stony Brook, NY
M. Balasubramanian, J. McBreen, , A. Moodenbaugh, X. Sun, X. Q. Yang, and W.S. Yoon	Brookhaven National Laboratory Upton, NY 11973
P. Bruce and A. Robertson	St. Andrews
Y. Xia and M. Yoshio	Saga U/ONRI
J. Xu	Rutgers U.
M. Okada	Tosoh Corp.
K. Zaghib	Hydro Quebec Varennes, J3X 1S1 Quebec Canada
G. Amatucci	Telecordia
A. Mansour	Naval Surface Warfare Center West Bethesda, MD 20817-5700
K. Hämäläinen and A. Mattila	U. Helsinki
M. Giorgetti and W. Smyrl	U. Minnesota Corrosion Research Center Minneapolis, MN 55455
Anodes and Cathodes	
M. Doeff, M. Dollé, T. Eriksson, J. Hollingsworth, Y. Hu, F. Hu, , S.W. Song and K. Striebel	Lawrence Berkeley National Laboratory Berkeley CA 94720-8168
D. Abraham, N. Dietz, C. S. Johnson, J-S. Kim, A. J. Kropf, and J. T. Vaughey	Argonne National Laboratory Chemical Technology Division Argonne IL 60439
B. Cushing, R. Dass, J. Goodenough, F. Rivadulla and S. Schougaard	University of Texas at Austin Austin, TX 78712

Long-Term Battery Research	
K. Edström, L. M. Fransson, and M. Herstedt	Uppsala University, Sweden
S. Hackney	Michigan Technological University Houghton, MI 49931-1295
C. P. Grey and Y. Paik	State University of New York at Stony Brook, Department of Chemistry Stony Brook, NY
D. Curtis	University of Michigan
T. Malinski	Ohio University
M. Anderson and W. Zeltner	University of Wisconsin – Madison
Electrolytes	
N. Balsara, Y. B. Han, J. Kerr, G. Liu, Y. Matsumiya, C. Reeder, L. Odusanya, X. Sun and J. Xie,	Lawrence Berkeley National Laboratory Berkeley CA 94720-8168
H. Watanabe	Institute of Chemical Research, Kyoto University
M. Amin, O. Borodin, and G. D. Smith	Department of Materials Science and Engineering University of Utah Salt Lake City, UT
G. L. Baker	Department of Chemistry Michigan State University East Lansing, MI 48824-1322
S. A. Khan and P. S. Fedkiw	Department of Chemical Engineering North Carolina State University, Raleigh, NC 27695
S. E. Creager, D. D. DesMarteau, O. E. Geiculescu and R. V. Rajagopal	Department of Chemistry Clemson University Clemson, SC 29634-0973.

Appendix B

List of Acronyms

AFM	Atomic force microscopy
ALT	Accelerated life test
ANL	Argonne National Laboratory
AOP	Annual operating plan
ARC	Accelerated rate calorimetry
ASI	Area specific impedance
ATD	Advanced Technology Development
BATT	Batteries for Advanced Transportation Technologies
BHT	Butylated hydroxytoluene
BNL	Brookhaven National Laboratory
CPE	Composite polymer electrolyte
CSAFM	Current-sensing atomic force microscopy
CV	Cyclic voltammetry
DEC	Diethyl carbonate
DFT	Density functional theory
DMC	Dimethylcarbonate
DMF	Dimethyl formamide
DSC	Differential scanning calorimetry
DOD	Depth-of-discharge
DOE	Department of Energy
DSOC	Differential state of charge
DSC	Differential scanning calorimetry
EA	Ethylene acetate
EC	Ethylene carbonate
EDS	Electron dispersive spectroscopy
EDX	Energy dispersive x-ray analysis
EIS	Electrochemical impedance spectroscopy
EMC	Ethyl methyl carbonate
EQCM	Electrochemical quartz crystal microbalance
EV	Electric vehicle
EVOH	Ethylene vinyl alcohol polymer
EXAFS	Extended x-ray absorption fine structure
FCV	Fuel cell vehicle
FCVT	FreedomCAR and Vehicle Technology
FR	Flame retardant
FTIR	Fourier transform infrared
GC	Gas chromatography
γBL	γ-butyrolactone

HDPE	High density polyethylene
HETAP	Hexa-ethoxy-tri-aza-phosphazene
HEV	Hybrid electric vehicle
HMTAP	hexa-methoxy-tri-aza-phosphazene
HPPC	Hybrid pulse power characterization
HQ	Hydro-Québec
ICL	Irreversible capacity loss
IIT	Illinois Institute of Technology
INEEL	Idaho National Engineering and Environmental Laboratory
IR	Infrared
IRAS	Infrared absorption spectroscopy
LBNL	Lawrence Berkeley National Laboratory
LDPE	Low density polyethylene
LiBETI	$LiN(SO_2C_2F_5)_2$
LiBOB	Lithium bis(oxolato)borate
LiTFSI	Lithium bis(trifluoromethane-sulfonyl)imide
LN	Liquid nitrogen
MAS	Magic angle spinning
MCT	Mercury Cadmium Telluride
MD	Molecular dynamics
MIT	Massachusetts Institute of Technology
MW	Molecular weight
NFE	Nonflammable electrolyte
NG	Natural graphite
NMR	Nuclear magnetic resonance
NREL	National Renewable Energy Laboratory
OAAT	Office of Advanced Automotive Technologies
OCV	Open circuit voltage
PA	Power-assist
PC	Propylene carbonate
PCL	Power capability loss
PE	Polyethylene
PEG	Polyethylene glycol
PEO	Poly(ethylene oxide)
PF	Power fade
PMO	Poly(methylene oxide)
PNGV	Partnership for a New Generation of Vehicles
PPO	Poly(propylene oxide)
PTMO	Poly(trimethylene oxide)
PVdF	Poly(vinylidene fluoride)
RDE	Rotating disk electrode
R-F	Resorcinal formaldehyde
SAXS	Small angle x-ray scattering
SBIR	Small Business Innovative Research

SEI	Solid electrolyte interface
SEM	Scanning electron microscopy
SIMS	Secondary ion mass spectroscopy
SNFTIR	Subtractive normalization Fourier transform infrared
SOC	State of charge
SPE	Solid polymer electrolyte
SUNY	State University of New York
TEM	Transmission electron microscopy
TESA	Tetra-ethyl-sulfamide
TM	Transition metal
TMO	Trimethylene oxide
TPP	Tetraphenylporphyrin
UHV	Ultra high vacuum
USABC	United States Advanced Battery Consortium
VC	Vinylene carbonate
VEC	Vinyl ethylene carbonate
WAXD	Wide-angle x-ray diffraction
XAS	X-ray absorption spectroscopy
XPS	X-ray photoelectron spectroscopy
XRD	X-ray diffraction